

INFORMATION TO USERS

This reproduction was made from a copy of a document sent to us for microfilming. While the most advanced technology has been used to photograph and reproduce this document, the quality of the reproduction is heavily dependent upon the quality of the material submitted.

The following explanation of techniques is provided to help clarify markings or notations which may appear on this reproduction.

1. The sign or "target" for pages apparently lacking from the document photographed is "Missing Page(s)". If it was possible to obtain the missing page(s) or section, they are spliced into the film along with adjacent pages. This may have necessitated cutting through an image and duplicating adjacent pages to assure complete continuity.
2. When an image on the film is obliterated with a round black mark, it is an indication of either blurred copy because of movement during exposure, duplicate copy, or copyrighted materials that should not have been filmed. For blurred pages, a good image of the page can be found in the adjacent frame. If copyrighted materials were deleted, a target note will appear listing the pages in the adjacent frame.
3. When a map, drawing or chart, etc., is part of the material being photographed, a definite method of "sectioning" the material has been followed. It is customary to begin filming at the upper left hand corner of a large sheet and to continue from left to right in equal sections with small overlaps. If necessary, sectioning is continued again—beginning below the first row and continuing on until complete.
4. For illustrations that cannot be satisfactorily reproduced by xerographic means, photographic prints can be purchased at additional cost and inserted into your xerographic copy. These prints are available upon request from the Dissertations Customer Services Department.
5. Some pages in any document may have indistinct print. In all cases the best available copy has been filmed.

**University
Microfilms
International**

300 N. Zeeb Road
Ann Arbor, MI 48106

1327007

Martin, Kipp Alan

BEHAVIOR AND DESIGN OF MONOTUBE SIGN SUPPORT STRUCTURES

The University of Arizona

M.S. 1985

**University
Microfilms
International** 300 N. Zeeb Road, Ann Arbor, MI 48106

PLEASE NOTE:

In all cases this material has been filmed in the best possible way from the available copy. Problems encountered with this document have been identified here with a check mark .

1. Glossy photographs or pages
2. Colored illustrations, paper or print _____
3. Photographs with dark background
4. Illustrations are poor copy _____
5. Pages with black marks, not original copy _____
6. Print shows through as there is text on both sides of page _____
7. Indistinct, broken or small print on several pages
8. Print exceeds margin requirements _____
9. Tightly bound copy with print lost in spine _____
10. Computer printout pages with indistinct print _____
11. Page(s) _____ lacking when material received, and not available from school or author.
12. Page(s) _____ seem to be missing in numbering only as text follows.
13. Two pages numbered _____. Text follows.
14. Curling and wrinkled pages _____
15. Dissertation contains pages with print at a slant, filmed as received _____
16. Other _____

University
Microfilms
International

BEHAVIOR AND DESIGN OF MONOTUBE SIGN SUPPORT STRUCTURES

by

Kipp Alan Martin

A Thesis Submitted to the Faculty of the
DEPARTMENT OF CIVIL ENGINEERING AND ENGINEERING MECHANICS

In Partial Fulfillment of the Requirements
For the Degree of

MASTER OF SCIENCE
WITH A MAJOR IN CIVIL ENGINEERING

In the Graduate College
THE UNIVERSITY OF ARIZONA

1 9 8 5

STATEMENT BY AUTHOR

This thesis has been submitted in partial fulfillment of the requirements for an advanced degree at The University of Arizona and is deposited in the University Library to be made available to borrowers under the rules of the Library.

Brief quotations from this thesis are allowable without special permission, provided that accurate acknowledgement of source is made. Requests for permission for extended quotation from or reproduction of this manuscript in whole or in part may be granted by the head of the major department or the Dean of the Graduate College when in his or her judgment the proposed use of the material is in the interest of scholarship. In all other instances, however, permission must be obtained from the author.

SIGNED: Kipp A. Martin

APPROVAL BY THESIS DIRECTORS

This thesis has been approved on the date shown below:

Reidar Bjorhovde

REIDAR BJORHOVDE

Professor of Civil Engineering
and Engineering Mechanics

DEC. 13, 1985

Date

M. R. Ehsani

MOHAMMAD R. EHSANI

Assistant Professor of Civil Engineering
and Engineering Mechanics

12/13/85

Date

TABLE OF CONTENTS

	<u>Page</u>
LIST OF FIGURES	vii
LIST OF TABLES	x
ABSTRACT	xii
1. INTRODUCTION	1
2. SCOPE	7
3. STRUCTURAL RESPONSE UNDER WIND LOADS	9
4. ANALYSIS OF MONOTUBE STRUCTURES	20
4.1 Modeled Structures	20
4.2 Computer Programs	27
4.3 Finite Element Model Development	29
4.4 Static Loads on Structure	35
4.5 Dynamic Loads on Structure	36
4.6 Natural Frequencies of Vibration	41
4.7 Static Load Results	50
4.8 Dynamic Load Results	63
4.9 Conclusions for Analytical Studies	73
5. FIELD TESTING OF FULL-SCALE STRUCTURES	76
5.1 Description of Equipment and Software	76
5.2 Procedure for Gage Installation	82
5.3 Theory of Strain Gage Operation	85
5.4 Data Reduction Procedure	90
5.5 Statistical Analysis of Results	92
5.6 Calibration of Equipment	101
6. COMPARISON OF ANALYTICAL AND EXPERIMENTAL RESULTS	106
6.1 Tucson Structure	106
6.2 Phoenix Structure	113
7. SUMMARY, CONCLUSIONS AND RECOMMENDATIONS	118
7.1 Summary and Conclusions	118
7.2 Recommendations for Further Studies	121

TABLE OF CONTENTS (Continued)

	<u>Page</u>
APPENDIX A: DATA COLLECTION SOFTWARE FOR THE HP-41CX CALCULATOR ..	123
APPENDIX B: DATA REDUCTION SOFTWARE FOR HP SERIES 200 COMPUTER ...	129
APPENDIX C: SET-UP AND OPERATION OF FIELD TESTING EQUIPMENT	138
APPENDIX D: DATA TRANSFER FROM CASSETTE DRIVE TO HP SERIES 200 COMPUTER	142
APPENDIX E: DATA TRANSFER SOFTWARE FOR HP 41CX CALCULATOR	146
APPENDIX F: DATA TRANSFER SOFTWARE FOR HP SERIES 200 COMPUTER ...	148
REFERENCES	150

LIST OF FIGURES

<u>Figure</u>		<u>Page</u>
1	Typical Truss Sign Support Structure	3
2	Typical Monotube Sign Support Structure	3
3	Long Span Monotube Sign Support Structure	5
4	Typical Monotube Structure Beam-to-Column Connection	5
5	Airfoil Illustrating Principle of Lift	12
6	Drag on Plate in an Air Stream	12
7	Vortices for Flow Around a Cylinder	14
8	Karman Vortex Sheet	14
9	Standing Vortices for Flow Around a Cylinder	17
10	Relationship between the Reynolds Number and the Strouhal Number	17
11a	Tucson Monotube Structure	21
11b	Phoenix Monotube Structure	21
12	Dimensions of Tucson Monotube Structure	23
13	Beam-to-Column Connection for Tucson Monotube Structure	24
14	Column Foundation for Tucson Monotube Structure	25
15	Dimensions of Phoenix Monotube Structure	26
16	Beam-to-Column Connection for Phoenix Monotube Structure	28
17a	Finite Element Model of Tucson Monotube Structure	30
17b	Finite Element Model of Phoenix Monotube Structure	31
18	First Natural 3D Mode for Tucson Monotube Structure	46

LIST OF FIGURES (Continued)

<u>Figure</u>	<u>Page</u>
19	Second Natural 3D Mode for Tucson Monotube Structure 47
20	First Natural 3D Mode for Phoenix Monotube Structure 48
21	Second Natural 3D Mode for Phoenix Monotube Structure 49
22a	Deflected Shape for Tucson Monotube Structure Subjected to Static Loads 51
22b	Deflected Shape for Phoenix Monotube Structure Subjected to Static Loads 52
23a	Static Stresses at Midspan of Tucson Monotube Structure 56
23b	Static Stresses at Midspan of Phoenix Monotube Structure 57
24a	Static Stresses at Column Base of Tucson Monotube Structure 58
24b	Static Stresses at Column Base of Phoenix Monotube Structure 59
25a	Static Stresses at Joint of Tucson Monotube Structure 61
25b	Static Stresses at Joint of Phoenix Monotube Structure 62
26	Typical Histogram for Dynamic Analysis of Monotube Structures 64
27	Periodic Histogram for Dynamic Analysis of Monotube Structures 69
28	Typical Strain Gage 78
29	Anemometer Mounted on Structure 78

LIST OF FIGURES (Continued)

<u>Figure</u>		<u>Page</u>
30	Data Acquisition Equipment	81
31	Locations of Strain Gages on Monotube Structure	83
32a	Two-wire Quarter Bridge Circuit	84
32b	Three-wire Quarter Bridge Circuit	84
33a	Mounted Strain Gage with Cable Attached	86
33b	Mounted Strain Gage with Protective Wax Coating	86
34	Typical Wheatstone Bridge	88
35	Dynamic Deflections in Monotube Structure at Various Times	93
36a	Stress Envelope for Midspan Stresses of Tucson Monotube Structure	95
36b	Stress Envelope for Midspan Stresses of Phoenix Monotube Structure	96
37a	Stress Envelope for Column Base Stresses of Tucson Monotube Structure	99
37b	Stress Envelope for Column Base Stresses of Phoenix Monotube Structure	100
38	Apparent Strain in Strain Gage Due to Temperature	102
39	Correlation of Stresses for Tucson Monotube Structure	111
40	Total Stresses for Tucson Monotube Structure	112
41	Correlation of Stresses for Phoenix Monotube Structure	116
42	Total Stresses for Phoenix Monotube Structure	117

LIST OF TABLES

<u>Table</u>	<u>Page</u>
1 Coefficient of Drag for Various Shapes	11
2a Element Thicknesses and Diameters for Tucson Monotube Structure	33
2b Element Thicknesses and Diameters for Phoenix Monotube Structure	34
3a Drag Forces on Signs for Tucson Monotube Structure	37
3b Drag Forces on Signs for Phoenix Monotube Structure	38
4 Average Diameter of Finite Element Subassemblies	40
5a Natural Frequencies of Tucson Monotube Structure	44
5b Natural Frequencies of Phoenix Monotube Structure	45
6a Midspan Static Deflections for Tucson Monotube Structure	53
6b Midspan Static Deflections for Phoenix Monotube Structure	54
7a Stresses at Critical Points for Dynamic Analysis of Tucson Monotube Structure	65
7b Stresses at Critical Points for Dynamic Analysis of Phoenix Monotube Structure	66
8 Wind Speeds for which Periodic Oscillation Occur in Beam	70
9a Stresses for Tucson Monotube Structure for Dynamic Loading with Structural Mass	71
9b Stresses for Phoenix Monotube Structure for Dynamic Loading with Structural Mass	72
10a Deflections of Tucson Monotube Structure for Dynamic Loading with Structural Mass	74

LIST OF TABLES (Continued)

<u>Table</u>		<u>Page</u>
10b	Deflections of Phoenix Monotube Structure for Dynamic Loading with Structural Mass	75
11a	Results of Data Acquisition Unit Calibration Test - Day One	105
11b	Results of Data Acquisition Unit Calibration Test - Day Two	105
12	Computed and Measured Stresses for 60-Foot Structure	107
13	Computed and Measured Stresses for 100-Foot Structure	114

ABSTRACT

Results of field testing and analytical studies are presented for two monotube sign structures. One structure had a span of 60 feet, the other had a span of 100 feet. Both structures were instrumented with strain gages and an anemometer to determine in-service strains due to wind loading.

The structures were analyzed by two- and three-dimensional finite element modeling. The loading included static and dynamic (vortex shedding) loads. It was found that the analytical study correlated well with the field measurements, especially when the complexities of the analysis are considered.

It is concluded that current designs of monotube sign support structures tend to be conservative, very much prompted by the AASHTO dead load deflection criterion. Recommendations are made for improved design and construction criteria, along with additional studies that need to be undertaken.

Chapter 1

INTRODUCTION

For almost as long as there have been roads, there has been a need for road signs to display information to travelers. As the width of the roads grew, so did the size of the structures, until today spans in excess of 100 feet are not uncommon.

To support signs over these large spans, truss type structures have traditionally been used. These typically consist of two columns supporting a truss or tri-cord element. The traffic signs are arranged in the desired locations and bolted in place. Figure 1 shows a typical truss type structure.

The design of sign support structures is based on the American Association of State Highway and Transportation Officials' (AASHTO) 1975 "Standard Specifications for Structural Supports for Highway Signs, Luminaries and Traffic Signals" (1), which was revised in 1978 and 1979, and one of its predecessors, the AASHTO 1968 "Specifications for the Design and Construction of Structural Supports for Highway Signs". In the remainder of this report these will be referred to as the Specifications.

The Specifications set minimum performance guidelines. Among these are criteria governing deflections. Essentially, the maximum

static dead load deflection, in units of feet, is limited to the empirical value of $d^2/400$, where d is the depth of the sign in feet. If the deflection of a sign-support structure is found to be excessive, the designer can satisfy the Specifications simply by specifying a deeper sign (i.e., larger d). The rationale and consequences of this approach will be discussed in some detail in later chapters. An extensive evaluation of the deflection requirement has been given by Ehsani and Bjorhovde (2).

Over the years, the performance of the truss structures has generally been satisfactory. However, there are some drawbacks to their use. They are expensive to fabricate and in many cases the application of the deflection requirement produces a structure which is not as economical as some of the pre-engineered structures that are available. One of the latter types that has seen increased use is the monotube sign support structure. In addition to being more economical, the monotube structure also has the advantage of being more attractive than most truss structures.

As shown in Fig. 2, monotube structures are constructed of linearly tapering tubular elements that have a constant wall thickness. They consist of two columns supporting a beam in a fashion similar to the truss type structures. The columns are one piece tapered members, with the largest diameter at the base. The beam normally consists of two tapered pieces that are joined with the largest diameter at mid-

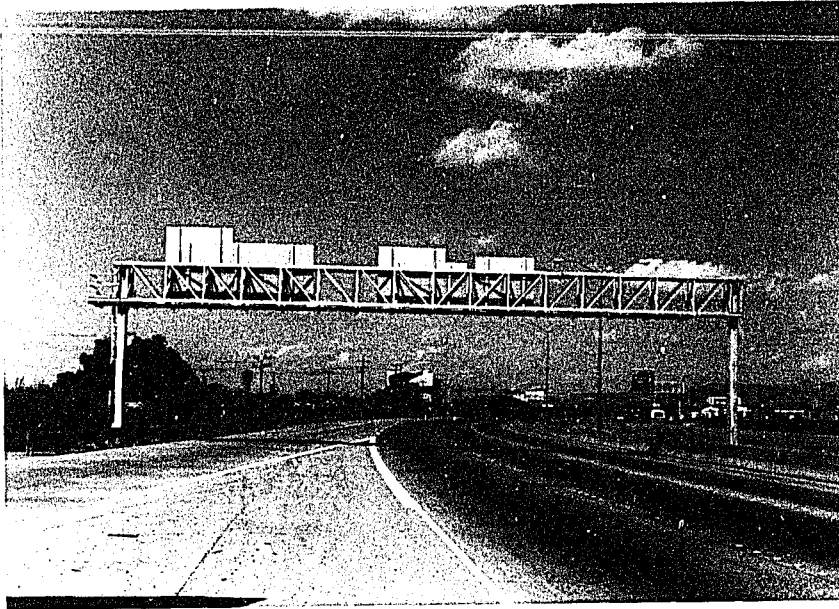


Figure 1 Typical Truss Sign Support Structure

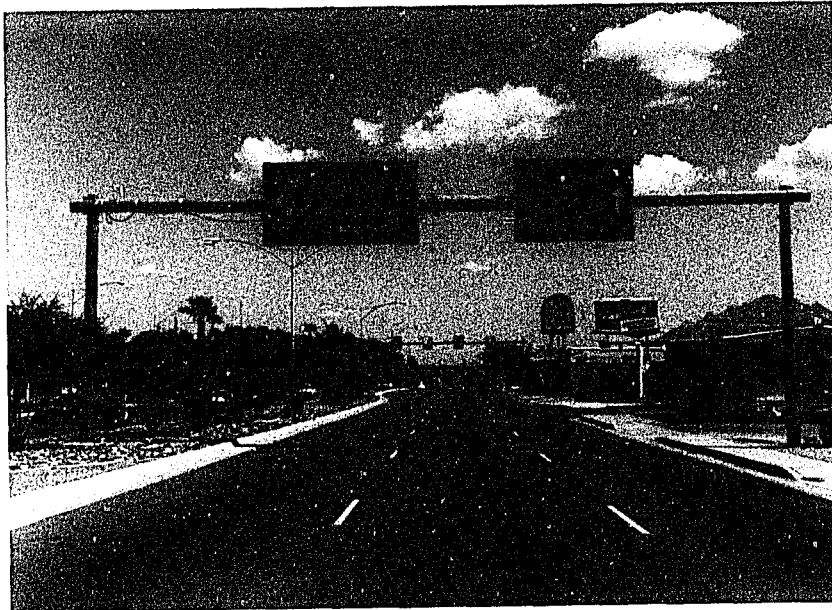


Figure 2 Typical Monotube Sign Support Structure

span. Beams of longer spans may consist of 3 pieces, with the middle one having a constant diameter. Figure 3 shows one of these longer 3-piece spans. For both types, the beam is connected to the column by simple supports, as shown in Fig. 4.

Currently, the Specifications do not provide sufficiently detailed guidelines for the design of monotube structures. As a result, the manufacturers of these structures utilize individual design criteria that make direct comparisons between different products very difficult. In addition, the structures tend to vary widely in material as well as cross-sectional properties. This has placed the transportation authorities in the position of having to accept or reject different designs with no rational guidelines to follow.

The absence of adequate design guidelines can partly be attributed to the sparsity of research and engineering data on the strength and behavior of monotube structures. The first major work in this area was a project conducted by Ehsani and Bjorhovde (3) in 1984 at the University of Arizona. This study modeled a monotube structure using the finite element method to determine its response to various static and dynamic loads. It was found that the $d^2/400$ deflection criterion was inappropriate for monotube structures. Dead load deflections in excess of the $d^2/400$ limit were calculated, although the stresses associated with these deflections were well below the magnitudes of the allowable levels.

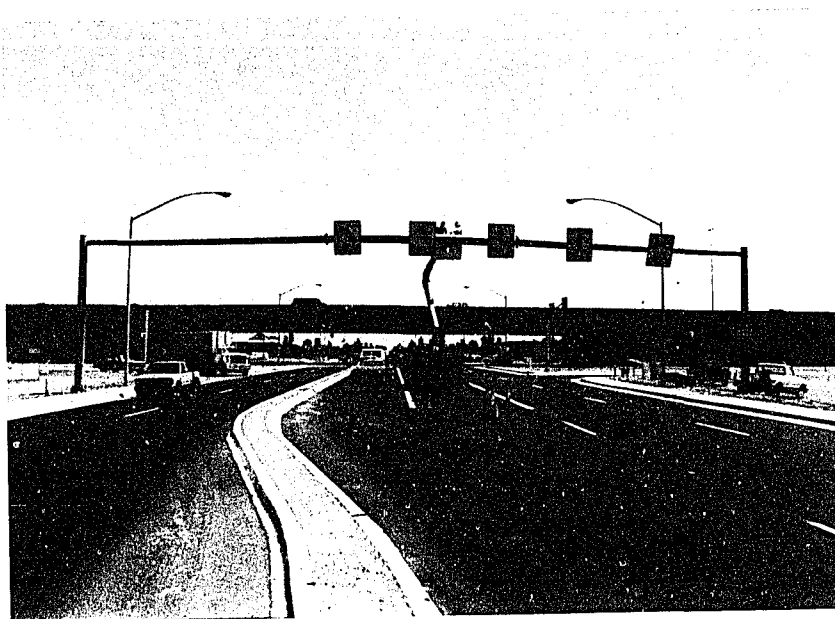


Figure 3. Long Span Monotube Sign Support Structures

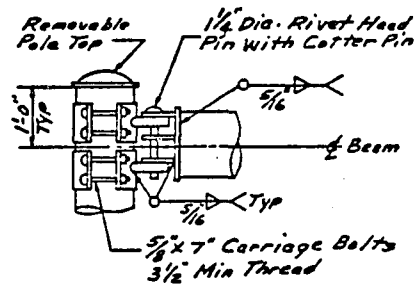


Figure 4. Typical Monotube Structure Beam-to-Column Connection

The first monotube study was purely analytical and the accuracy of the results obtained is a function of the assumptions that were made to model the structure. It is important to compare such theoretical results with actual performance data for a real structure, to verify the modeling as well as the responses that have been found. The latter should be obtained from testing, preferably using a full scale structure being subjected to a variety of service conditions. With such test data and correlations in hand, improved design guidelines can be developed.

Chapter 2

SCOPE

Before the validity of any analytical study can be fully accepted, its results should be compared to the actual behavior of the subject in question. While the study by Ehsani and Bjorhovde (3) provided detailed data on the behavior of monotube structures, it lacked comparison with the performance of an actual structure.

The study presented here was conducted in three parts. In the first, two actual structures were modeled for computer analysis. These were analyzed for various static and dynamic loads to determine their response to different wind speeds. The data that were collected include dynamic histograms, deflections and stresses for a variety of wind speeds.

Part two involved field testing of the same two structures. By testing the structures under service conditions, the true response was obtained. Strains at critical points on the structure were recorded, along with the wind speed corresponding to these strains.

The final part of the study was aimed at comparing and evaluating the results obtained in the first two parts. Through this comparison, it would be possible to judge the validity of the computer model, as well as to reveal any problem conditions such as resonance.

This study has been limited to monotube structures as described in Chapter 1. Cantilever structures were not considered, and fatigue related problems have also been ignored due to time limitations.

Chapter 3

STRUCTURAL RESPONSE UNDER WIND LOADS

For most sign structures, the only loads acting on the structure are gravity and wind. The forces due to gravity are simply the self weight of the structure; their magnitude and effect on the structure are relatively easy to determine.

In contrast to the gravity loads, which are static, wind loads are dynamic. There are a number of reasons for this dynamic nature. First, the magnitude of the wind is not constant. The wind tends to gust. The direction of the wind also changes. Finally, the cross-sectional shape of the structural elements may cause dynamic behavior.

An object placed in an air stream will cause a disturbance in that air stream. This disturbance will create pressure on the object, the size and shape of which will determine the intensity and distribution of the pressure. As an illustration, it is this phenomenon that creates the lift on an airplane wing. The wing is shaped such that as air flows around it, the pressure on the wing surface is larger on the bottom than on the top, as shown in Fig. 5. Thus, the airplane rises.

In addition to lift, another force that is exerted on the object is drag. This has been experienced by anyone trying to pedal a

bicycle into the wind. As long as the velocity of the airstream is constant, the drag force remains constant. Drag is therefore considered a static force.

The magnitude of the drag force, shown in Fig. 6, can be computed as:

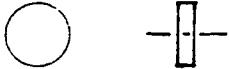

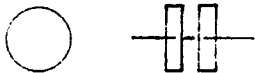
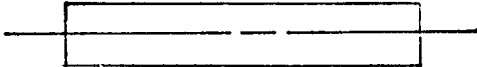
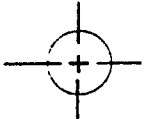

$$F = \rho C_D A V_0^2 \quad (1)$$

where F is the drag force, A is the projected area of the object perpendicular to the flow, ρ is the density of the air, V_0 is the velocity of the airstream, and C_D is the coefficient of drag for the object (4). Table 1 gives the coefficient of drag for some common shapes.

If the object in the air stream has an irregular shape, the pressure distribution will also be irregular. Thus, for a certain range of wind speeds, the object may develop vibrations or oscillations normal to the direction of flow (5). A common example of the phenomenon is the oscillation observed in telephone cables in a strong wind. Sometimes, these oscillations can result in excessive deformations or even collapse of a structure. This happens when the vibrations induced by the airflow have a frequency that is equal or close to one of the natural frequencies of the structure, and reflects the condition of structural resonance.

The occurrence of resonance means that the structure will continue to oscillate with no additional energy or load applied to the

TABLE 1. Drag Coefficient for Various Shapes

Form of Body	L/D	R	C_D
Circular Disk 		$>10^3$	1.12
Rectangular Plate (L = length, D = width) 	1 3 20 8	$>10^3$	1.16 1.20 1.50 1.90
Tandem Disks (L = Spacing) 	0 1 2 3	$>10^3$	1.12 0.93 1.04 1.54
Cylinder (axis parallel to flow) 	0 1 2 4 7	$>10^3$	1.12 0.91 0.85 0.87 0.99
Cylinder (axis perpendicular to flow) 	1 5 20 8 5 8	10^5 $>5 \times 10^5$	0.63 0.74 0.90 1.20 0.35 0.33
Streamlined Foil 	8	$>4 \times 10^4$	0.07

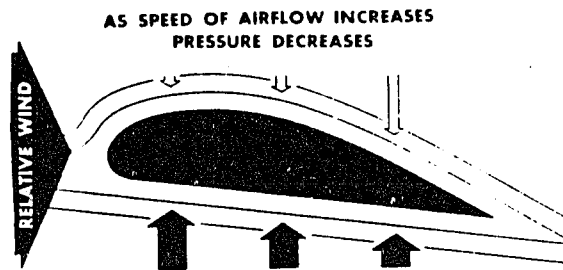


Figure 5. Airfoil Illustrating Principle of Lift



Figure 6. Drag on Plate in Air Stream

structure. Probably the most famous structural failure where resonance at least played a part was the collapse of the Tacoma Narrows Bridge in the State of Washington. This bridge failed at a wind speed of 42 mph, although it had been designed to withstand winds up to 100 mph if no oscillations had occurred (6). However, the wind-induced vibrations were close to one of the natural frequencies of the bridge and this contributed to the collapse.

The wind-induced vibrations are caused by a phenomenon known as vortex shedding. Fluid flowing around an object will develop vortices in the wake. These will alternate from one side of the object to the other, as illustrated in Fig. 7 for flow around a cylinder.

The study of these vortices was originated by von Karman (6), using a double row of vortices in two-dimensional flow. He found that the only stable equilibrium configuration for the double row resulted when the vortices of one row were exactly opposite to points half-way between the vortices in the other row. Von Karman also found that for the rows to be stable, they would have to be spaced at 0.281 times the distance between two adjacent vortices of one row. Such an arrangement is known as a Karman vortex sheet and is illustrated in Fig. 8.

Von Karman based this treatment of vortex shedding on the assumption of a perfect fluid. By definition, the only property possessed by a perfect fluid is density. Therefore, this treatment does not reflect the influence of fluid viscosity. Flow of a viscous

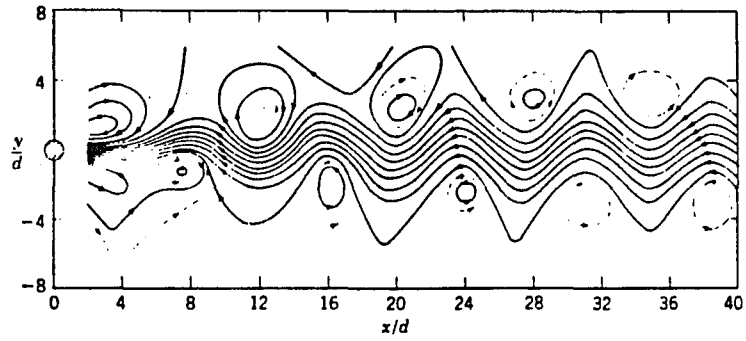


Figure 7. Vortices for Flow Around Cylinder

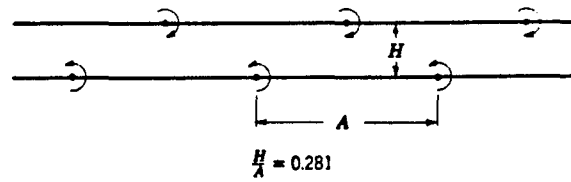


Figure 8. Kármán Vortex Sheet

fluid is accompanied by a pressure gradient that is proportional to the dynamic viscosity of the fluid. Since the density and viscosity for air are both relatively small, the viscosity can have as much effect on fluid flow as the density and must be taken into account. The Reynolds number, R , characterizes the relative importance of viscous action, with a higher number indicating a lesser importance (4). Therefore, an infinite value of R corresponds to a flow in which viscous resistance plays no part.

For flow past a cylinder, a number of changes occur as the Reynolds number increases. For instance, for small values of R , the flow is smooth and unseparated. For higher values of R , two symmetrical standing vortices form behind the cylinder, as shown in Fig. 9. As R increases, these vortices stretch downstream. When R is approximately 40, the vortices alternate in detaching from the two sides of the cylinder and move downstream. This is the start of vortex shedding.

For R values between 40 and 300, the shedding is very regular in both amplitude and frequency and can be approximated by a Karman sheet. As R increases past 300, the flow becomes irregular. The vortices are still shedding with a predominant frequency, but their amplitude is not easily determined, since it is more or less random. This irregular flow continues until R equals 3×10^5 . At this point,

the flow is so turbulent that the vortex sheet is no longer recognizable.

For the range of Reynolds numbers where vortex shedding does occur, the frequency with which the vortices are shed can be expressed non-dimensionally by the Strouhal number, S . Since the vortex shedding frequency varies with R , S also varies with R , as shown in Fig. 10.

For monotube structures, the fluid is air and the structure can be considered a long cylinder. The Reynolds number is then defined as (6):

$$R = 780.5 \cdot V \cdot D \quad (2)$$

where V is the airspeed in miles per hour and D is the cylinder diameter in inches. It can be seen that except when dealing with very small cylinders and low wind speeds, R will be greater than 300. For values of R between 300 and 3×10^5 , the shedding frequency is sinusoidal but with a random amplitude. For R larger than 3×10^5 , both the frequency and the amplitude are random.

For the range of $300 < R < 3 \times 10^5$, the vortex shedding forces must be determined from the pressure distribution.

The generally accepted expression for this force is (7):

$$F(t) = 1/2 \gamma V^2 A_p C_L \sin \Omega t \quad (3)$$

where $F(t)$ is the time dependent vortex shedding force, γ is the density of air, V is the wind velocity, A_p is the projected area of the cylinder, C_L is the coefficient of lift, Ω is the shedding frequency,

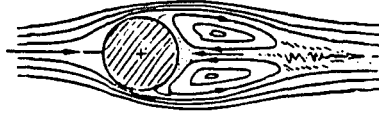


Figure 9. Standing Vortices for Flow Around Cylinder

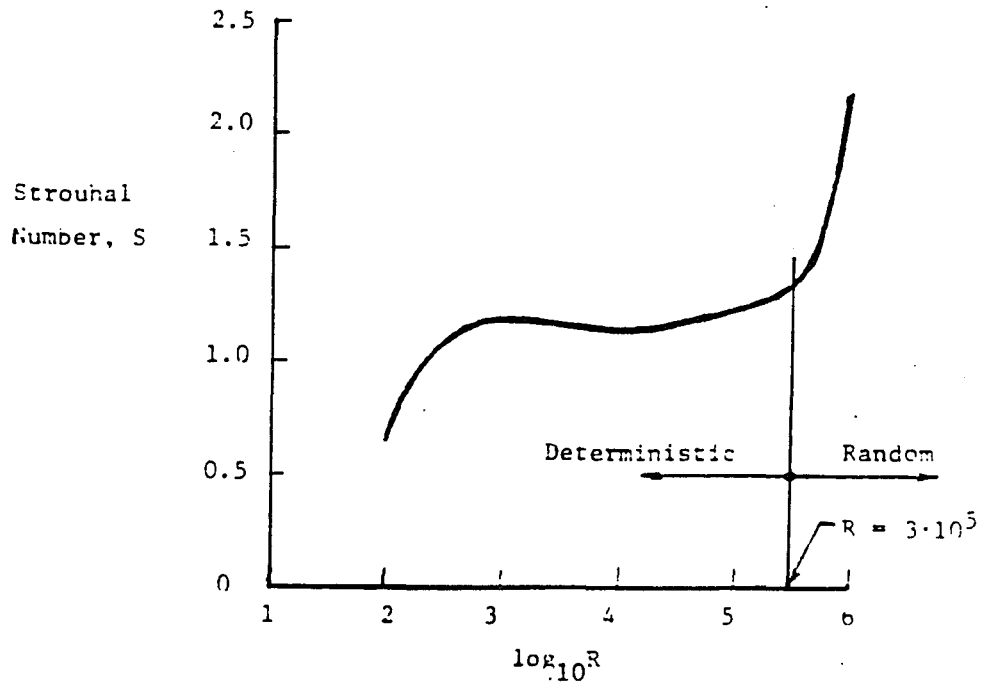


Figure 10. Relationship Between the Reynolds Number and the Strouhal Number

and t is the time. To account for the random force amplitude, Weaver (8) experimentally determined the root-mean-square (rms) values of C_L , denoted as \bar{C}_L , and using these, the expression for the vortex shedding forces becomes (4):

$$F(t) = 1/2 \gamma A_p \bar{C}_L \sin \Omega t \quad (4)$$

The determination of Ω is critical in the use of this equation. The vortex shedding frequency is determined from the equation (2)

$$\Omega = \frac{SV}{D} \quad (5)$$

where S is the Strouhal number, V is the air speed, and D is the cylinder diameter.

As an example, the forcing function for a wind speed of 15 mph and a cylinder 14 in. in diameter will be determined. From Eq. (2), $\log_{10} R = \log_{10} (780.5 \cdot 15 \cdot 14) = 5.21$. From Fig. 11, the corresponding Strouhal number is $S = 1.48$.

From Eq. (5), using $S = 1.48$, $V = 15 \text{ mph} = 264 \text{ in/sec}$. and $D = 14 \text{ in.}$, the value of Ω is found to be

$$\Omega = \frac{1.48(264)}{14} 27.91 \text{ rad/sec.}$$

$F(t)$ is now determined from Eq. (4), using $\bar{C}_L = 1.0$, as

$$\begin{aligned} F(t) &= 1/2 (0.002378) (22.0)^2 A_p (1.0) \sin (27.91t) \\ &= 0.575 A_p \sin (27.91t) \end{aligned}$$

where the wind speed is 22.0 ft/sec. From this expression, the forces on the structure can be determined, given the corresponding values of A_p .

For the monotube structure, the vibrations caused by the vortex shedding are more pronounced in the beam, as it is a simply supported element. These vibrations are also more pronounced in longer spans. In the range of wind speeds where $300 < R < 3 \times 10^5$, the vibrations are usually of small amplitude, unless their frequency is close to the resonant frequency of the structure. In this case, the deflections may be excessive.

As stated in Chapter 1, the quantity $d^2/400$ is an empirically derived value. This criterion was originally developed primarily for use with truss type structures, where vortex shedding has a much smaller effect. This provision is very restrictive. Even structures with large signs (≈ 7 feet deep) can deflect no more than 0.125 inches. Other codes (9,10) are not as restrictive in their deflection criterion. A deflection criterion should be developed for the monotube structures, independent of that used for trusses. This criterion should be based on the stiffness of the monotube structure, as well as provide for serviceability.

Chapter 4

ANALYSIS OF MONOTUBE STRUCTURES

To help in developing the design guidelines, as well as to provide data for a detailed comparison with the results of full-scale testing, extensive structural analyses were performed. This evaluation was done by modeling the two tested structures using the finite element method. The response of the models under static and dynamic loading was found, including the determination of the first ten natural frequencies for two- and three-dimensional behavior. Detailed stress and deflection computations were also made.

4.1 Modeled Structures

For this study, the Arizona Department of Transportation provided shop drawings and site plans for two sign structures. Both of these structures had been designed in accordance with the AASHTO specifications (1). The first structure has a span of 60 feet, and is located across the north-bound lanes of Miracle Mile, just north of Glenn Avenue in Tucson, Arizona. This structure is shown in Fig. 11a. The second structure has a span of 100 feet, and is located across University Drive at the intersection of University Drive and Hohokam Expressway in Phoenix, Arizona. This structure is shown in Fig. 11b.



Figure 11a Tucson Monotube Structure

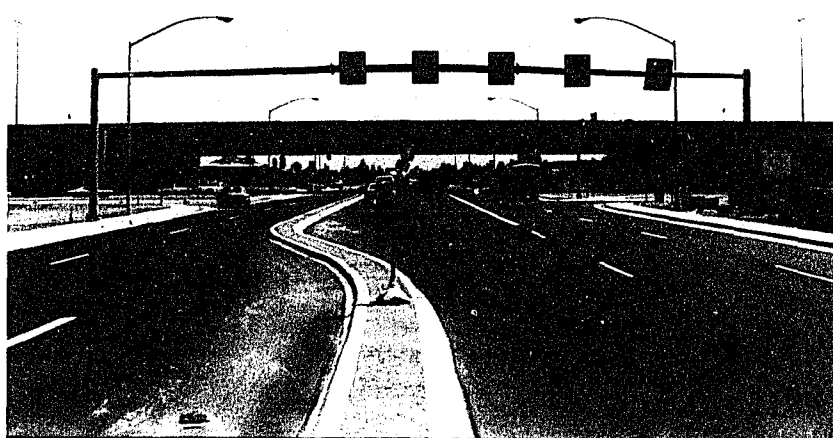


Figure 11b Phoenix Monotube Structure

The dimensions of the Tucson structure are given in Fig. 12. The columns are linearly tapering single tubes, with the largest diameter at the base. Due to the site topography, the west column is 21" shorter than the east column, in order for the beam to be level. The beam is also constructed of linearly tapering elements. It is spliced with the largest diameter at midspan.

The beam-to-column connection is shown in Fig. 13. It provides some moment resistance to vertical loads and essentially free rotation under horizontal loads. This connection also offsets the center line of the beam 18" from the centerline of the column, thus producing a true three-dimensional structure.

The details of the column base and foundation are shown in Fig. 14. The column base can be reasonably assumed to be fully fixed in all directions. The location of the traffic signs can be seen in Fig. 12.

The dimensions of the Phoenix structure are given in Fig. 15. The columns are of similar construction to the Tucson structure. The beam, however, is made of three segments instead of two, with the splices between segments at approximately the third points. The two outer segments have their largest diameter at the splices and taper linearly to the ends. The interior segment is of constant diameter. The beam is also cambered, so that the centroidal axis at midspan is 17" above the centroidal axis at the ends of the beam.

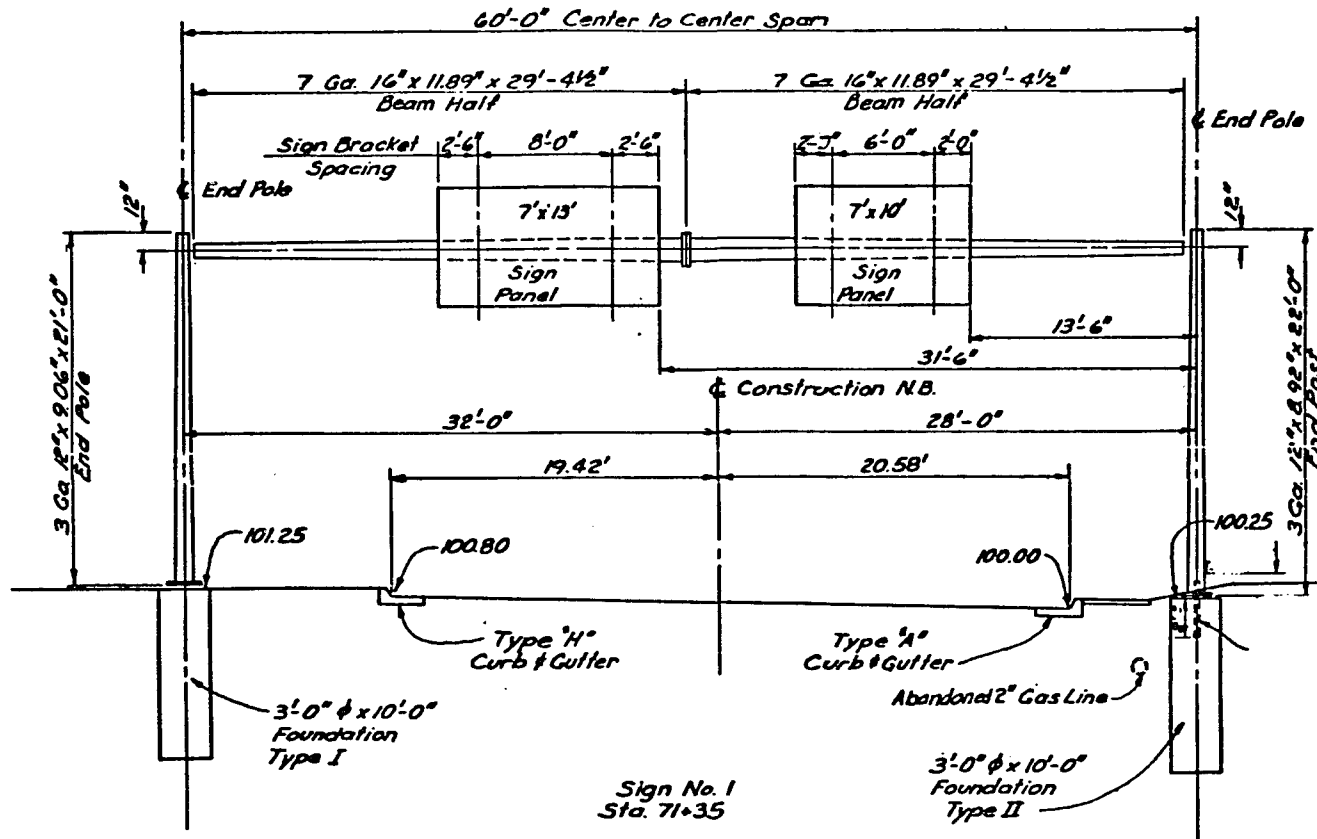


Figure 12. Dimensions of Tucson Monotube Structure

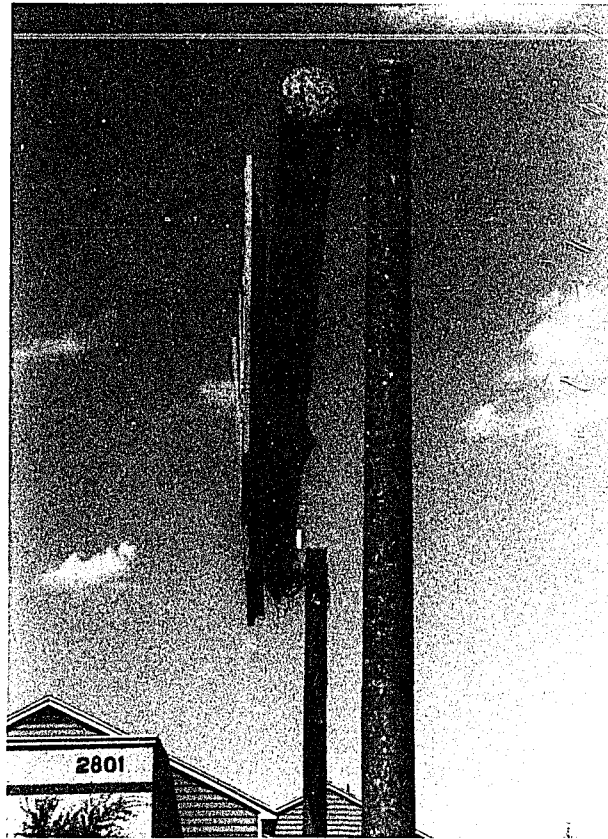


Figure 13 Beam-to-Column Connection for Tucson Monotube Structure

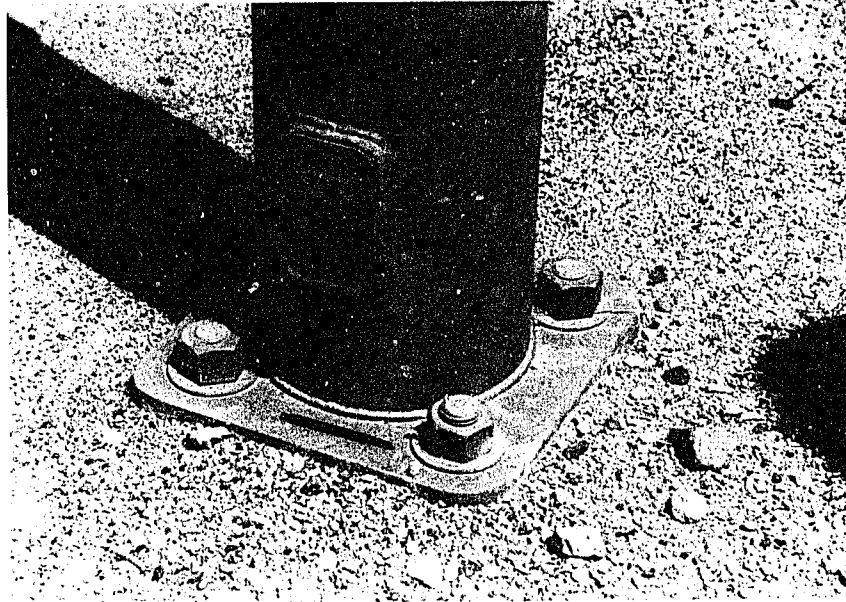


Figure 14 Column Foundation for Tucson Monotube Structure

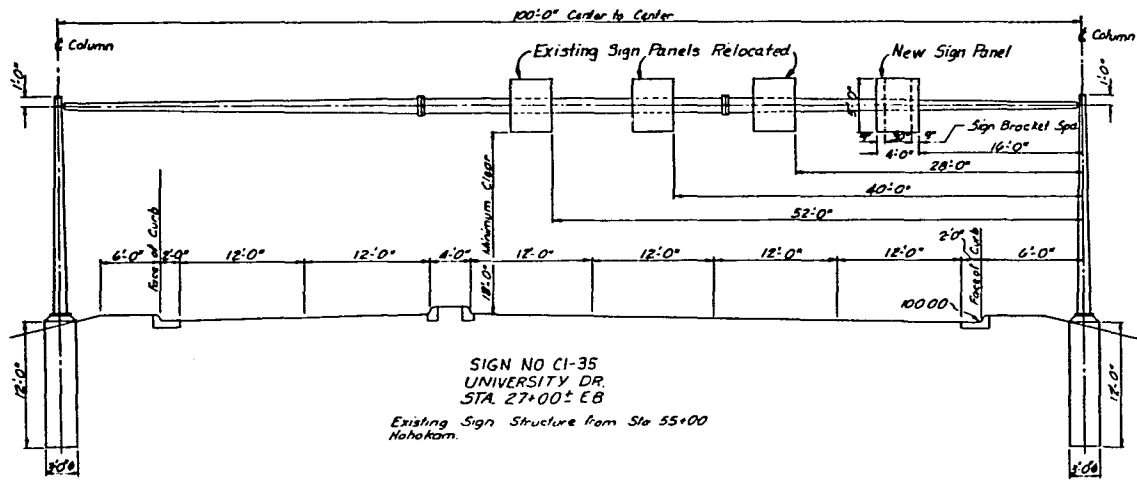


Figure 15. Dimensions of Phoenix Monotube Structure

The beam-to-column connection for the Phoenix structure is not the same as the Tucson structure. While the moment resistances are comparable, the connection is such that the axes of the columns and the beam all lie in the same plane. This connection is shown in Fig. 16. The column base is similar to that shown in Fig. 14 and can also be assumed to be fully fixed. The locations of the signs for this structure are shown in Fig. 15.

4.2 Computer Programs

The structural analysis of the monotube structures was accomplished using a set of computer programs collectively known as GIFTS (Graphics-oriented Interactive Finite element analysis Time-sharing System) (8). These programs constitute a finite element pre- and post-processing and analysis package, which can be loaded and run on a variety of minicomputers and time-sharing systems. It can be used with a standard alphanumeric terminal or with a graphics terminal. For this study, the GIFTS package was run on a Data General Eclipse computer of the Department of Aerospace and Mechanical Engineering at the University of Arizona.

Each of the GIFTS programs (modules) is fully compatible with all of the other modules. A module may perform a specific function, such as computing the natural frequencies of a structure, or a class of functions such as mesh definition and element generation. Many of the

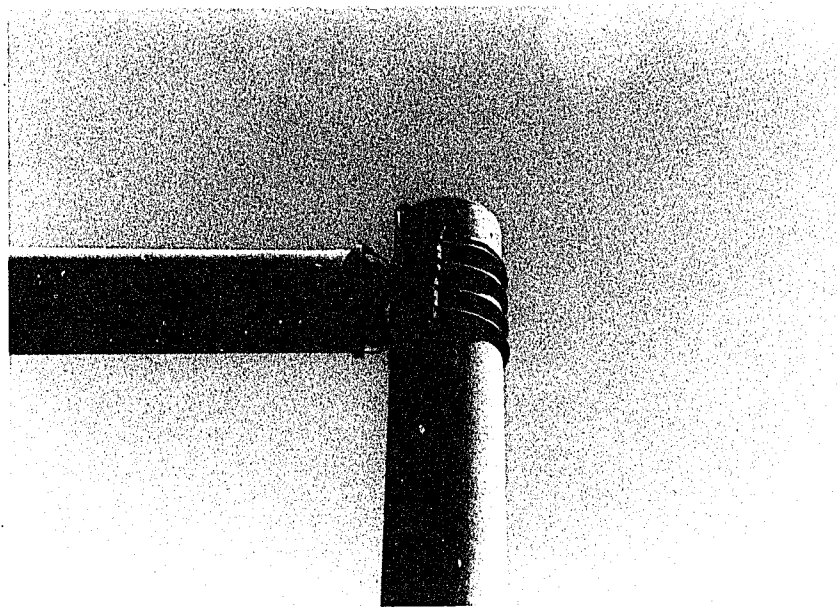


Figure 16 Beam-to-Column Connection for
Phoenix Monotube Structure

modules can be operated in either batch mode or interactively. In batch mode, the modules obtain commands and data from a pre-existing steering file. In interactive mode, the user must input the commands and data through the keyboard.

GIFTS can handle many different loads and load cases, and the stresses and deflections can be computed for each load case. Plots of the deflected structure or the stress distribution on any cross-section can also be provided.

4.3 Finite Element Model Development

Using the guidelines of the GIFTS package (11), a finite element model for each structure was developed. These models are shown in Figs. 17a and 17b for the Tucson and Phoenix structures, respectively.

The elements in both structures were modeled as beam elements with one node at each end. In order to be as realistic as possible, each node was allowed to have three translational degrees of freedom (i.e., displacements in the x-, y-, and z-directions), as well as three rotational degrees of freedom (rotations about the x-, y-, and z-axes). The x-, y-, and z-axes for each model are shown in Figs. 17a and 17b. These axes were considered to be the global axes for each model.

In GIFTS, a variety of cross-sectional shapes can be used for the beam elements, including the standard I-section and a hollow,

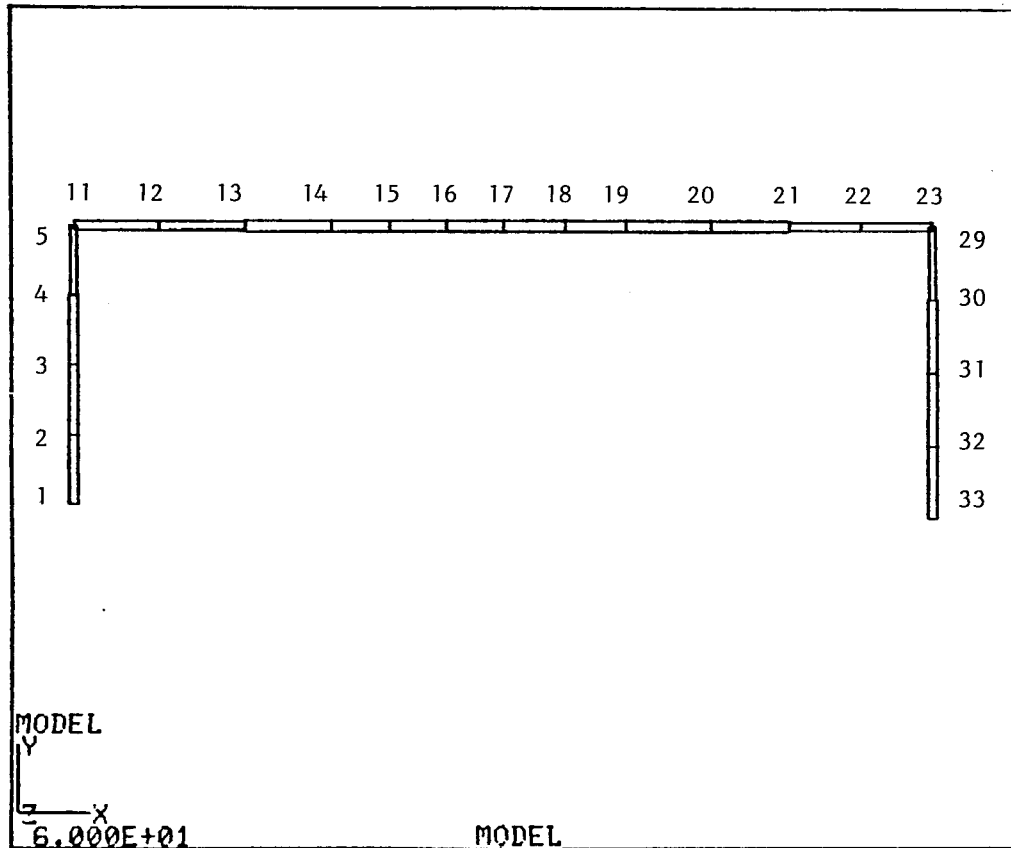


Figure 17a Finite Element Model of Tucson Monotube Structure
Showing Nodal Mesh.

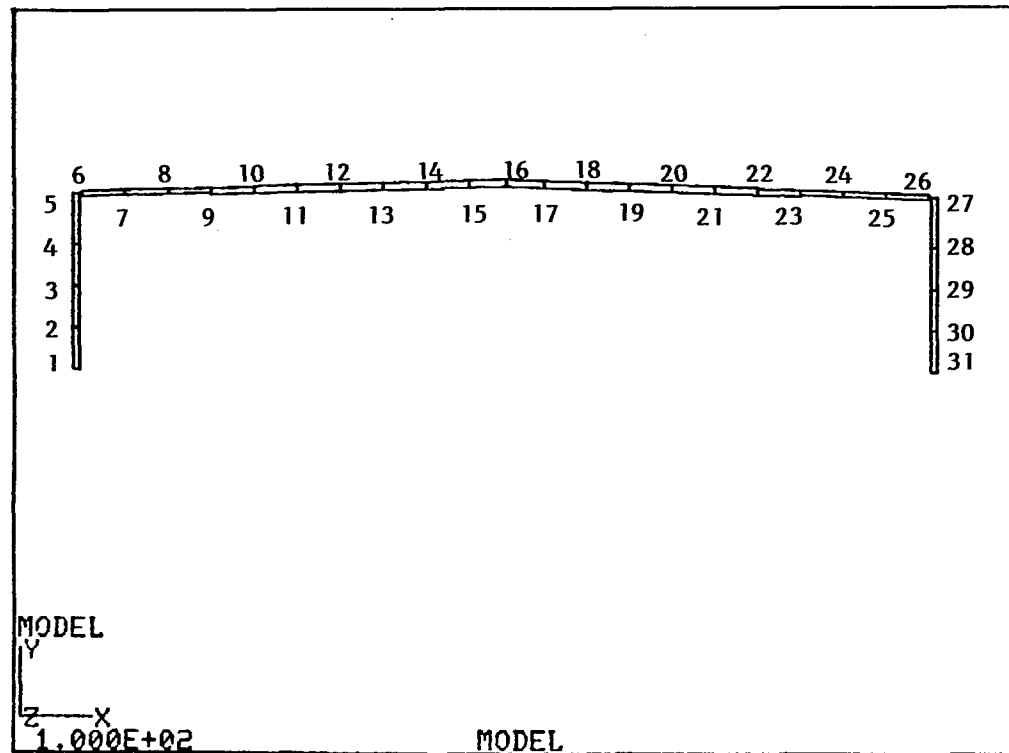


Figure 17b Finite Element Model of Phoenix Monotube Structure Showing Nodal Mesh

circular section. Thus, the hollow circular sections were used for the beam and column elements while the I-shape was used for the elements connecting the beam and the columns. GIFTS, however, cannot accept non-prismatic (e.g., tapered) elements. To circumvent this limitation, each element was assumed to have a constant cross-section, with dimensions equal to the average of the two end cross-sections of the element in the actual structure. In addition, a larger number of elements than would normally be required were used in each model. The wall thickness of the circular elements were taken as the minimum specified on the shop drawings. A list of element diameters and thicknesses is given in Tables 2a and 2b.

The most difficult element to model was that representing the beam-to-column connection. The shear capacity of a connection is based on its cross-sectional area, while the flexural capacity depends on the moment of inertia. To ensure a realistic behavior for shear, the connection was modeled as a short I-section beam with the same area as the actual connection. The weak axis of the I-beam was oriented to give the least bending resistance in the horizontal direction, reflecting the simple support condition for the beam under the action of horizontal (perpendicular to the plane of the monotube structure) loads. The element was proportioned to give a moment capacity in the vertical direction approximating that of the real connection. The I-section was actually similar to a flat plate, as the flanges were only

Table 2a. Element Diameters and Thicknesses for Tucson Structure.

<u>Element No.</u>	<u>I-Node</u>	<u>J-Node</u>	<u>Dia. (in)</u>	<u>Thicknesses (in.)</u>
3	1	2	12.78	0.239
4	32	33	12.92	"
5	2	3	11.92	"
6	31	32	12.04	"
7	3	4	11.08	"
8	30	31	11.14	"
9	4	5	10.22	"
10	29	30	10.24	"
11	11	12	12.96	0.179
12	12	13	13.72	"
13	13	14	14.48	"
14	14	15	15.12	"
15	15	16	15.18	"
16	16	17	15.68	"
17	17	18	16.12	"
18	18	19	15.58	"
19	19	20	14.92	"
20	20	21	14.20	"
21	21	22	13.42	"
22	22	23	12.90	"

Table 2b. Element Diameters and Thicknesses for Phoenix Structure.

<u>Element No.</u>	<u>I-Node</u>	<u>J-Node</u>	<u>Dia. (in)</u>	<u>Thicknesses (in.)</u>
3	1	2	14.40	0.239
4	30	31	14.40	"
5	2	3	14.18	"
6	29	30	14.18	"
7	3	4	13.50	"
8	28	29	13.50	"
9	4	5	12.80	"
10	27	28	12.80	"
11	6	7	11.60	0.179
12	7	8	12.54	"
13	8	9	13.48	"
14	9	10	14.40	"
15	10	11	15.32	"
16	11	12	16.26	"
17	12	13	17.20	"
18	13	14	17.66	"
19	14	15	17.66	"
20	15	16	17.66	"
21	16	17	17.66	"
22	17	18	17.66	"
23	18	19	17.66	"
24	19	20	17.20	"
25	20	21	16.26	"
26	21	22	15.32	"
27	22	23	14.40	"
28	23	24	13.48	"
29	24	25	12.54	"
30	25	26	11.60	"

slightly wider than the web and of negligible thickness (1×10^{-20} in.). The connection element for the Tucson structure was 10" x 0.825" in section and 18" long. The connection element for the Phoenix structure was 7.1" x 1.25" and 7.8" long.

In selecting the nodal mesh for each structure, a node was placed at the actual attachment points of each traffic sign for signs wider than 4 feet, and at the center of the sign for signs 4 feet wide or less. In this manner, the mass of the signs would be applied at a node. A node was also placed at the midspan of the beam, to be able to determine deflections and stresses at this important point.

The element lengths were maintained between 4 and 6 feet, and wherever it was possible, the elements were given the same length. This was difficult to accomplish for the Tucson structure, primarily due to the sign locations. The Phoenix structure, however, was more easily modeled with elements of constant length.

4.4 Static Loads on Structure

As explained in Chapter 3, air flowing past an object will create a drag force. However, for wind speeds less than about 23 mph the drag will be negligible, although the drag on the signs may be significant. The 23 mph wind speed is the upper limit for which the vortex shedding is deterministic. Using Eq. (1) and the tables for the coefficient of drag, C_D , published by Rouse (4), the drag force on the signs was computed for the wind speeds considered. These forces are

shown in Tables 3a and 3b for the Tucson and Phoenix structures, respectively. A static analysis was then performed for the various wind speeds, using the drag on the signs and the self weight of the structure. The results of this analysis will be discussed in detail later in this chapter.

The static analysis was performed by applying the drag force as a horizontal load, perpendicular to the axes of the beam and the columns. The loads were applied at the nodes corresponding to the attachment points of the signs. In addition, the weight of the signs was included as a lumped mass applied at these nodes. GIFTS can automatically calculate the mass of each element, and applies these masses in lumped form at the nodes.

4.5 Dynamic Loads on Structure

The equation for the vortex shedding frequency, Eq. (5), is heavily dependent on the diameter of the cylinder. This means that for the tapered cylinders of the monotube structure, the shedding frequency will vary along the length of the member. This condition is difficult, if not impossible to model. Therefore, each structure was divided into three subassemblies, where the columns and the beam each was considered as one. An average diameter was determined for each subassembly, using the diameters of the elements in the subassembly. This average

Table 3a. Drag Forces on Signs of Tucson Structure (lbs.). *

<u>Wind Speed (MPH)</u>	<u>7' x 13' Sign</u>		<u>7' x 10' Sign</u>	
	<u>Node 14</u>	<u>Node 16</u>	<u>Node 19</u>	<u>Node 20</u>
2.5	0.785	0.785	0.605	0.605
5.0	3.145	3.145	2.410	2.410
7.5	7.075	7.075	5.425	5.425
10.0	12.580	12.580	9.640	9.640
12.5	19.655	19.655	15.650	15.650
15.0	28.305	28.305	21.690	21.690
17.5	38.525	38.525	29.525	29.525
20.0	50.32	50.32	38.560	38.560
22.5	63.685	63.685	48.805	48.805
23.2	67.710	67.710	51.885	51.885

*See Fig. 17a for node locations.

Table 3b. Drag Forces on Signs of Phoenix Structure (lbs.).*

<u>Wind Speed (MPH)</u>	<u>All Signs are 4' x 5'</u>			
	<u>Node 15</u>	<u>Node 18</u>	<u>Node 20</u>	<u>Node 22</u>
2.5	0.353	0.353	0.353	0.353
5.0	1.411	1.411	1.411	1.411
7.5	3.175	3.175	3.175	3.175
10.0	5.644	5.644	5.644	5.644
12.5	8.819	8.819	8.819	8.819
15.0	12.699	12.699	12.699	12.699
17.5	17.285	17.285	17.285	17.285
20.0	22.576	22.576	22.576	22.576
22.1	27.566	27.566	27.566	27.566

* See Fig. 17b for node locations.

diameter was then used to compute the vortex shedding frequency and the corresponding forces for each node. The average diameters of each substructure are given in Table 4.

To perform a dynamic analysis of a structure using GIFTS, the loads on the structure at specific points in time must be entered into the GIFTS modules. GIFTS assumes a linear load variation over any individual time interval. For this study, the loads were determined at 0.5 second intervals for a total time of 32 seconds. This gives a sum of 64 load increments. The time of 32 seconds was chosen on the basis of the earlier monotube study (3), which found that this would be a sufficient period to detect any form of excessive deformation (i.e., resonance). However, it should be noted that apart from a wind tunnel, the probability of a structure experiencing a constant wind speed for as long a period as 32 seconds will be extremely small. The wind generally blows in gusts, and while the variation in velocity may not be great, it is sufficient to keep the structure from vibrating at one frequency for any extended period of time. The probability of actual resonance occurring is therefore negligible (2,3).

The loads were given as nodal loads. The magnitudes of these loads were determined using Eq. (4), the average diameter of the subassemblies, and the tributary projected area of each node. The loads were determined as acting normal to the axis of the subassembly and perpendicular to the direction of the wind.

Table 4. Average Diameters of Finite Element Subassemblies (in).

	<u>Tucson</u>	<u>Phoenix</u>
Column 1	11.50	13.81
Column 2	11.59	13.81
Beam	14.40	15.20

Dynamic analyses were performed for each structure for wind speeds ranging from 2.5 mph to 20 mph in steps of 2.5 mph. For the Tucson structure, additional analyses were performed for wind speeds of 22.5 and 23.2 mph. For the Phoenix structure, an additional analysis was performed for a wind speed of 22.1 mph. Above these maximum wind speeds, the vortex shedding forces are of random magnitude, and thus considered beyond the scope of this study. The 2.5 mph interval was chosen as a compromise between accuracy, data entry time, and computer cost.

GIFTS allows the user to choose one of four approaches for dynamic analysis. These are Houbolt's Scheme, Newmark's Beta Method, Wilson's Theta Method, and the Trapezoidal Rule (8). Houbolt's Scheme was chosen for this study, since it is generally more accurate than the Trapezoidal Rule and does not need to use the arbitrary constants of Newmark's and Wilson's Methods. While recommended values for these constants exist, it is not known if they are applicable for monotube structures.

4.6 Natural Frequencies of Vibration

The natural frequencies of a structure are representative of the dynamic response of the structure in the absence of any external loads. They are the frequencies at which the structure will vibrate when no energy is being provided to the structural system and can be determined by an iterative technique such as subspace iteration.

The natural vibration characteristics of a structure are important when the structure is subjected to dynamic forces. The frequencies of the loads and those of the structure may combine in such a manner as to give a response that is a magnification of a natural frequency. In the worst case, the loading frequency equals a natural frequency. This causes the structure to develop ever-increasing deflections and thus constitutes resonances; the consequences of which were discussed in Chapter. 3.

The structure can be modeled as a distributed or lumped mass system. The distributed mass system results in a structure with an infinite number of degrees of freedom. The lumped mass system results in a structure with the number of degrees of freedom given by:

$$\text{NDF} = (\text{NP} \cdot \text{NFP}) - (\text{NFP})_s \quad (6)$$

where NP = the number of nodal points in structure, NFP = the number of degrees of freedom at each node, and $(\text{NFP})_s$ is the total number of suppressed degrees of freedom. The value of NDF therefore takes into account whether the structure has been modeled as a two- (2D) or three-dimensional (3D) system.

GIFTS uses the subspace iteration technique, which is based on the lumped mass approach. In the computation of the natural frequencies, the models that were used for the static and dynamic analyses also were utilized. The structural damping has been conservatively assumed to be zero.

Tables 5a and 5b give the natural frequencies for the first 10 modes for both structures. These include 2D as well as 3D data. The 2D data represents displacements in the x- and y-directions, since the displacements in the out-of-plane direction (z-direction) have been suppressed.

From Table 5a, it can be seen for the Tucson (60 foot) structure, the following 2D and 3D modes have the same frequencies:

$$f_1 (2D) = f_2 (3D)$$

$$f_2 (2D) = f_3 (3D)$$

$$f_3 (2D) = f_6 (3D)$$

$$f_4 (2D) = f_8 (3D)$$

$$f_5 (2D) = f_{10} (3D)$$

Similarly, for the Phoenix (100 foot) structure, Table 5b gives

$$f_1 (2D) = f_1 (3D)$$

$$f_2 (2D) = f_3 (3D)$$

$$f_3 (2D) = f_5 (3D)$$

$$f_4 (2D) = f_8 (3D)$$

$$f_5 (2D) = f_{10} (3D)$$

Since the 2D modes are all in-plane, this indicates that the above mentioned 3D modes are dominated by in-plane behavior.

Figures 18 and 19 show the first two 3D mode shapes for the Tucson structure. Figures 20 and 21 show the first two 3D mode shapes for the Phoenix structure. It should be understood that the deflected

Table 5a. Natural Frequencies of Tucson Structure (CPS).

<u>Mode</u>	<u>2-D</u>	<u>3-D</u>
1	2.834	2.295
2	3.265	2.834
3	12.290	3.265
4	27.301	4.293
5	31.760	7.925
6	34.714	12.290
7	47.312	16.646
8	74.169	27.301
9	92.693	29.307
10	102.730	31.934

Table 5b. Natural Frequencies of Phoenix Structure (CPS).

<u>Mode</u>	<u>2-D</u>	<u>3-D</u>
1	1.467	1.467
2	3.055	1.479
3	5.001	3.055
4	10.872	3.868
5	19.263	5.001
6	29.481	6.193
7	36.518	9.118
8	37.522	10.872
9	42.252	13.874
10	56.589	19.263

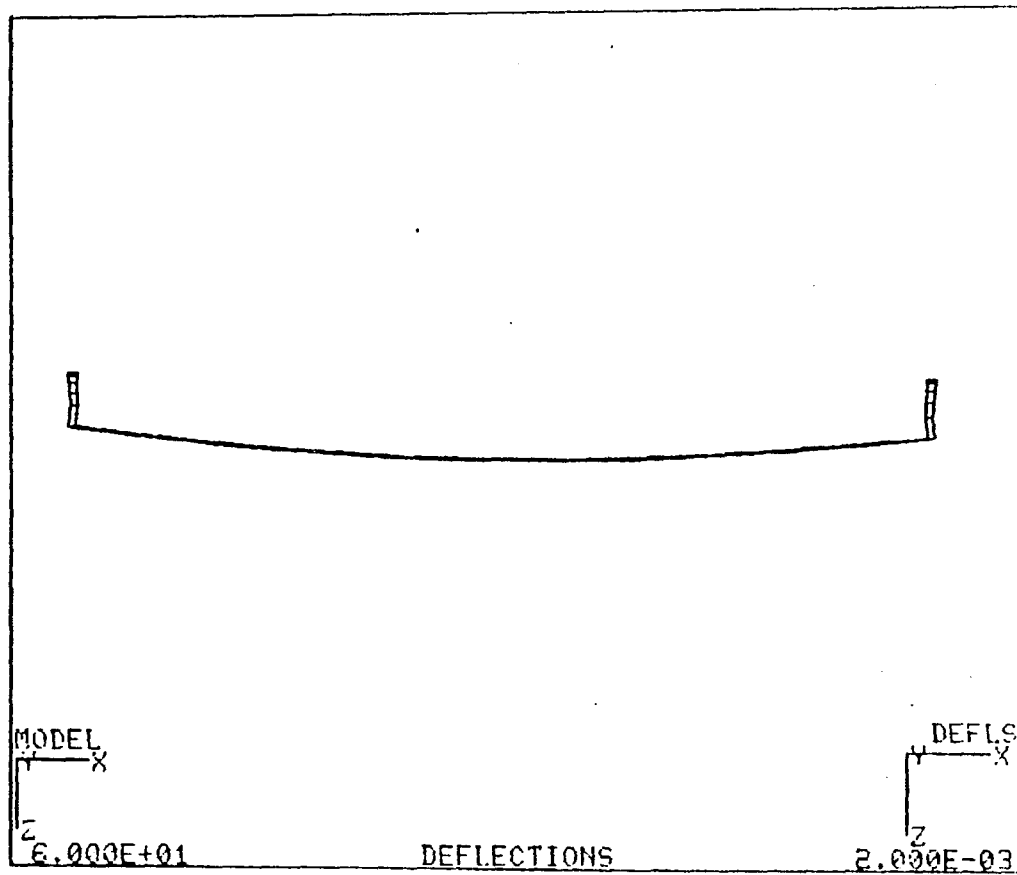


Figure 18 First Natural 3D Mode for Tucson Monotube Structure

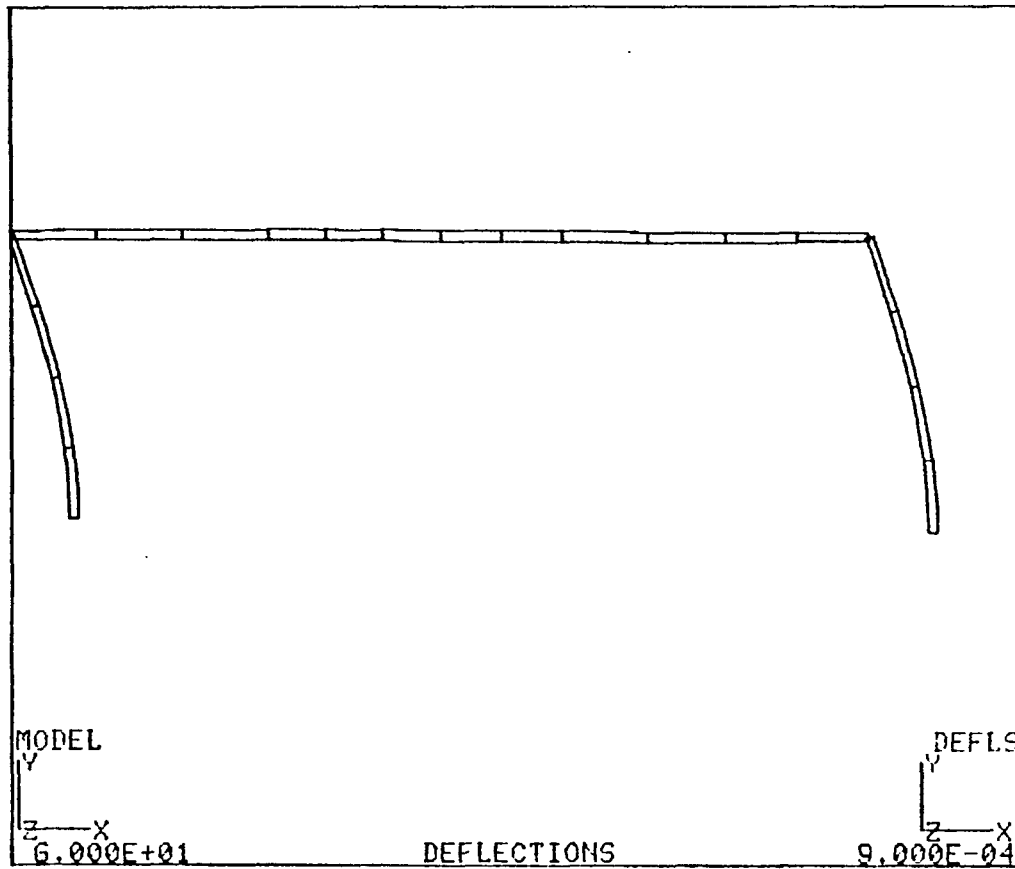


Figure 19 Second Natural 3D Mode for Tucson Monotube Structure

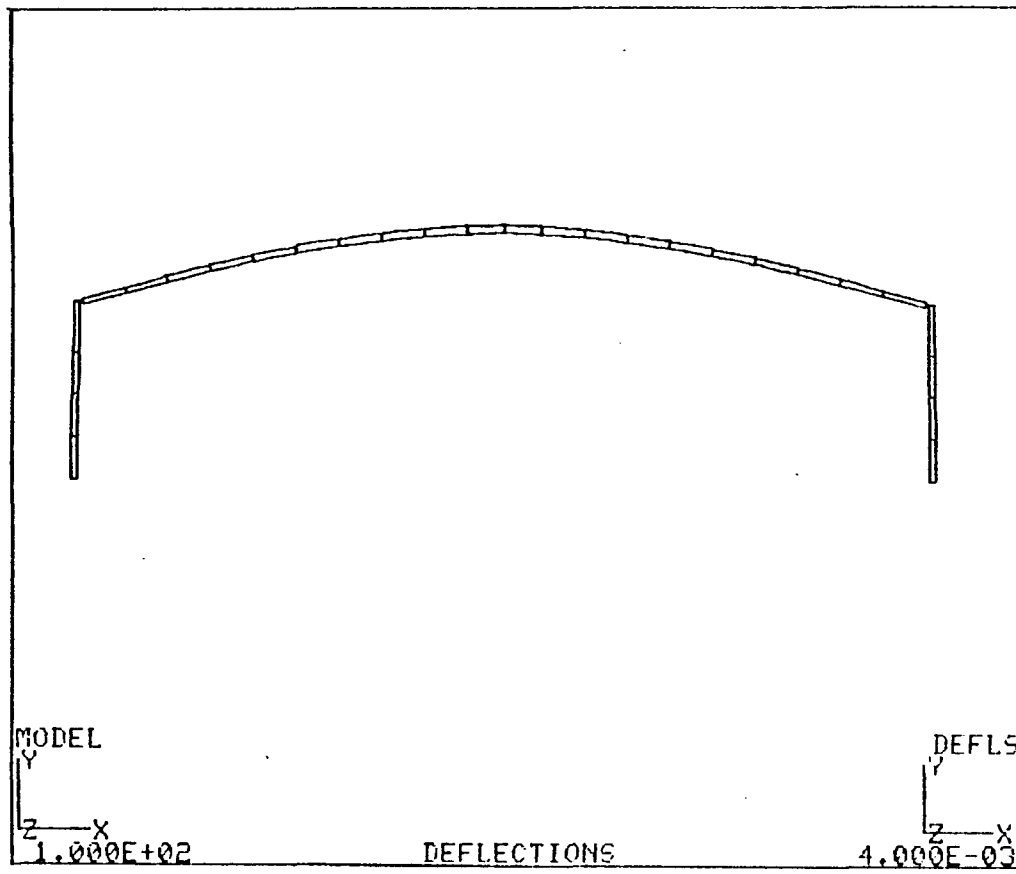


Figure 20 First Natural 3D Mode for Phoenix Monotube Structure

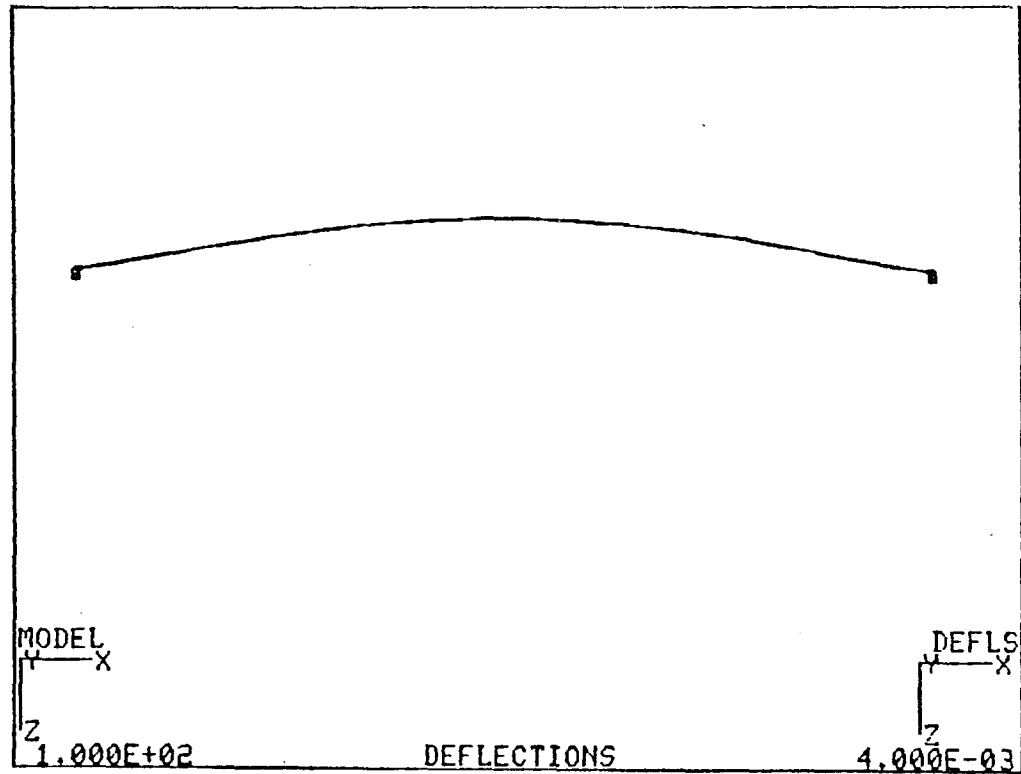


Figure 21 Second Natural 3D Mode for Phoenix Monotube Structure

shapes shown do not indicate actual displacements, since the natural frequencies are not associated with any load. However, they do give an indication of the shapes that can be expected for a vibrating structure.

4.7 Static Load Results

Both models were analyzed for a combination of static loads. These loads included the weight of the structural elements, the weight of the signs, and the drag on the signs. The drag forces for various wind speeds are shown in Table 3a for the Tucson (60 ft) structure and in Table 3b for the Phoenix (100 ft) structure. These forces were applied at the attachment points of the signs.

For the wind speeds considered, the gravity loads due to the weight of the structure govern in all cases. The deflected shape of the structures can be seen in Fig. 22a and 22b. The vertical deflections at the midspan of the beam are given in Tables 6a and 6b. It can be seen that they are identical in every case. The out-of-plane deflections did vary with the wind speed as shown in Tables 6a and 6b. However, the out-of-plane deflections are considerably smaller than the in-plane deflections. This is especially noteworthy in the case of the Tucson structure which has two relatively large signs. Even with these large signs, drag was not a major factor.

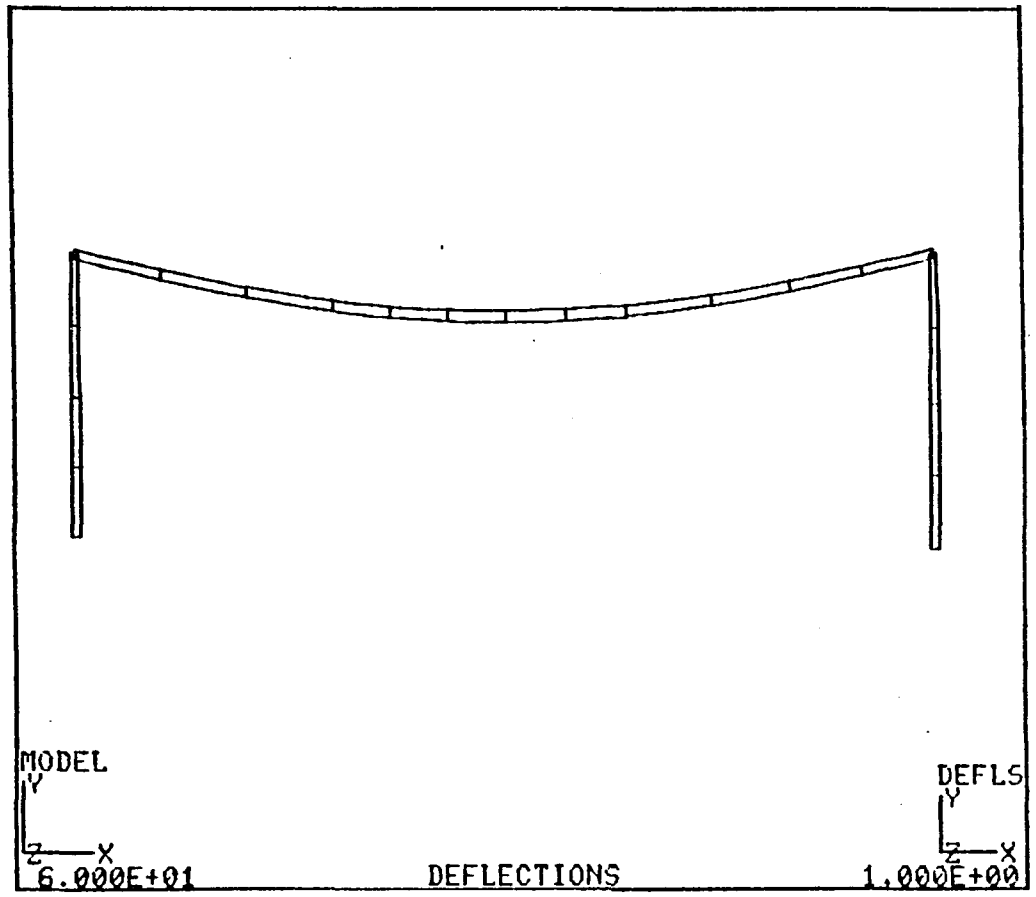


Figure 22a Deflected Shape for Tucson Monotube Structure Subjected to Static Loads

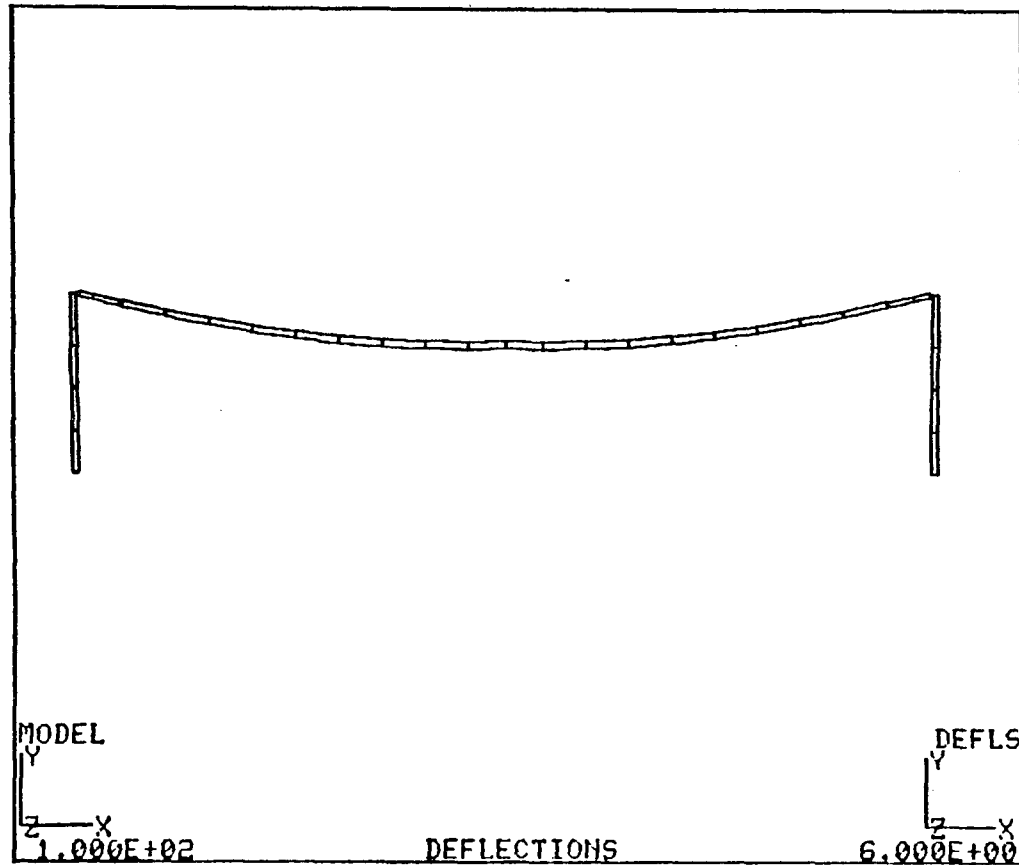


Figure 22b Deflected Shape for Phoenix Monotube Structure
Subjected to Static Loads

Table 6a. Midspan Static Deflections for Tucson Structure (in.).

<u>Wind Speed</u>	Direction*		
	<u>x</u>	<u>y</u>	<u>z</u>
2.5	0.002	1.123	0.008
5.0	0.001	1.123	0.019
7.5	0.001	1.123	0.038
10.0	0.001	1.123	0.065
12.5	0.001	1.123	0.099
15.0	0.001	1.123	0.141
17.5	0.001	1.123	0.190
20.0	0.000	1.123	0.247
22.5	0.000	1.123	0.312
23.2	0.000	1.123	0.331

*For labeling of x-, y- and z-axes, see Fig. 17a.

Table 6b. Midspan Static Deflections for Phoenix Structure (in.).

<u>Wind Speed</u>	<u>x</u>	<u>Direction*</u>	
		<u>y</u>	<u>z</u>
2.5	0.000	5.513	0.003
5.0	0.000	5.513	0.013
7.5	0.000	5.513	0.030
10.0	0.000	5.513	0.053
12.5	0.000	5.513	0.083
15.0	0.000	5.513	0.120
17.5	0.000	5.513	0.163
20.0	0.000	5.513	0.213
22.1	0.000	5.513	0.260

*For labeling of x-, y- and z-axes, see Fig. 17a.

The stresses at midspan are also principally due to weight of the structure. The stress distributions for shear stress and normal stress at midspan of the Tucson structure are shown in Fig. 23a. Figure 23b shows a similar plot for the Phoenix structure. The magnitudes of the stresses did not vary with the wind speed, but remained constant at the indicated values. For the Tucson structure, the maximum normal stress was ± 4.38 ksi, which is about 13% of the yield stress of 34 ksi. The magnitude of the normal stress for the Phoenix structure was 8.86 ksi, which is about 26% of the yield stress.

The stresses at the column base for the Tucson structure became larger as the wind speed increased. The stress for the Phoenix structure, however, remained close to constant. This is probably due to the larger sign area for the Tucson structure, which results in higher drag forces. The drag on the Phoenix signs appears to be negligible. The maximum normal stress at the column base for the Tucson structure is ± 1.34 ksi, and for the Phoenix structure ± 2.51 ksi. Both are well below the yield stress of the steel. The stress distributions at the column base are shown in Figs. 24a and 24b for the Tucson and Phoenix structures, respectively.

At the connection between the column and the beam, shear stress is the governing factor. For both structures, the finite element model showed some normal stress, but this is largely due to the way the joint was modeled rather than any actual stress. The shear

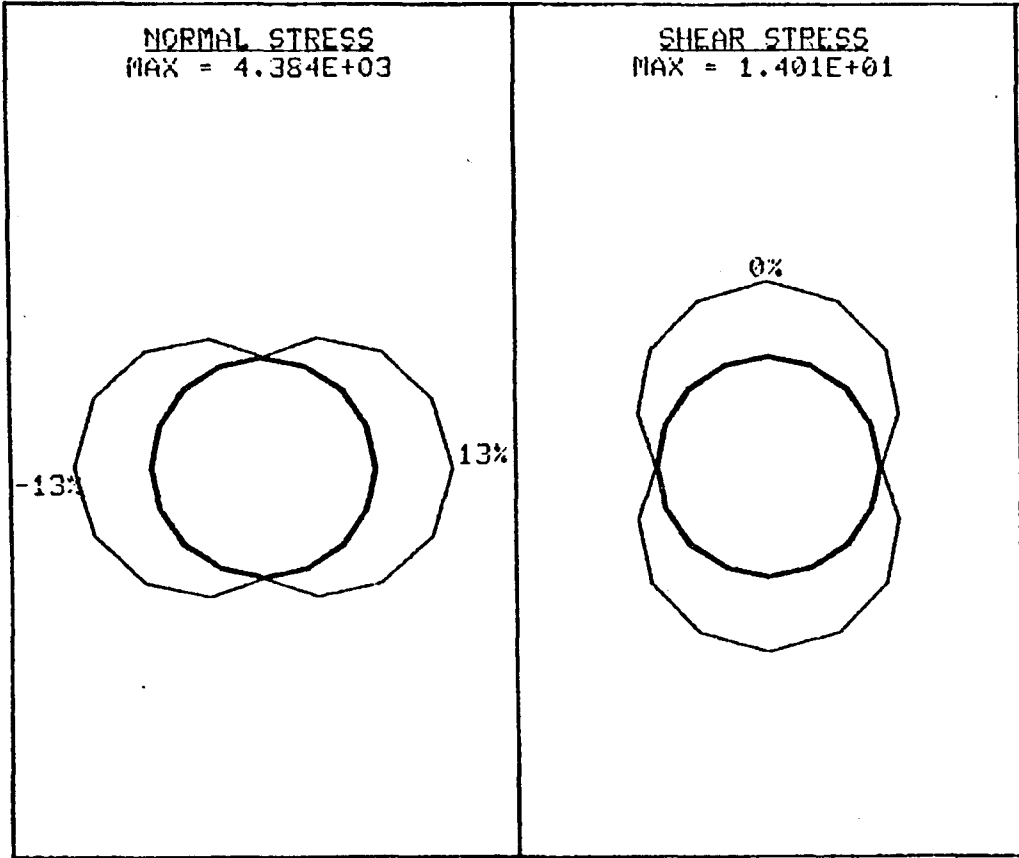


Figure 23a Static Stresses at Midspan of Tucson Monotube Structure

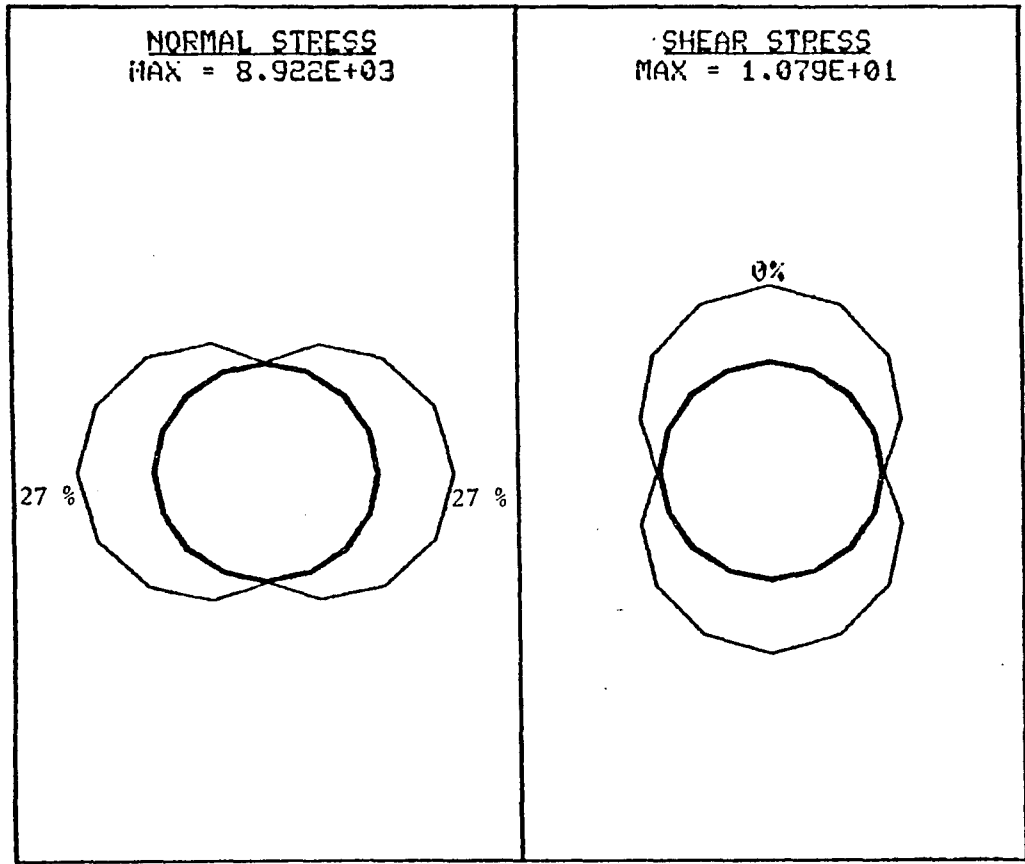


Figure 23b Static Stresses at Midspan of Phoenix Monotube Structure

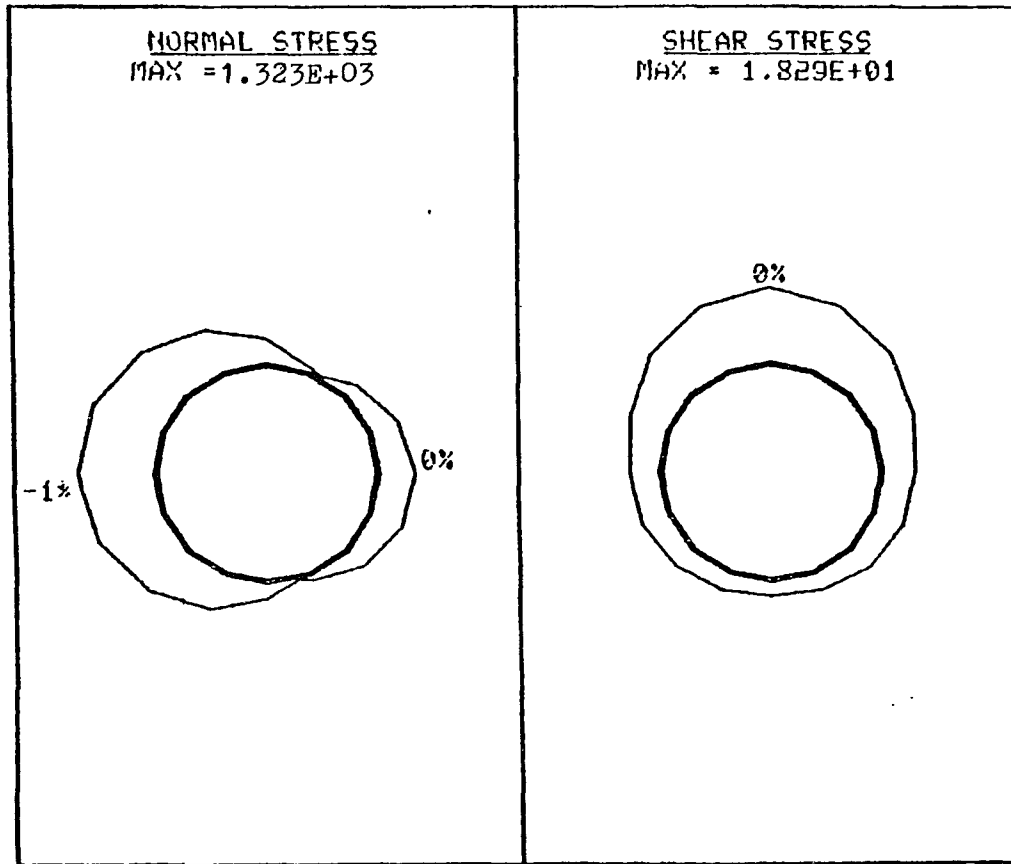


Figure 24a Static Stresses at Column Base of Tucson Monotube Structure

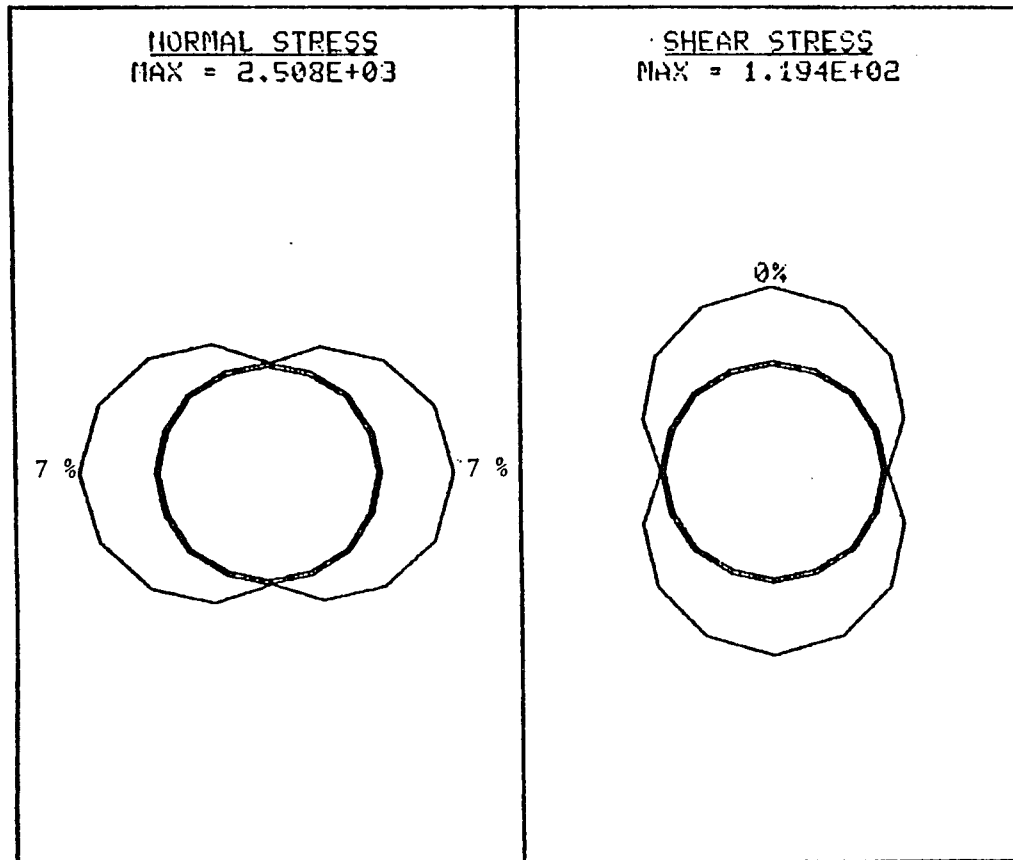


Figure 24b Static Stresses at Column Base of Phoenix Monotube Structure

stress at the joint was close to constant for both structures. The gravity loads appear to govern. For the Tucson structure the maximum shear stress is 2.64 ksi. For the Phoenix structure it is 3.22 ksi. Both are well below the shear yield stress of the steel, which is 19.4 ksi. The shear stress distributions are shown in Figs. 25a and 25b for the Tucson and Phoenix structures.

As has been seen, the stresses at the three critical locations on each structure are significantly below the representative yield values of the steel. However, neither structure was able to meet the $d^2/400$ deflection criterion. For the Tucson structure, which has a sign depth of 7 ft., the maximum allowable deflection according to Specifications is:

$$\frac{d^2}{400} = \frac{7^2}{400} = 0.123 \text{ ft.} = 1.48''$$

For the Phoenix structure with the 5 ft. deep sign, the allowable deflection is:

$$\frac{d^2}{400} = \frac{5^2}{400} = 0.063 \text{ ft.} = 0.76''$$

The actual deflection is 5.513 in. However, the stresses are very low for both cases. The above, therefore, illustrates why the $d^2/400$ deflection criterion is unrealistic for monotube structures.

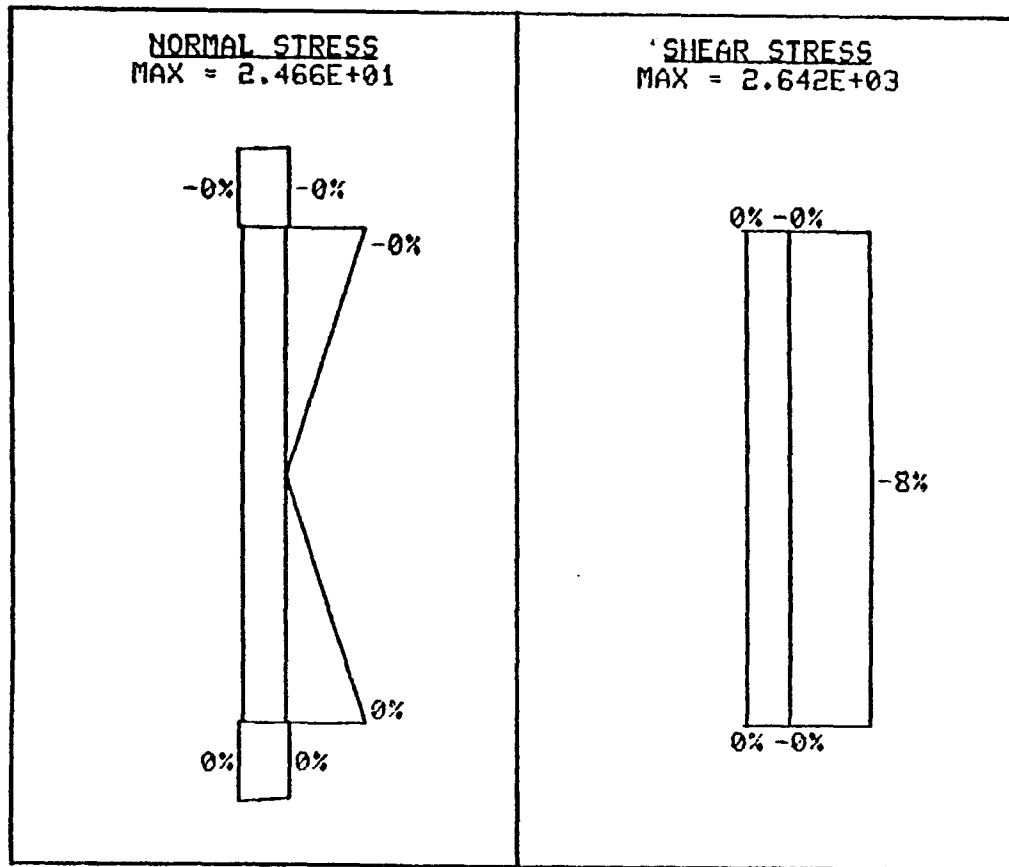


Figure 25a Static Stresses at Joint of Tucson Monotube Structure

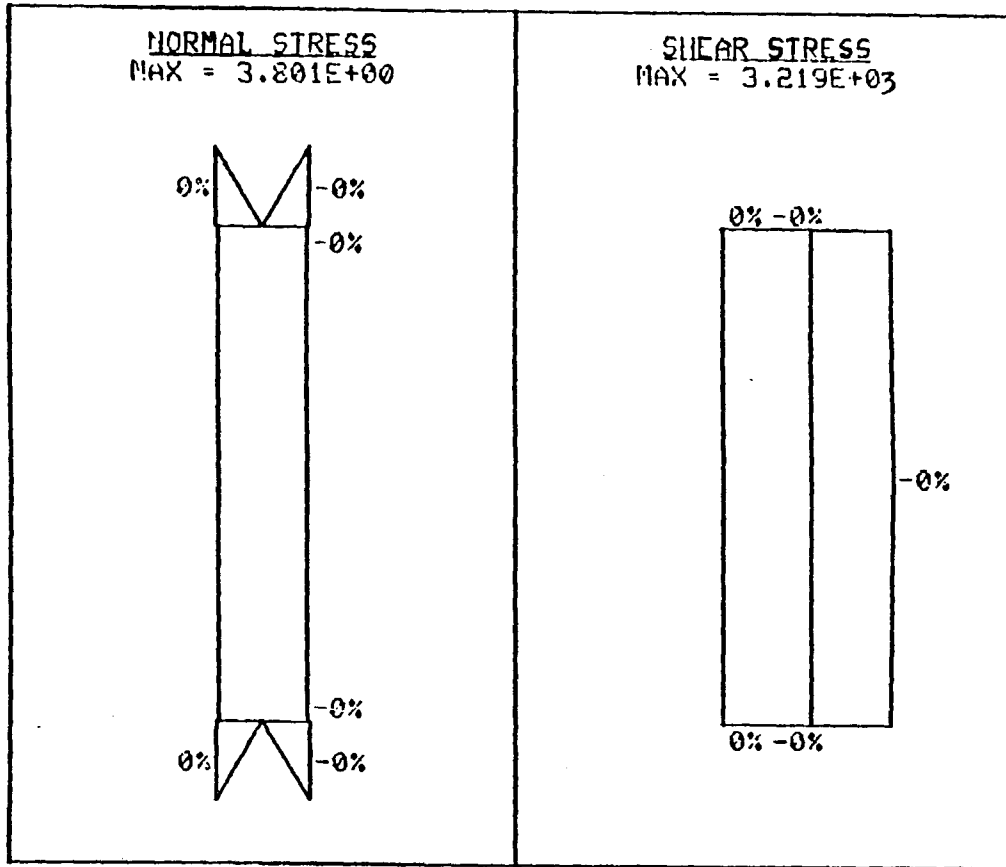


Figure 25b Static Stresses at Joint of Phoenix Monotube Structure

4.8 Dynamic Load Results

The same models used for the static load tests were used for the dynamic load tests. The loads for these tests were determined using Eq. (4). The loads were calculated for the same wind speeds as those used in the static analysis.

Initially, the loading included only those loads calculated from Eq. (4) and the drag forces on the signs. The transient analysis was conducted over a time period of 32 seconds, with the loads from the forcing function input at 0.5 second intervals. The weight of the structure was not included in these analyses.

In order to determine the critical stress levels for each wind speed, a histogram for various points was constructed, using the GIFTS modules. Points considered included the midspan of the beam for in-plane deflections, and the top of the left column for out-of-plane deflections. A typical histogram is shown in Fig. 26.

From the histogram, the times of the maximum deflections were determined, and the corresponding stresses are shown in Tables 7a and 7b. From Table 7a, it is apparent that the column base is the most critical point for the Tucson structure. However, Table 7b indicates that the critical point on the Phoenix structure is at the midspan of the beam. This shift in the critical location is probably due to the larger relative stiffness of the beam in the Tucson structure. The average moment of inertia, I_{ave} for the beam of the Tucson structure is

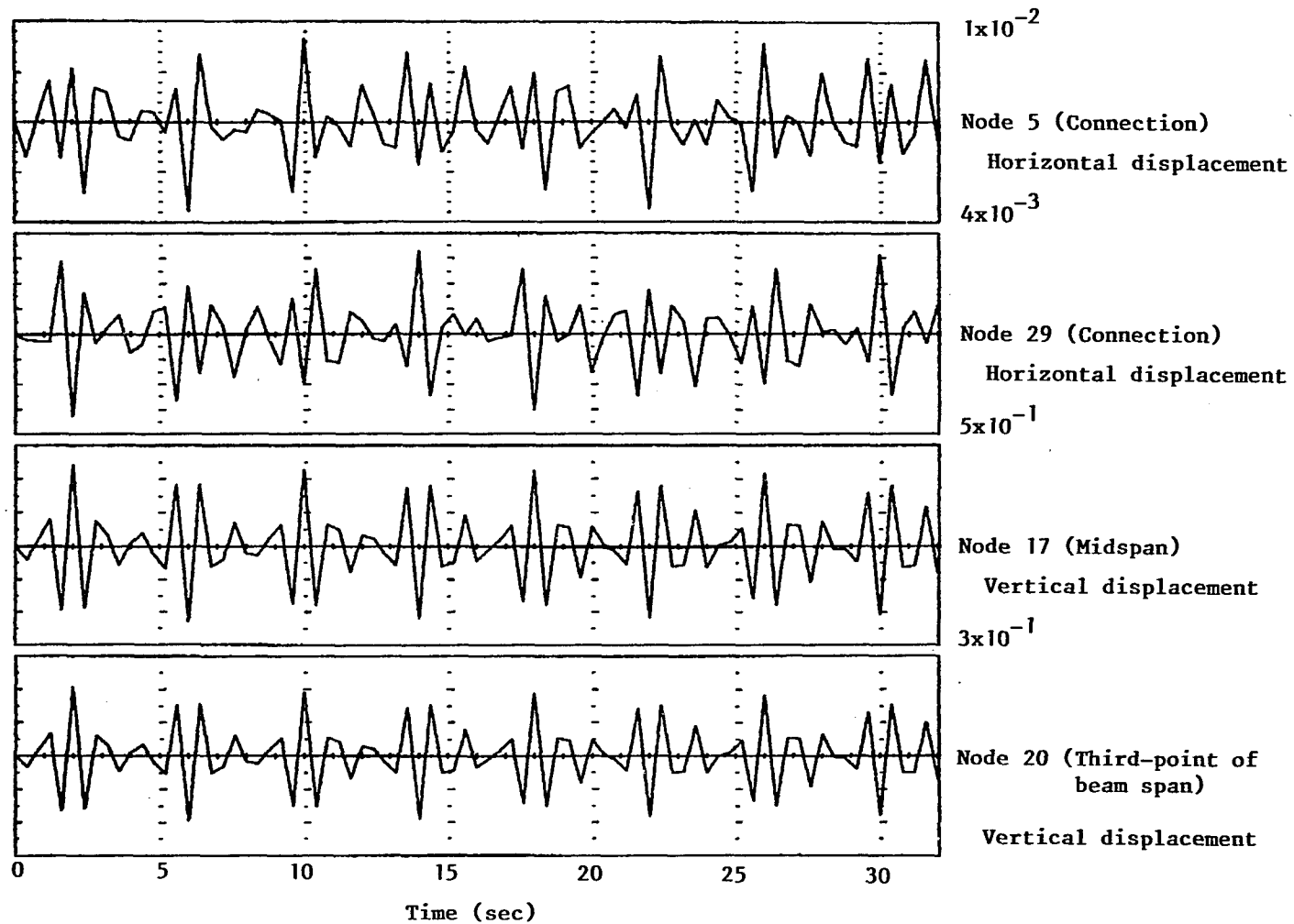


Figure 26 Typical Histogram for Dynamic Analysis of Monotube Structures

Table 7a. Stresses at Critical Points for Dynamic
Analysis of Tucson Structure (ksi).

<u>Wind Speed</u>	<u>Shear at Node 5</u>	<u>Normal at Node 1</u>	<u>Normal at Node 17</u>
2.5	0.005	0.019	0.012
5.0	0.028	0.036	0.048
7.5	0.026	0.078	0.540
10.0	0.038	0.148	0.095
12.5	0.025	0.174	0.101
15.0	0.042	0.265	0.157
17.5	0.053	0.357	0.210
20.0	0.072	0.474	0.276
22.5	0.026	0.595	0.329
23.2	0.128	1.301	0.727

Table 7b. Stresses at Critical Points for Dynamic Analysis of Phoenix Structure (ksi).

<u>Wind Speed</u>	<u>Shear at Node 5</u>	<u>Normal at Node 1</u>	<u>Normal at Node 16</u>
2.5	0.005	0.009	0.017
5.0	0.017	0.020	0.038
7.5	0.025	0.029	0.071
10.0	0.051	0.068	0.125
12.5	0.163	0.196	0.314
15.0	0.186	0.252	0.483
17.5	0.159	0.206	0.330
20.0	0.246	0.270	0.525
22.1	0.252	0.330	0.674

206.6 in⁴, while for the Phoenix structure it is 261.5 in⁴. If the stiffness is defined as I_{ave}/L , then the stiffness of the Tucson sign is $206.6/(60*12) = 0.29$. The corresponding values for the Phoenix structure's beam is $261.5/(100*12) = 0.22$. For a simply supported beam, a larger stiffness will result in a lower stress level for a given load, thus the stresses at the midspan of the Tucson structure are relatively less critical than for the Phoenix structure.

Another factor may be the size of the signs. The signs on the Tucson structure are significantly larger than on the Phoenix structure. The moment induced at the base by the drag on the signs will be much larger than the moment induced at midspan. This will cause a greater stress at the column base.

An interesting development occurs between the wind speeds of 22.5 mph and 23.2 mph for the Tucson structure. The stresses more than double for the small increase in wind speed. This does not occur at any other wind speed. The deflections also show a disproportionate increase in their magnitude. This increase is probably due to the frequency of the beam approaching one of its natural frequency. Prior studies (2,3) have indicated that a natural frequency may lie somewhere near 23 mph for a structure of this diameter (14").

Because the beam is simply supported, it can be considered to act by itself. For the wind speed of 23.2 mph, the beam vibrates at a frequency of 5.94 cps. The second 3D natural frequency of the beam is

6.44 cps. The deflections and stresses increase as the structural frequency approaches a natural frequency.

Another interesting phenomenon occurs for both the Tucson and Phoenix structures. For various wind speeds, the histogram for the node at the midspan of the beam shows a periodic vertical deflection. This is shown in Fig. 27. The frequency of these oscillations is very low (between 0.082 to 0.165 cps). These are well below any of the natural frequencies, nor do they cause excessive stresses or deflections, as would be expected of a natural frequency. These oscillations appear to have been caused by the 0.5 sec. time step chosen in the transient analysis. However, if these oscillations are real, additional studies are needed to determine their effect on the fatigue strength of the structure. The wind speeds for which these periodic oscillations occur are shown in Table 8.

The results discussed so far are somewhat misleading. For the dynamic analysis, the mass of the structure was not considered. However, the mass of the structure will increase the inertia of the vibrating structure. This may increase the deflections and stresses experienced by the structure. Therefore, additional computer analyses were run to include the mass of the structure.

The maximum stresses for each wind speed are given in Tables 9a and 9b for the three critical points on each structure. It is interesting to note that for both structures the magnitudes of the

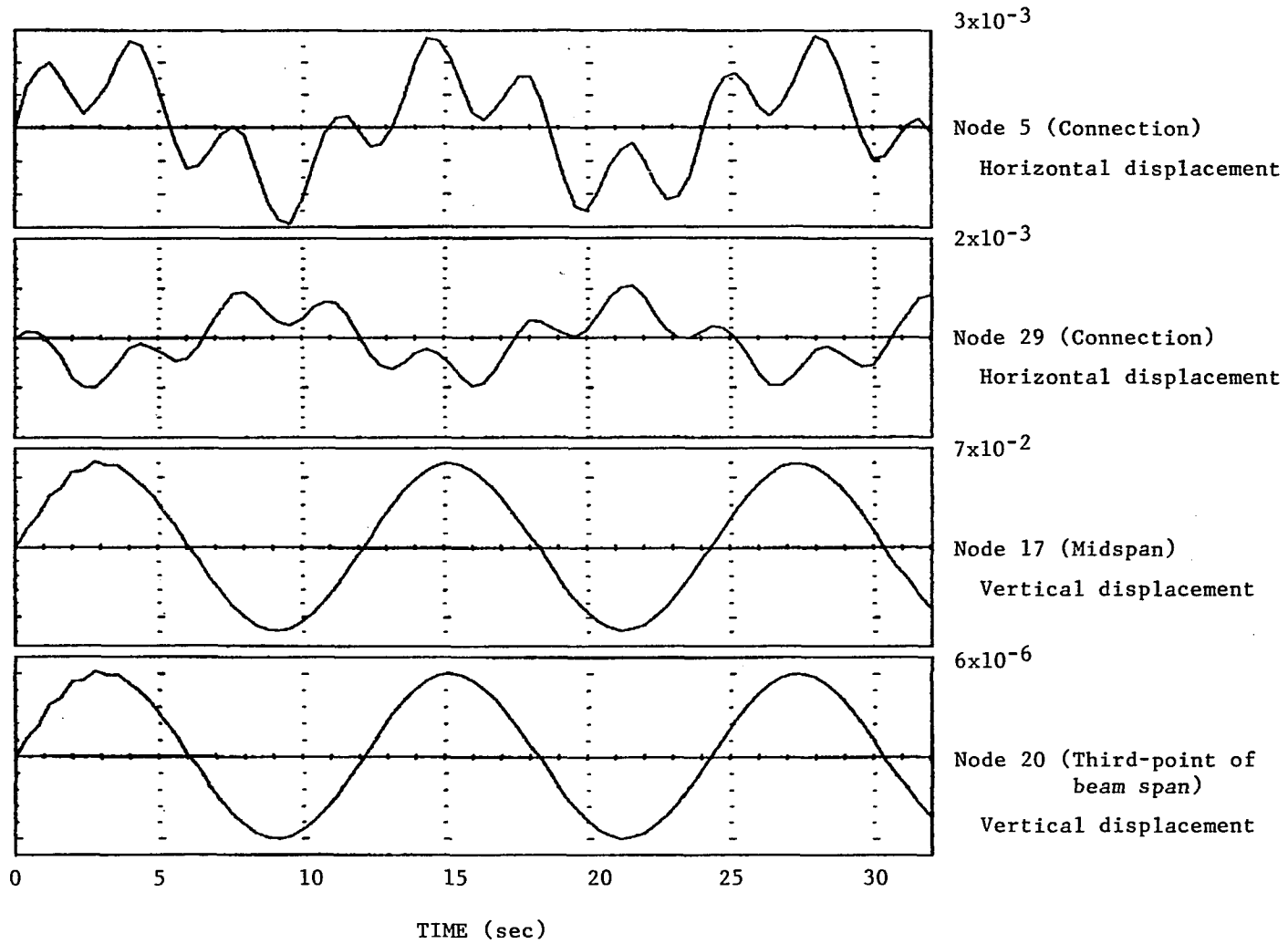


Figure 27 Periodic Histogram for Dynamic Analysis of Monotube Structures

Table 8. Wind Speeds (mph) for which Periodic Oscillation Occur in the Beam.

<u>Tucson (60')</u>	<u>Phoenix (100')</u>
10.0	7.5
17.5	10.0
20.0	17.5
	20.0

Table 9a. Stresses (ksi) for Tucson Structure for Dynamic Loading with Structure Mass.

<u>Wind Speed</u>	<u>Shear at Beam End</u>	<u>Normal at Column Base</u>	<u>Normal at Beam Midspan</u>
2.5	2.64	1.34	4.38
5.0	2.64	1.34	4.38
7.5	2.64	1.35	4.39
10.0	2.65	1.48	4.39
12.5	2.66	1.65	4.49
15.0	2.70	1.61	4.54
17.5	2.78	1.70	4.59
20.0	2.82	1.81	4.66
22.5	2.87	1.93	4.71
23.2	3.12	2.64	5.11

Table 9b. Stresses (ksi) for Phoenix Structure for Dynamic Loading with Structure Mass.

<u>Wind Speed</u>	<u>Shear at Beam End</u>	<u>Normal at Column Base</u>	<u>Normal at Beam Midspan</u>
2.5	0.04	2.84	10.11
5.0	0.05	2.87	10.18
7.5	0.07	2.91	10.23
10.0	0.09	2.95	10.29
12.5	0.22	3.11	10.51
15.0	0.22	3.16	10.70
17.5	0.25	3.12	10.53
20.0	0.32	3.19	10.75
22.1	0.32	3.25	10.92

maximum stresses equal the superimposed stresses from the static analysis and the first dynamic analysis. This can render the dynamic analysis simpler by removing the structural mass from the calculations. A simple static analysis will take care of that.

The deflections can also be superimposed. The deflections caused by the self weight (= dead load) dominate. The maximum deflections for the various wind speeds are given in Tables 10a and 10b.

4.9 Conclusions for Analytical Studies

From this, it can be seen that the monotube structures as modeled are safe for the wind speeds considered. The maximum stresses were less than 40% of the yield stress in all cases. The possibility of fatigue failure warrants further study, especially where the periodic oscillations occur. Neither of the structures modeled meets the $d^2/400$ deflection limitation. Since the stress levels were low, even for the large deflections computed, this indicates that the $d^2/400$ limitation may be unnecessarily restrictive when applied to monotube structures.

As stated previously, these parametric studies are only as accurate as the data used to model the structures and forces. The results presented in this chapter must be compared with the results of the full-scale field testing discussed in Chapter 5.

Table 10a. Deflections at Midspan for Tucson Structure
with Structure Mass.

<u>Wind Speed</u>	<u>Deflection (in.)</u>
2.5	1.12
5.0	1.13
7.5	1.13
10.0	1.14
12.5	1.13
15.0	1.14
17.5	1.14
20.0	1.15
22.5	1.16
23.2	1.18

Table 10b. Deflections at Midspan for Phoenix Structure
with Structure Mass.

<u>Wind Speed</u>	<u>Deflection (in.)</u>
2.5	5.52
5.0	5.53
7.5	5.55
10.0	5.55
12.5	5.63
15.0	5.75
17.5	5.65
20.0	5.74
22.1	5.86

Chapter 5

FIELD TESTING OF FULL-SCALE STRUCTURES

The second phase of the research study consisted of the testing of actual sign support structures under service conditions. This was accomplished by instrumenting two structures with electrical resistance strain gages, as well as an anemometer to determine wind velocity and direction. The data were used to determine the stresses and strains at a number of important locations in the structures, and subsequently to evaluate the correlation between theoretical and actual structural performance.

5.1 Description of Equipment and Software

The equipment used for the field testing can be categorized into two main groups: The first was the portable equipment used for the data collection, and included all sensors, electrical hardware and software used in obtaining data directly from the structures. The second group consisted of the equipment that was used for data reduction. This included all the electrical hardware and software that was utilized to manipulate and analyze the collected data. The data collection group can be further subdivided into six sections; namely, sensors, data acquisition, control, mass storage, communications, and support.

The sensors are the strain gages and the anemometer. The gages were of the bonded electrical resistance foil type, with a resistance of $120 \pm 0.3 \Omega$, a gage length of 10 mm, and a gage factor of 2.12. A typical gage is shown in Fig. 28. The anemometer was a Weathertronics Combination Wind Sensor, Model 2132, consisting of 3 standard anemometer cups connected to an AC generator, and a weather vane connected to a DC potentiometer. This unit can be seen in Fig. 29.

The data acquisition equipment was of crucial importance to the success of the field work. To read the strain gages as well as the anemometer, a Hewlett Packard (HP) Data Acquisition and Control Unit, Model 3421A, was used. This can measure AC and DC voltages, resistances, and amperages, and can also be used to control other devices. It also has a built-in power output that may be utilized to run peripheral devices. The unit can accept input from twenty different sources or channels. For the field measurements of this project, 16 channels were used by the strain gages, 1 by the wind speed sensor, and 1 by the wind direction sensor, for a total of 18.

The control unit of the data collection group was an HP-41CX calculator. This is a user programmable calculator whose software had been designed to control the data collection activities and a number of arithmetic functions. The calculator has a built-in clock and calendar, making it possible to record the data and time of each

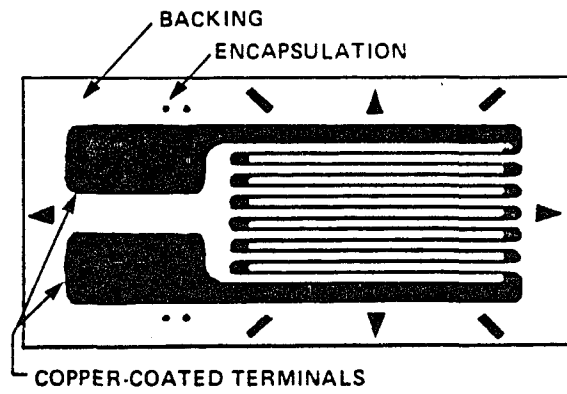


Figure 28. Typical Strain Gage

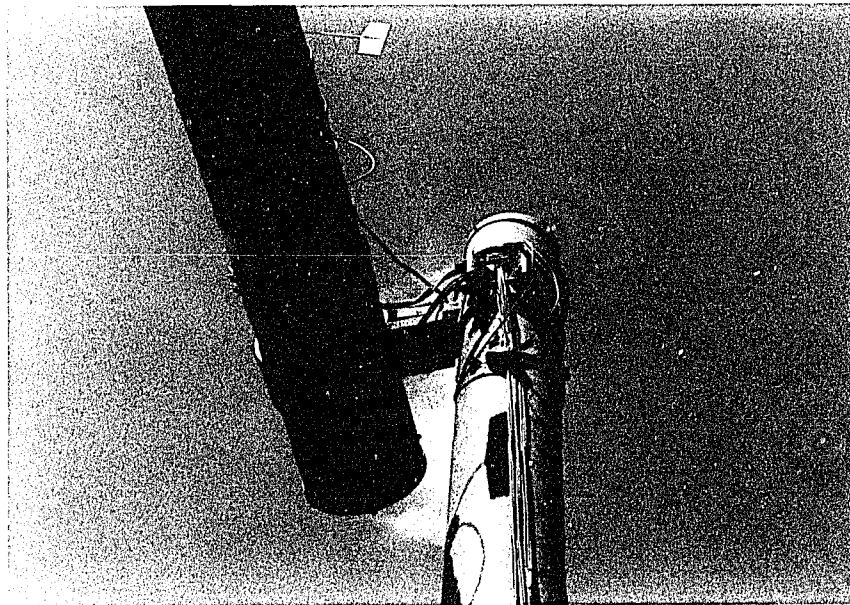


Figure 29. Anemometer Mounted on Structure

reading of the gages. The data were initially stored in the calculator's memory and subsequently transferred to the mass storage unit.

The software used by the HP-41CX was originally written by Geotechnical Engineering and Mining Services, Inc. of Littleton, Colorado. However, it was found necessary to modify portions of the code to better perform the required tasks. A complete listing of this software is given in Appendix A.

After the strain gages were read, the readings were stored in the calculator's memory. When this memory was full, the readings were transferred to the mass storage unit, an HP Model 82161A cassette drive. This tape drive uses micro-cassettes to record the data, and each cassette can store about 128 Kb of data, or slightly over 16,000 numbers.

The HP-3421A, -41CX, and tape drive were arranged to communicate by means of a HP Interface Loop (HP-IL). This is a serial loop that is controlled by the HP-IL module which is connected to the HP-41CX. Through this loop, directions and data are sent from one device to another. As this is a serial loop, any device that is shut off or disconnected will interrupt data flow in the loop.

The support equipment consisted of a multi-channel DC power supply, a Wheatstone Bridge circuit board, a 5 HP, 2000 Watt portable generator, and a radial blower. The power supply was used to provide a

voltage to the gages and the wind direction potentiometer. The Wheatstone Bridge circuits were connected to the strain gages to form quarter bridges. This will be discussed in detail later in this chapter. The portable generator was needed to provide power at the remote testing sites, and the blower was necessary to keep the power supply from overheating. Figure 30 shows the 3421A, 41CX, tape drive, power supply, Wheatstone Bridge board, and blower.

The data reduction equipment group comprised of the following items: an HP Model 9836 (Series 200) desk top computer, an HP Model 82169A HP-IL/HP-IB interface, an HP 82905B dot-matrix printer, and an HP Model 7470A two-pen plotter.

The HP- 9836 computer was equipped with two 270 Kb double-sided disk drives, and 640 Kb of random access memory. It communicated with peripheral devices through the Hewlett-Packard Interface Bus (HP-IB). The computer was used for all the computational work of the project, with the exception of running the GIFTS program.

The dot-matrix printer and the plotter are HP-IB peripheral devices and were used to obtain hard copy output of the information generated by the HP-9836.

The HP-IL/HP-IB interface allows an HP-IL device to communicate with an HP-IB device. It can be operated with a controller on the HP-IL side, the HP-IB side, or in "mailbox" mode, where controllers exist on both sides. The latter approach was chosen for

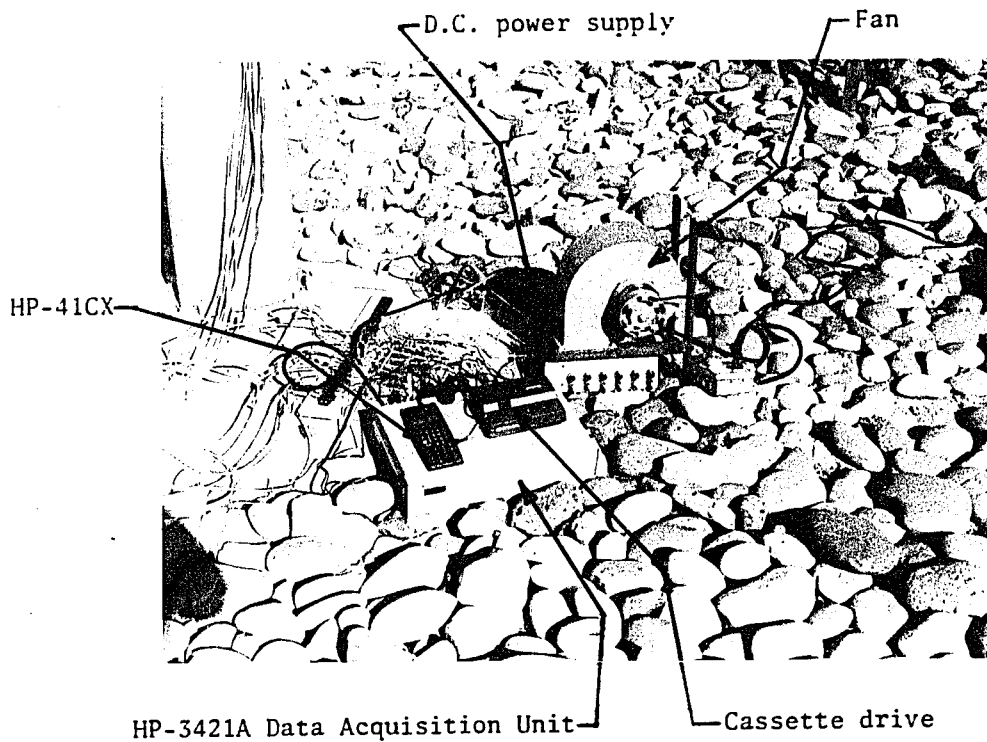


Figure 30 Data Acquisition Equipment

this project. Thus, the interface was used to allow data that were stored on the micro-cassette to be transferred to the HP-9836 for storage on 5-1/4" floppy disks. The controller consisted of the HP-41CX calculator on the HP-IL side and the HP 9836 on the HP-IB side. The data transfer required that programs be run simultaneously on the HP-41CX and the HP-9836. These are listed in Appendix B.

5.2 Procedure for Gage Installation

A total of 16 gages were attached to each structure. They were mounted in groups of four at the following locations: midspan of the beam, end of the beam, top of the column, and base of the column. The gages were arranged around the perimeter of the tube at 90° intervals such that one pair of gages measured in-plane strains and the other pair measured out-of-plane strains. The locations of the gages are indicated in Fig. 31.

The gages were installed in accordance with normal procedures (10), with the exception that Elmer's "Dura-Bond" contact cement was used instead of the suggested adhesive. This was done to facilitate gage installation in the field. Otherwise, the installation followed common procedures for cleaning of the steel, aligning and bonding of the gages, and so on.

Once the gages were installed, cables were soldered to the gage leads to connect them to the data acquisition unit. On the Tucson structure, a quarter bridge using two wires, as shown in Fig. 32a, was

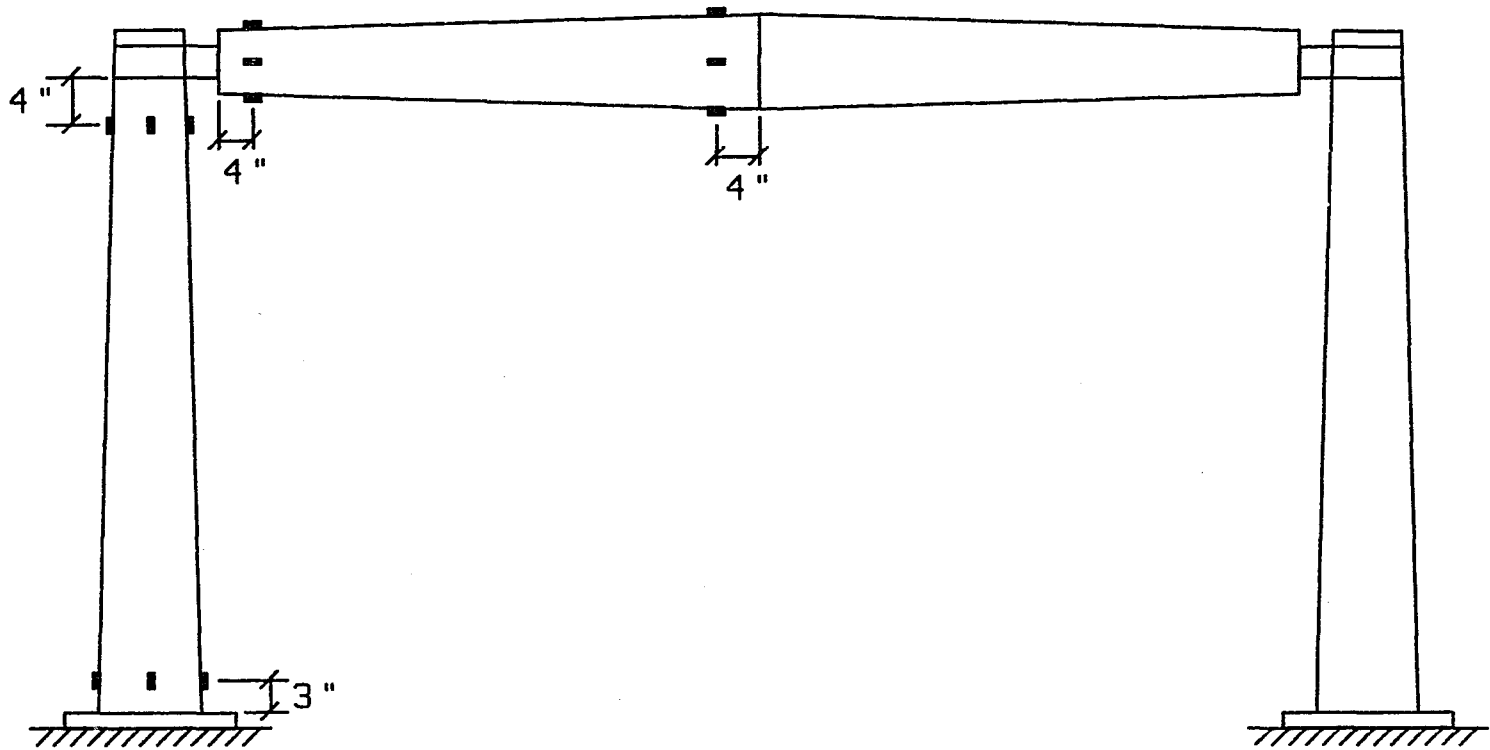


Figure 31. Locations of Strain Gages on Monotube Structures

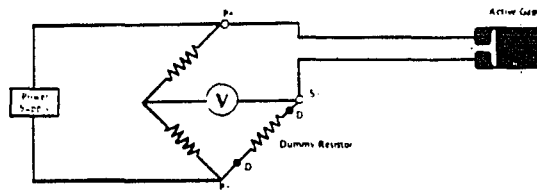


Figure 32a. Two-wire Quarter Bridge circuit

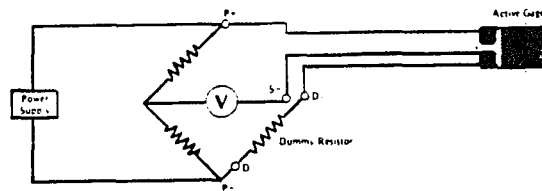


Figure 32b. Three-wire Quarter Bridge circuit

utilized. On the Phoenix structure, a quarter bridge was again used, but this time with a three-wire circuit, as shown in Fig. 32b. The three-wire arrangement helps eliminate the effect of lead wire resistance on the gage readings. After the cables had been attached, the gages were further protected by applying a covering of paraffin wax. Figure 33a shows a gage with the cables attached, and Fig. 33b shows the same gage after the wax has been applied.

5.3 Theory of Strain Gage Operation

The operational function of an electrical strain gage is based on Ohm's Law (15), which states that

$$V = IR \quad (6)$$

where V is voltage, I is current in amperes, and R is the resistance in ohms. For a constant I , a change in the resistance will cause a proportional change in the voltage. The electrical strain gage functions as a resistor, and as the gage is strained in tension, the resistance increases; as the gage is compressed, the resistance decreases. The corresponding change in voltage is measured to determine the strain. However, in order to keep the magnitude of the current constant, it must be supplied at a constant voltage. If the strain gage were the only element in the circuit, this would be impossible. Fortunately, by adding other elements to the gage circuit, it becomes possible to supply the current to the circuit at a constant



Figure 33a Mounted Strain Gage with Cable Attached



Figure 33b Mounted Strain Gage with Protective Wax Coating

value. One arrangement for the gage circuit is the Wheatstone Bridge, as shown in Fig. 34.

The Wheatstone Bridge consists of four resistors arranged to form a closed circuit. The voltage (and current) is supplied at a constant value across nodes A and C, and the change in voltage is measured across nodes B and D. The drop in voltage from A to B is (13):

$$V_{AB} = \frac{R_1}{R_1 + R_2} V \quad (7)$$

where R_1 and R_2 are the resistances of the resistors, and V is the applied voltage. Similarly, the voltage drop from A to D is:

$$V_{AD} = \frac{R_4}{R_3 + R_4} V \quad (8)$$

The output voltage, E , from the bridge is equivalent to:

$$E = V_{BD} = V_{AB} - V_{AD}$$

or

$$E = \frac{R_1 R_3 - R_2 R_4}{(R_1 + R_2)(R_3 + R_4)} \quad (9)$$

The bridge is considered balanced when $E = 0$ or $R_1 R_3 = R_2 R_4$. When the bridge is balanced, any change in the resistance will cause a voltage differential E to develop across BD. If $\Delta R_1, \Delta R_2, \Delta R_3$, and ΔR_4 are the changes in resistance of R_1, R_2, R_3 , and R_4 , respectively, then ΔE has a value equal to:

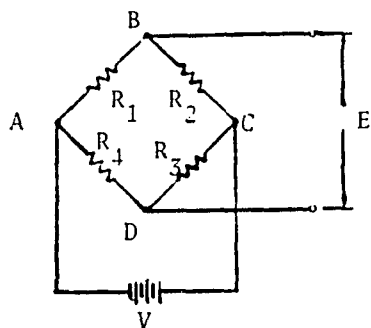


Figure 34 Typical Wheatstone Bridge

$$\Delta E = \frac{\begin{vmatrix} (R_1 + \Delta R_1) & (R_2 + \Delta R_2) \\ (R_3 + \Delta R_3) & (R_4 + \Delta R_4) \end{vmatrix}}{\begin{vmatrix} (R_1 + \Delta R_1 + R_2 + \Delta R_2) & 0 \\ 0 & (R_3 + \Delta R_3 + R_4 + \Delta R_4) \end{vmatrix}} \quad (10)$$

Simplifying Eq. (10) and neglecting second-order terms gives:

$$\Delta E = V \frac{R_1 R_2}{(R_1 + R_2)} \left(\frac{\Delta R_1}{R_1} - \frac{\Delta R_2}{R_2} + \frac{\Delta R_3}{R_3} - \frac{\Delta R_4}{R_4} \right) \quad (11)$$

For quarter bridge circuits, such as those used for the sign structures, the strain gage is the only resistor that will show a change in resistance. Therefore, $\Delta R_2 = \Delta R_3 = \Delta R_4 = 0$ and Eq. (11)

becomes:

$$\Delta E = V \frac{r}{(1+r)^2} \frac{\Delta R}{R_1} \quad (12)$$

where $r = R_1/R_2$.

The quantity $\Delta R/R$ represents a change in resistance and is related to the strain as

$$\Delta R/R = S_g \epsilon \quad (13)$$

where S_g is a proportionality constant known as the gage factor, and ϵ is the strain. The gage factor allows the manufacturer to calibrate his gages to give the proper values.

For this study, $R_1 = R_2$, and r becomes 1.0. Substituting into Eq. (12) gives:

$$\Delta E = \frac{V}{4} S_g \epsilon \quad (14)$$

Rearranging and solving for the strain then yields:

$$\epsilon = 4\Delta E / (VS_g) \quad (15)$$

This equation was used to determine the strains from the voltages recorded by the data acquisition unit.

5.4 Data Reduction Procedure

Data reduction is the process by which the strain gage voltage readings are manipulated to determine the corresponding values of stress and strain. The only unknown in Eq. (15) is ΔE . If it were possible to balance each Wheatstone Bridge before each gage reading, the gage reading (voltage) would have been ΔE , since it was recording zero before the strain occurred. However, due to the dynamic nature of the structural loading, such balancing is normally not possible. It was, therefore, necessary to determine an initial value, or offset, of the gage voltage.

After the data had been transferred to a file on a floppy disk, the HP-9836 was used to search through the data file for gage readings that were made at wind speeds of less than 0.1 mph. This value was selected as the basic "zero" wind speed, after experimentation on calm days showed that strains induced by a wind of that magnitude were negligible. An average value of all such readings was computed for each gage, and these were then defined as the gage offsets and stored on a floppy disk in a data file. The offsets were recomputed for each day of data collection. This was necessary to do,

as disconnecting the data acquisition unit from the gage cables caused the offsets to change from day to day. (It is noted that the data acquisition unit had to be disconnected from the gage cables every day, as it was not possible to monitor the unit 24 hours a day, and no provision could be made to secure the unit from weather and vandals).

Once the offsets had been determined, the strains were computed. The true value of E was determined from Eq. (16):

$$\Delta E = V_i - V_o \quad (16)$$

where V_i is the voltage reading for a strain gage, and V_o is the offset for that gage. If V_i is less than V_o , a negative value of ΔE is obtained. This indicates compression. A positive value of ΔE indicates tension.

With the value of ΔE computed, the strain was determined using Eq. (14). The value of the corresponding stress was then calculated using Hooke's Law (17)

$$\sigma = E\epsilon \quad (17)$$

where σ is the stress and E is the modulus of elasticity of steel, taken as 29×10^3 ksi. The stress and strain data were all stored, along with the corresponding normal wind component. This made them available for further data reduction and evaluations of the results, such as determining statistical characteristics of the stresses.

5.5 Statistical Analysis of Results

The data collection equipment was capable of reading the anemometer and strain gages approximately every 34 seconds. The data acquisition unit would first read and store the wind speed and direction in the calculator's memory, which took approximately 5 seconds. Using these values, the calculator would then compute the magnitude of the wind component perpendicular to the plane of the structure and store this value in its memory. This process consumed about 2 seconds. All strain gages were now scanned, one after the other, which required about 3 seconds. The remaining 24 seconds was needed to transfer the gage readings from the data acquisition unit to the calculator's memory.

Due to the vibrating nature of the structures, the strain gage readings were not necessarily always at the maximum, as indicated by Fig. 35. As can be seen from this figure, the stress at time t_1 , will be less than at time t_2 . The readings might have been taken at any point in the cycle, and it was therefore determined that a statistical evaluation of the data was the only way in which logical explanations of the results could be provided.

The analysis was conducted for each gage for all wind speeds, using increments of 1 mph. Each nominal wind speed covered a range of 0.5 mph on either side of the nominal value. Therefore, actual wind speed values exactly halfway between two nominal wind speed increments were rounded up to the higher value.

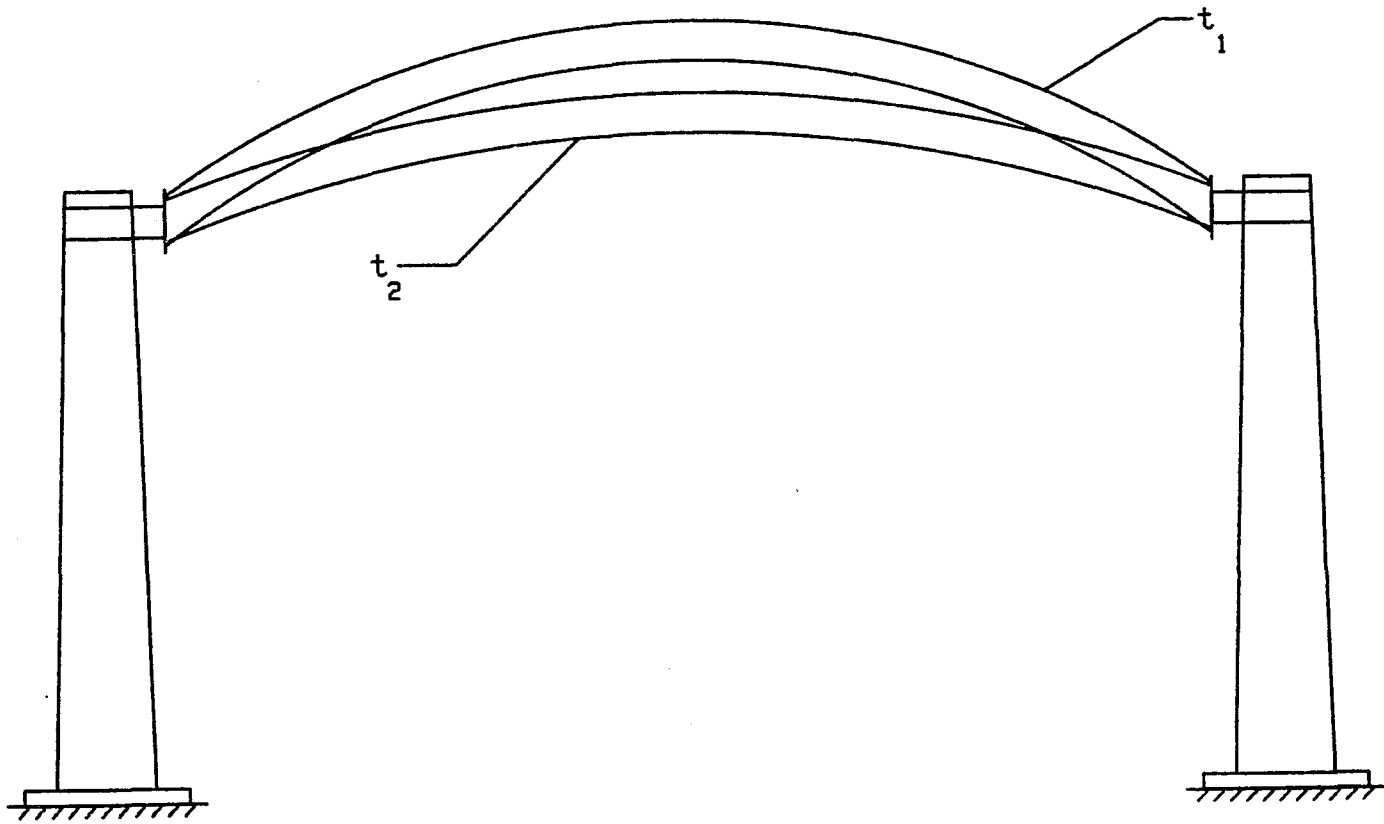


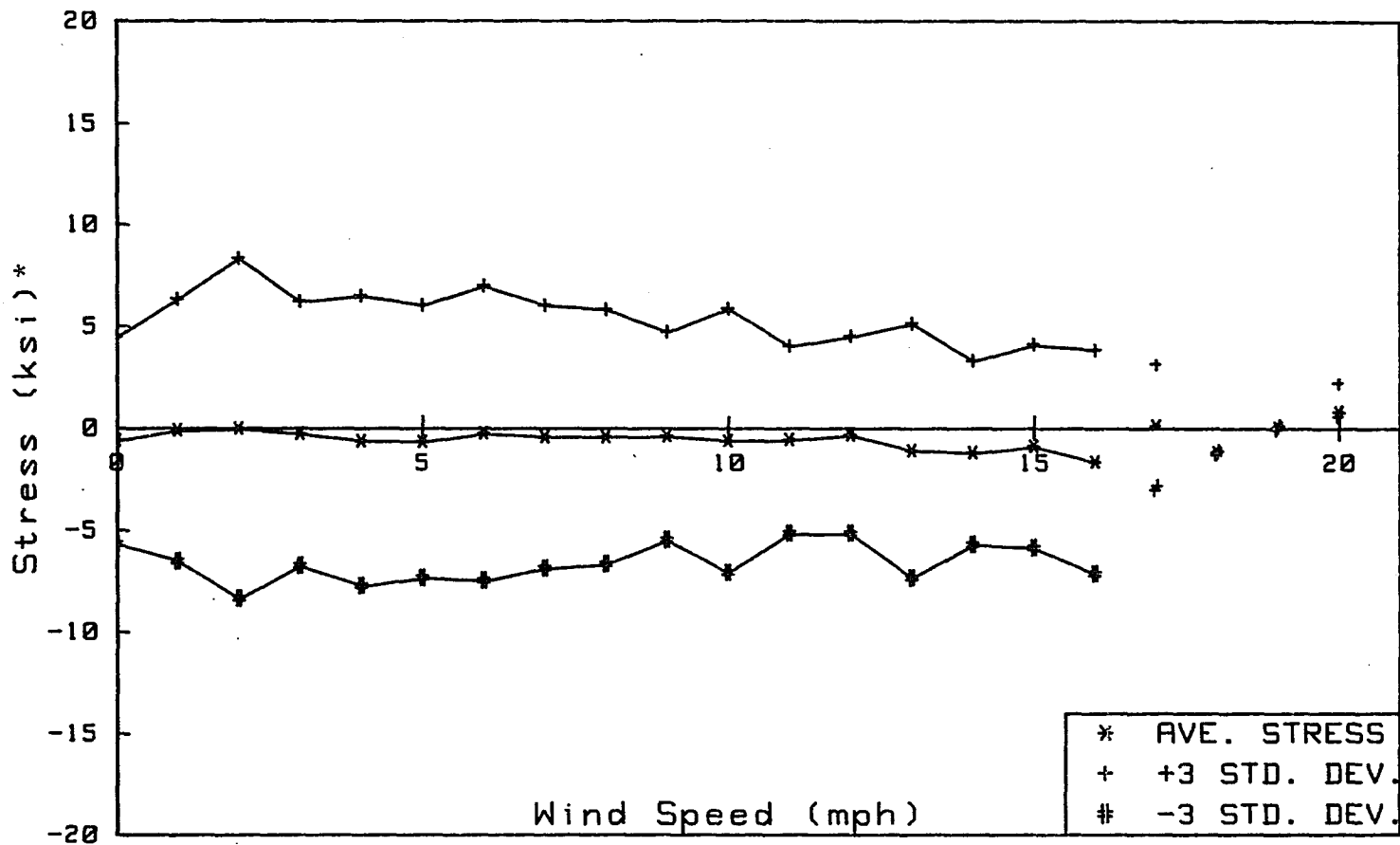
Figure 35. Dynamic Deflections in Monotube Structure at Various Times

For the Tucson structure, a total of 1244 readings were made by each gage. For the Phoenix structure, 1133 readings were taken per gage. For each nominal wind speed, the maximum positive and negative stresses were found, and the average stress and standard deviation were computed. The average positive and negative stresses, along with their respective deviations were then determined. The standard deviations were calculated using:

$$\sigma = \sqrt{\frac{n\sum x^2 - (\sum x)^2}{n(n-1)}} \quad (18)$$

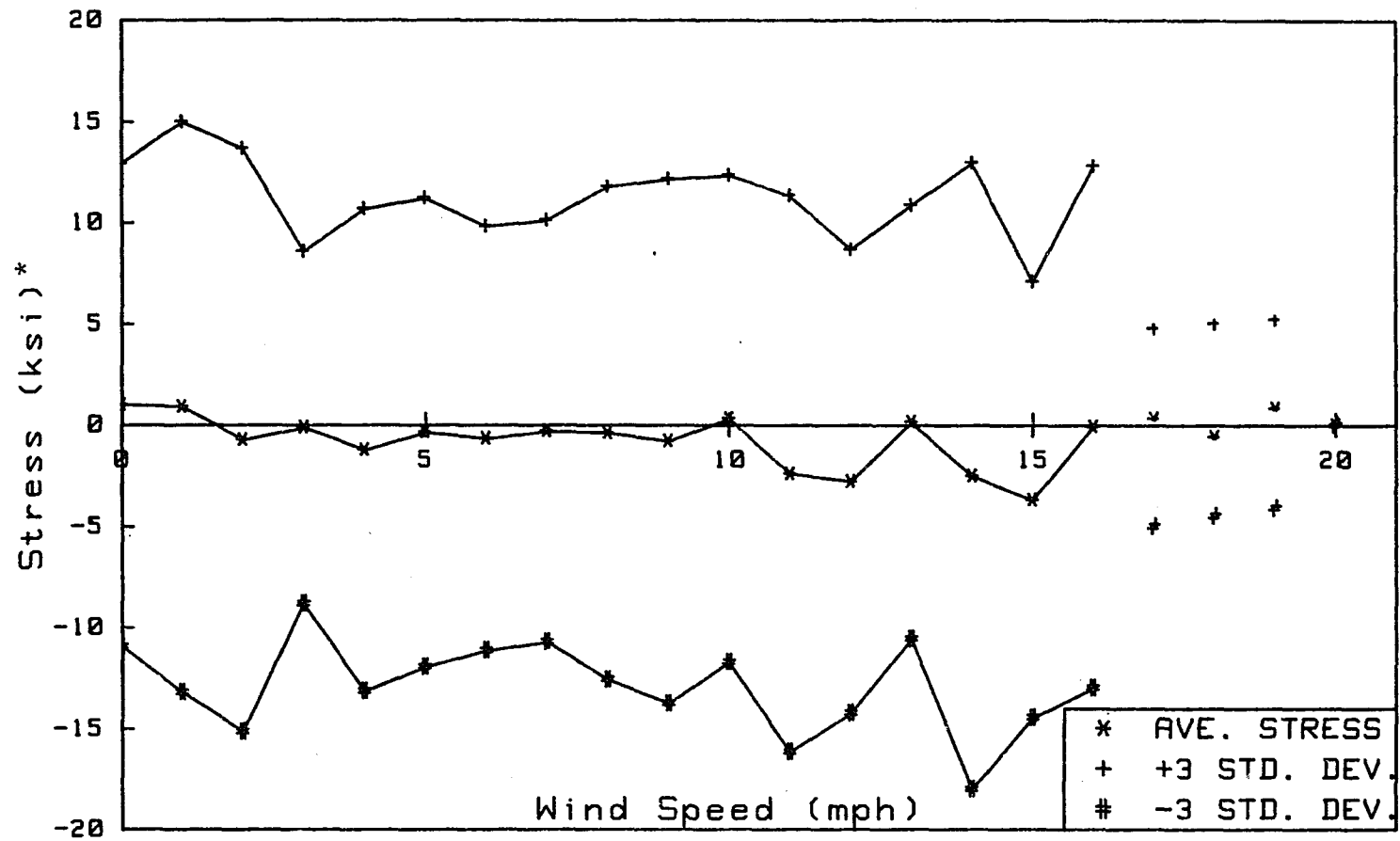
where σ is the standard deviation, n is the number of data points for a certain nominal wind speed, and $X_1, X_2, X_3, \dots, X_n$ are the data points.

The two locations of primary interest for each structure are at the midspan of the beam and at the base of the column. A stress envelope was determined for each of these by plotting the average stresses, along with points identifying values of plus and minus 3 standard deviations to either side of the average. This envelope includes 99.5% of all possible stress levels (14), assuming that the readings are normally distributed. The envelopes for the midspan of the Tucson and Phoenix structures are shown in Figs. 36a and 36b, respectively.



*For wind speeds greater than 16 mph, the statistical population is too small for accurate analysis

Figure 36a Stress Envelope for Midspan Stresses of Tucson Monotube Structure



*For wind speeds greater than 16 mph, the statistical population is too small for accurate analysis

Figure 36b Stress Envelope for Midspan Stresses of Phoenix Monotube Structure

It can be seen that the maximum values of the stress envelope are well within the safe range. For the Phoenix (100' span) structure, the maximum value given by the envelope is 18 ksi, which is only 53% of the yield stress of 34 ksi. For the Tucson (60' span) structure, the margin of safety is even larger. The maximum value given by the envelope is 8.2 ksi, or 24% of the yield stress. Furthermore, it is emphasized that these values tend to be extremes. The large number of tests that were made lend confidence to the statistical evaluations; further data are not likely to alter the averages nor the + 3 standard deviations to a significant degree. It is therefore clear that the low level of service load stress that was predicted by the analytical study has been substantiated.

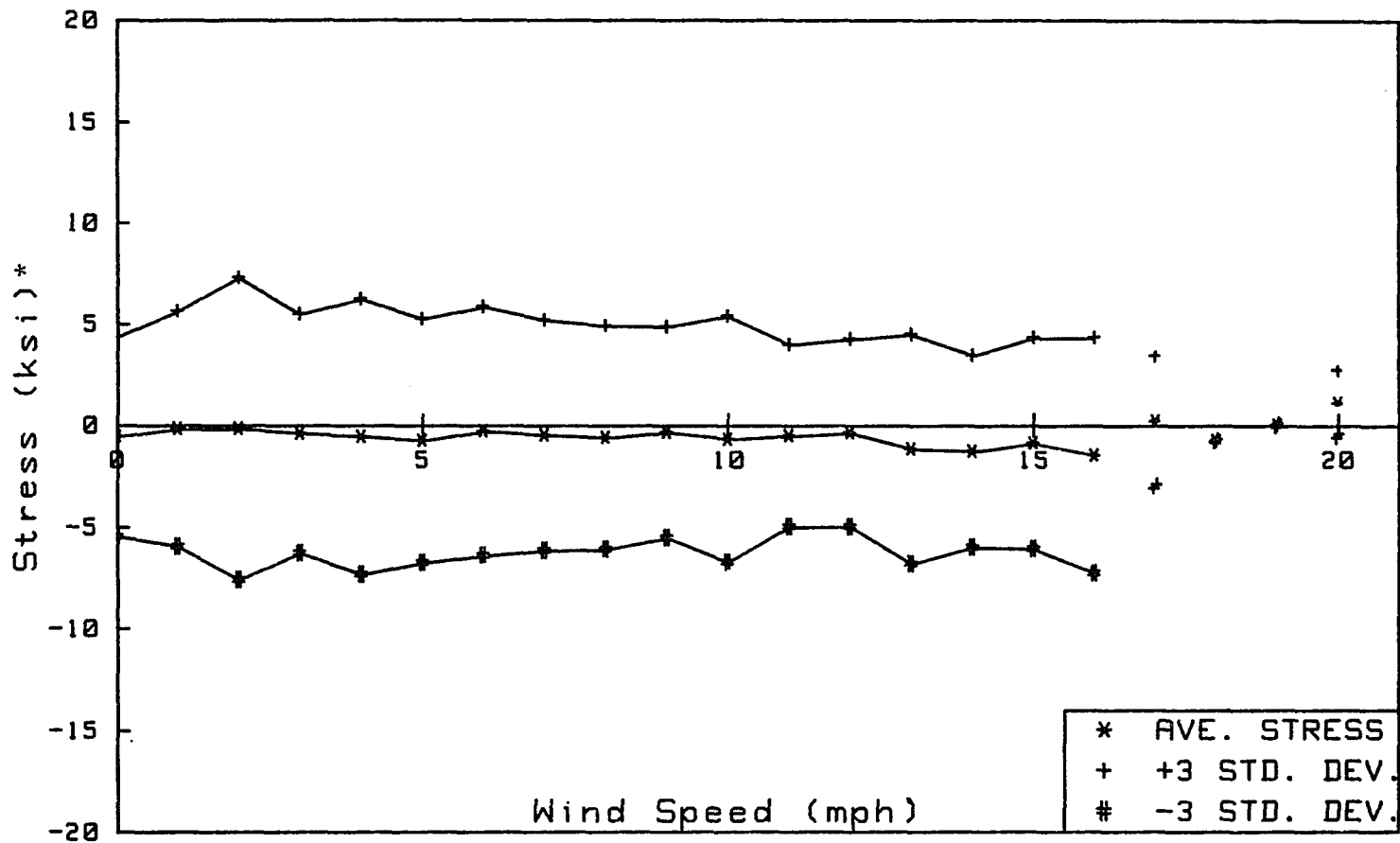
It is interesting to note that both structures exhibit local maxima in the envelopes at wind speeds of approximately 2 mph, and again at 14 to 16 mph. The frequency of oscillations at 2 mph is well below any natural frequency for both structures. However, between wind speeds of 15 and 16 mph, both structures are near a natural frequency. For the Tucson structure, the frequency corresponds to the third 3D mode of 3.26 cps. For the Phoenix structure, the mode is also the third 3D mode, at a frequency of 3.06 cps. It is believed that the maxima observed in the stress envelopes at this wind speed indicates that the structure is tending toward resonance at these points. However, due to the structural damping and the gusting of the wind, the

resonance condition is not achieved. This is the same finding that was made in the original monotube study (3).

The stresses at the column bases are not as large as their midspan counterparts. The envelopes for the out-of-plane stresses for both structures are shown in Figs. 37a and b. The maximum value for the Tucson structure is 7.7 ksi, and for the Phoenix structure it is 17.0 ksi. This demonstrates that the span length has a greater influence on the column base stresses than does the sign size. It is noted that the signs on the Tucson structure were about twice as large as those on the Phoenix structure, but the latter has a span that is 67% longer.

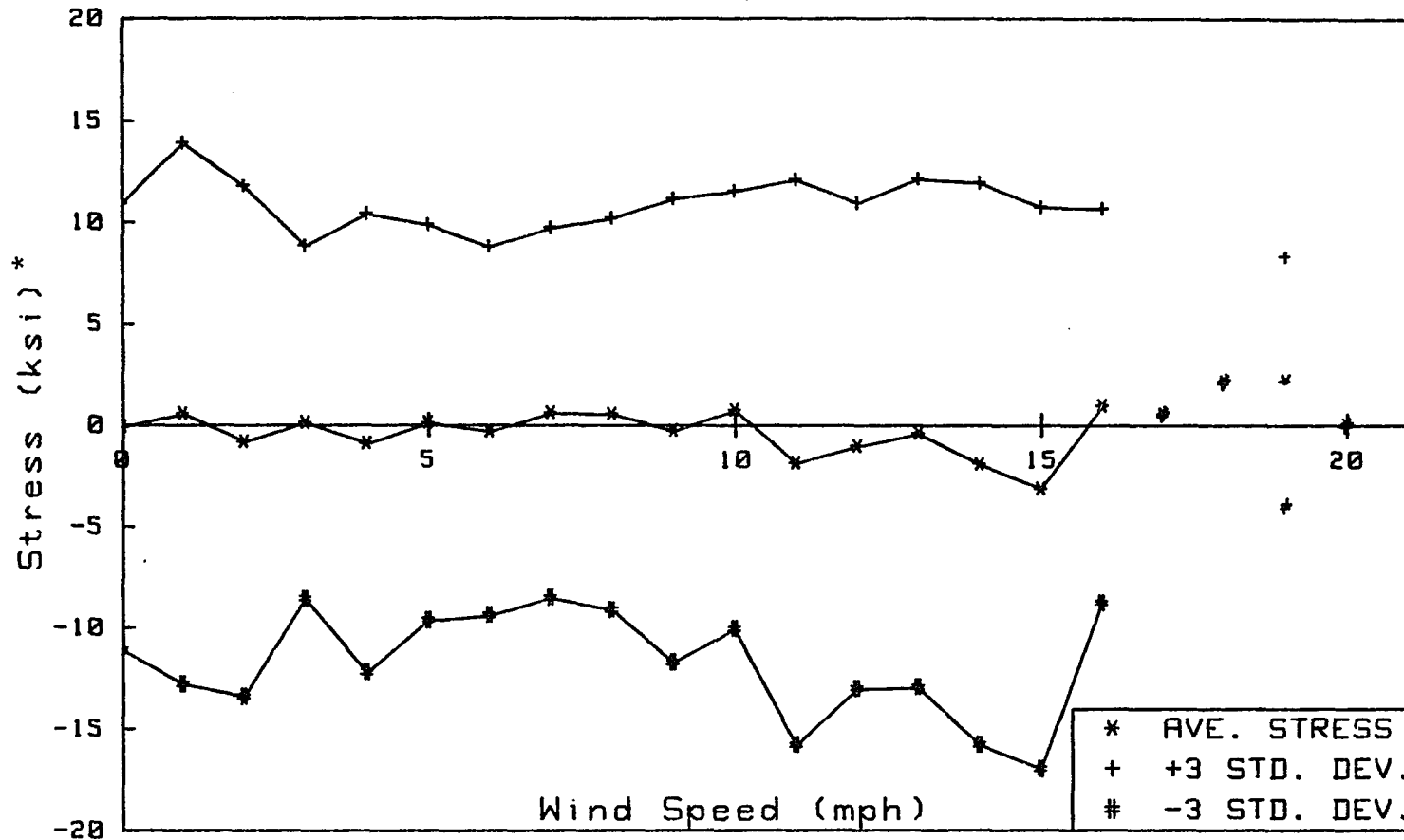
The column base stresses also exhibit local maxima at approximately the same wind speeds as was found for the beam. Here, again, the structure is vibrating at close to a natural frequency, but is prevented from reaching a resonance condition by the inherent structural damping, as well as the fact that the wind only blows for short periods of time.

The maximum stresses discussed so far were not the actual maximum stresses recorded, but the maximum values that are likely to occur, given the statistical distribution of the data. The recorded stresses were less than those presented. For example, at 16 mph, the wind speed for which the stress envelope is the widest for the Tucson structure, the maximum recorded stress was 7.3 ksi, as compared to



*For wind speeds greater than 16 mph, the statistical population is too small for accurate analysis

Figure 37a Stress Envelope for Column Base Stresses of Tucson Monotube Structure



*For wind speeds greater than 16 mph, the statistical population is too small for accurate analysis

Figure 37b Stress Envelope for Column Base Stresses of Phoenix Monotube Structure

12.2 ksi of the envelope. It is therefore clear that the use of a statistical approach has made it possible to include essentially all of the possible stress levels in the analysis. This also reflects the cyclic nature of the structural behavior, as well as the influence of the time lapse involved in the reading of the gages.

5.6 Calibration of Equipment

Due to the high ambient temperatures during the times when the data for the Phoenix structure were collected, it was necessary to calibrate the equipment and the gages to reflect the higher than normal operating temperatures. The data were collected during the months of June and July, with ambient temperatures ranging between 100° and 115°F. Data for the Tucson structure were also collected on one day during this period, with an ambient temperature of 102°F. It was not found necessary to apply calibration constants to the other Tucson data which were collected during the month of March when the temperature was in the mid 80's.

The first correction was made to account for the apparent and true strains caused by thermal conditions. The gages that were used had been calibrated to read zero strain at 75°F. However, much of the time these gages were used when the ambient temperature was over 100°F, and the surface temperature of the structure was greater than 140°F. The temperature response curve of the gage that is shown in Fig. 38 indicates that this can cause an error of -50 micro strain, which

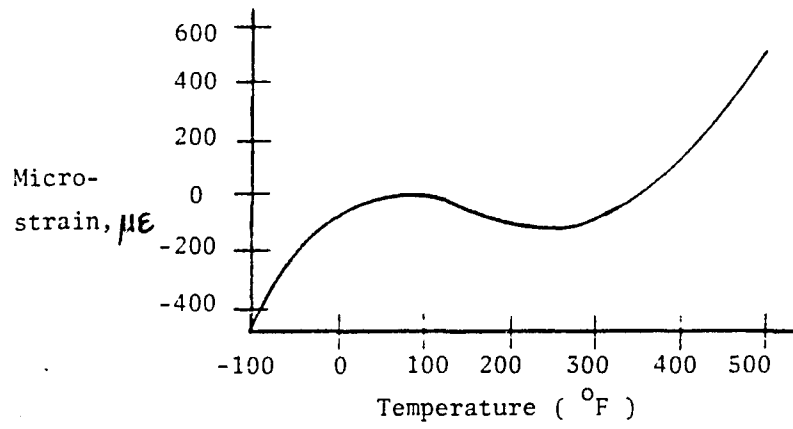


Figure 38 Apparent Strain in Strain Gage
Due to Temperature

corresponds to approximately 1.5 ksi compressive stress. To compensate for this, a separate gage was bonded to a piece of steel of the same thickness as the wall of the structure. The gage was covered and protected exactly as the other 16 gages were. It was then placed in the sun and read along with the other gages. When the gage readings were reduced, the voltage difference of the separate gage was subtracted from the voltage difference of the other gages, thereby canceling the elevated temperature effects.

A more significant correction was needed to compensate for the influence of higher operating temperatures on the Data Acquisition Unit. The service manual (17) states that the optimum operating temperature is in the range of 62^o to 78^oF. In the field, the unit would have to work in temperatures as high as 135^oF, resulting in some impairment of accuracy. Since the unit had been routinely run in the sun at temperatures between 120^o and 130^oF, a test was conducted to see if the error was systematic, and how it could be accounted for.

The unit was set in the sun on a warm day. It was connected to a Wheatstone Bridge, across which a known voltage was applied. At intervals of approximately one hour, the bridge voltage was read by the Data Acquisition Unit, as well as by a voltmeter that was kept at its optimum temperature. The voltages and the time and temperature were recorded over a period of two days.

The results of the experiment are shown in Tables 11a and 11b. For temperatures above 105°F, it is seen that the voltages read by the Data Acquisition Unit were 43% greater than the actual voltages. This difference appears to be independent of the level of temperature above 105°F. During the data reduction, the voltage differences were reduced by this amount to correct for the temperature effects on the equipment.

All stress and strain values that are given in this chapter reflect these correction factors.

TABLE 11a - Results of Data Acquisition Unit Calibration Test - Day One

Time	Temperature (°F)	Voltage Read	Actual Voltage	% Error
9:00	100	0.8321	0.5658	32.0
10:00	105	0.9047	0.5130	43.3
11:00	113	0.9181	0.5242	42.9
12:00	121	0.8989	0.5142	42.8
1:00	123	0.9015	0.5121	43.2
2:00	127	0.9086	0.5106	43.8
3:00	128	0.9011	0.5190	42.4
4:00	127	0.8974	0.5151	42.6
5:00	127	0.8983	0.5075	43.5

Average % Error = 43.1%

TABLE 11b - Results of Data Acquisition Unit Calibration Test - Day Two

Time	Temperature (°F)	Voltage Read	Actual Voltage	% Error
9:00	102	0.8596	0.5587	35.0
10:00	106	0.8778	0.5030	42.7
11:00	112	0.8753	0.4998	42.9
12:00	118	0.8897	0.5053	43.2
1:00	123	0.8924	0.5149	42.3
2:00	128	0.8975	0.5044	43.8
3:00	128	0.8997	0.5101	43.3
4:00	129	0.8814	0.5033	42.9
5:00	129	0.8873	0.5066	42.9

Average % Error = 43.0%

Chapter 6

COMPARISON OF ANALYTICAL AND EXPERIMENTAL RESULTS

The full-scale test results that have been obtained in the present research project represent a new contribution to the pool of information that previously provided only theoretical data on the response of monotube sign support structures. In the following discussion, a detailed evaluation of the data will be given, affording comparisons between actual in-service behavior of the structures and the theoretical studies that have been made. In addition to giving unique comparisons between analytical and experimental research, the results will also be used to examine and verify the design recommendations that were made earlier (3).

6.1 Tucson Structure

The 60-foot Tucson structure is the lower limit of what is considered a normal span for monotube structures. The analytical and the experimental results both showed that the point of maximum in-plane stress was at the midspan of the beam; these are detailed in columns 2 and 3 of Table 12. It should be noted that the measured stresses for the 20 mph wind speed represents only two individual readings, and no readings were obtained for wind speeds greater than 20 mph. The stresses that are given for the full-scale tests are the absolute

TABLE 12. Computed and Measured Stresses for 60-Foot Structure

Wind Speed, mph	In-plane at midspan, ksi		Out-of-plane at column base, ksi	
	Computed	Measured	Computed	Measured
2.5	4.38	5.52	1.34	1.74
5.0	4.38	5.69	1.34	2.08
7.5	4.39	4.33	1.35	1.08
10.0	4.39	4.86	1.48	2.03
12.5	4.49	4.36	1.65	1.73
15.0	4.54	4.10	1.61	2.43
17.5	4.59	4.01	1.70	2.58
20.0	4.66	1.30 ⁺	1.81	1.65
22.5	4.71	*	1.93	*
23.2	5.11	*	2.64	*

* No data collected for this wind speed.

⁺ Only two readings obtained at this wind speed.

values of the maximum stresses that were recorded. In most cases, the absolute values of the positive and negative stresses were almost identical, as would be expected for the type of cross section that is used in the structures. It is also noted that the stress levels do not vary a great deal over the range of wind speeds that were measured.

The data in Table 12 illustrate the good correlation that was obtained between the analytical and the experimental results. This is further emphasized when the complexities of full-scale testing, modeling of actual structures, and so on, are considered. Thus, the three-dimensional, non-prismatic nature of the structure makes it particularly difficult to model, especially when dynamic wind loads must be accounted for. The strain gages were not installed under ideal laboratory conditions, and the field measurements had to be made in a very demanding climate. In spite of these obstacles, the results of the analytical and experimental investigations are in good agreement.

The largest deviation between the measured and computed stresses occurs at a wind speed of 5 mph, although it is noted that the numerical value of the difference is still small. Also, the magnitudes of the stresses are well below the yield stress. The reasons for the differences and their magnitudes can be explained in part by examining the statistical characteristics of the measurement results.

As shown in Chapter 5, the maximum stress that is likely to appear at a wind speed of 5 mph is 7.32 ksi, which equals the mean

stress of 0.63 ksi plus 3 standard deviations. The maximum recorded stress of 5.69 ksi is greater than 95% (mean plus 2 standard deviations) of the stresses that can be expected to develop at this wind speed.

It is also interesting to note that at the higher wind speeds, the analytical model consistently predicts a higher level of stress than was measured. This may be partly due to the lower number of readings that were taken at the higher wind speeds, as compared to at the lower wind speeds. However, it is clear that the major influence is provided by the modeling of the structure. For example, the use of prismatic elements results in a smaller section at midspan of the analytical model, as compared to the real structure. This by itself will lead to somewhat higher stresses at the midspan location. The modeling of the beam-to-column connection also is important in the sense that a low restraint of same will lead to higher stresses in the beam. This difference between the results is not as consistent at the lower wind speeds, because random electrical disturbances that may have occurred during the data collection process would tend to cancel the modeling effects. The sensitivity of the equipment is also a factor in this case.

The experimental and theoretical results agree that the point of maximum out-of-plane stress is at the column base. These stresses are given in columns 4 and 5 of Table 12. The correlation between the

computed and measured stresses is good, although maybe not as satisfactory as for the midspan location. However, it is emphasized that the column base stresses are very low. At these levels, a 0.5 ksi difference appears large.

It is observed that the full-scale test results are consistently higher than those of the analytical study. This is most likely due to the element chosen to model the beam-to-column connection. The in-plane bending stiffness underestimates that of the actual connection and, therefore, less of the moment in the beam is transferred to the column. As a consequence, the stresses at the column base in the model are lower.

Perhaps the best way to comprehend how well the two studies correlate is to view the data graphically. Figure 39 displays the results for the measured and computed column base and beam midspan stresses. When drawn to scale, it is readily apparent how well the findings support each other.

The figure shows the stresses due to the dynamic effects of the wind, which is the primary live load the monotube structures will experience. However, the structural designer must know the total stress from both live and dead loads. Therefore, the computed dead load stresses (no measurements could be taken for dead loads) were added to those due to the wind load, and the sums for the in-plane and the out-of-plane directions are shown in Fig. 40. It is clear that the

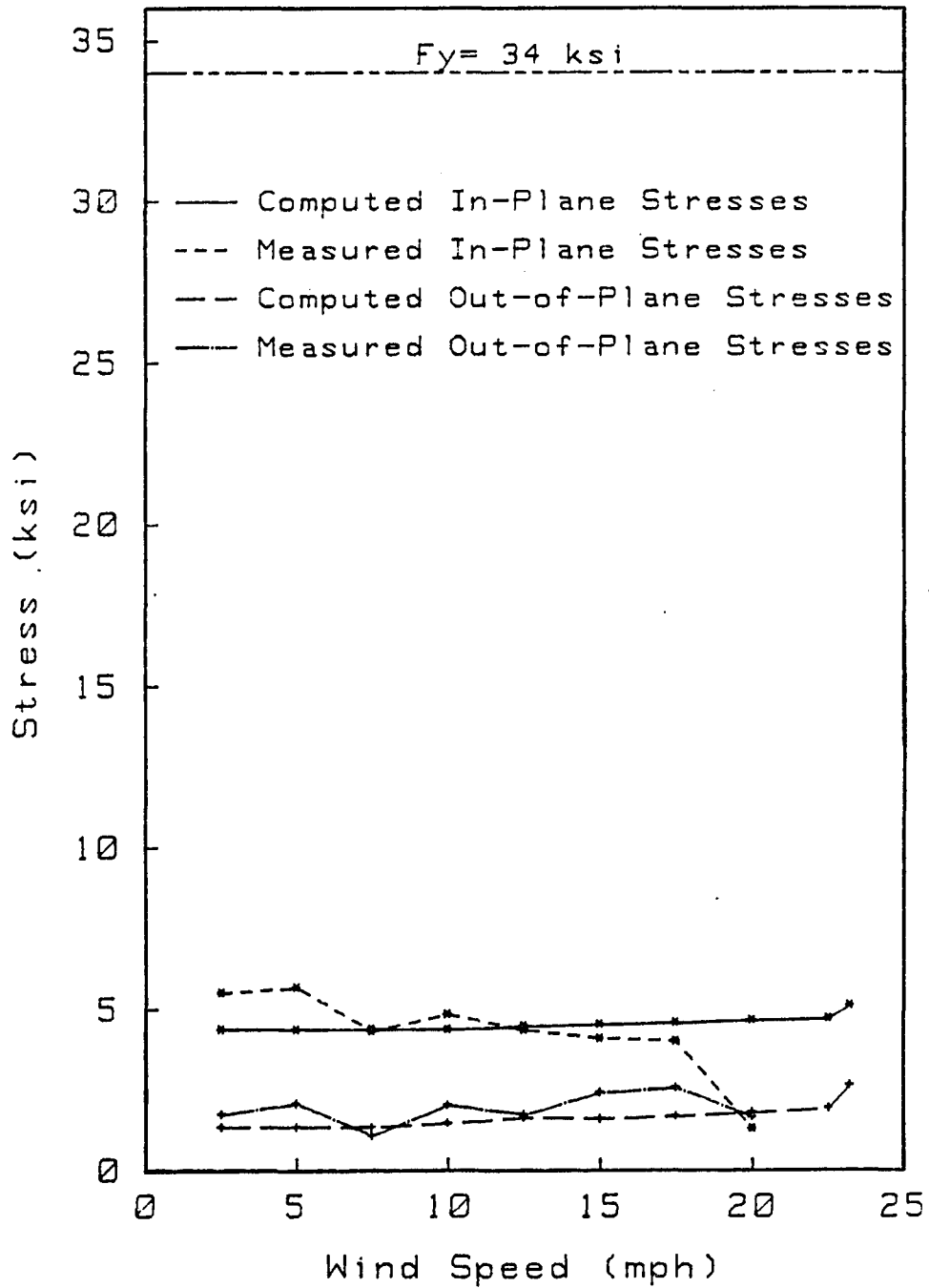


Figure 39 Correlation of Stresses for Tucson Monotube Structure

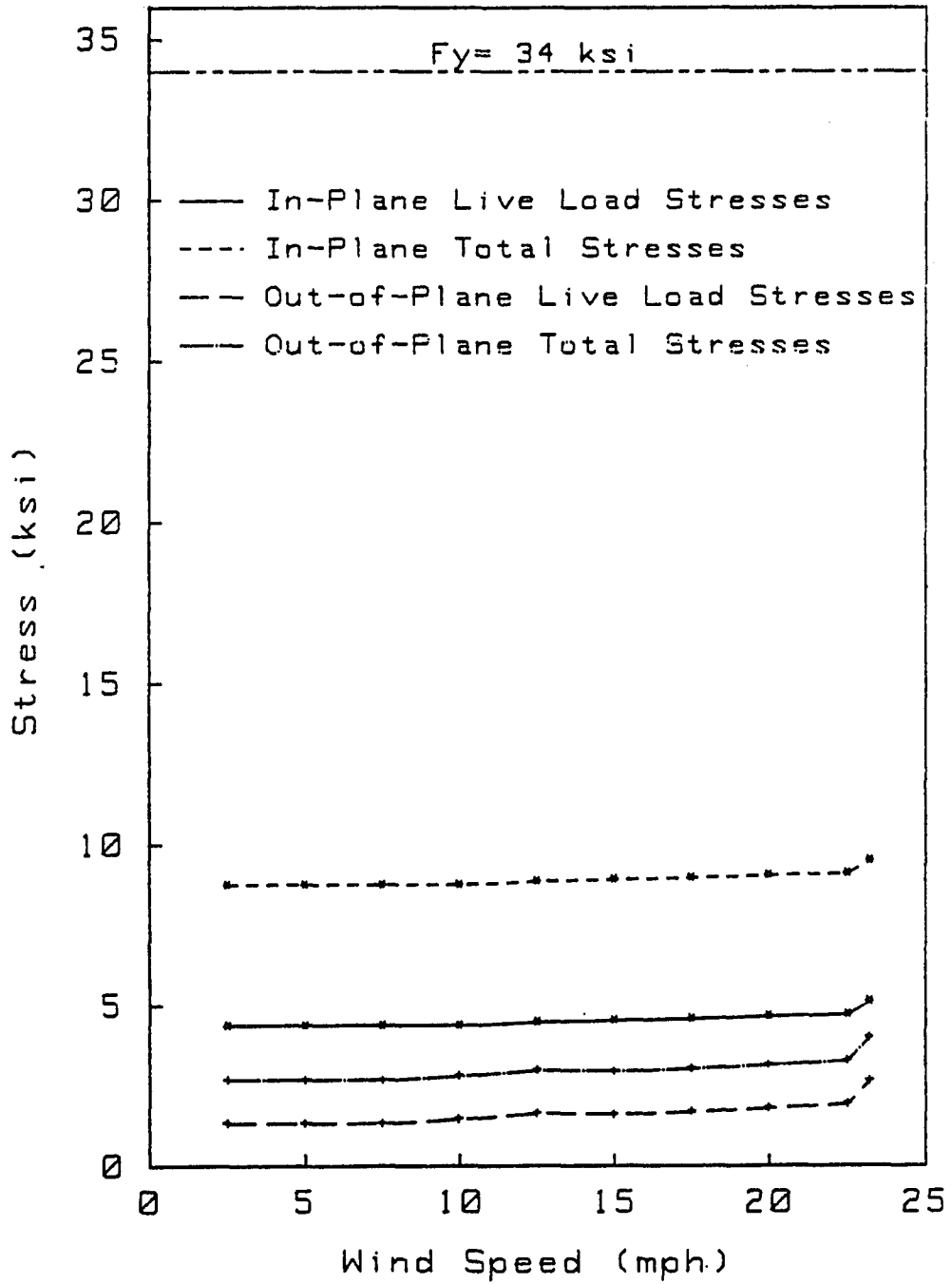


Figure 40 Total Stresses for Tucson Monotube Structure

stress levels are still well below the yield stress of the steel. In fact, the margin of safety indicates that the Tucson structure appears to have been designed quite conservatively.

6.2 Phoenix Structure

The 100-foot Phoenix structure is close to the upper limit of the normal spans for monotube structures. Longer spans may prove to be uneconomical. As for the Tucson structure, the computations and the testing both determined that the point of maximum in-plane stress was at the midspan of the beam. Columns 2 and 3 of Table 13 give the maximum stress at each wind speed as determined by computations and measurements. It should be noted that for the wind speed of 17.5 mph only one reading was obtained, and none could be had for wind speeds of 20.0 mph or greater.

It is seen that the correlation between the theoretical and actual stresses is good. The stresses are greater than at the corresponding point in the Tucson structure, as would be expected due to the longer span. The analytical study also predicts stresses that are consistently higher than the measured ones. The reasons for this were detailed in the description of the Tucson test results.

In the out-of-plane direction, both studies agree that the point of maximum stress is at the base of the column, and these data are given in columns 4 and 5 of Table 13. The stresses are low, and

TABLE 13 - Computed and Measured Stress for 100-Foot Structure

Wind Speed, mph	In-plane at midspan, ksi		Out-of-plane at column base, ksi	
	Computed	Measured	Computed	Measured
2.5	10.11	9.74	2.84	3.25
5.0	10.18	9.96	2.87	5.39
7.5	10.23	9.96	2.91	4.98
10.0	10.29	9.91	2.95	4.13
12.5	10.51	9.60	3.11	4.04
15.0	10.70	9.13	3.16	5.36
17.5	10.53	4.33 ⁺	3.12	1.47
20.0	10.75	*	3.19	*
22.1	10.92	*	3.25	*

⁺ Only one reading taken at this wind speed.

* No data collected for this wind speed.

hence the numerical values of the differences between the measured and the computed data appear more significant than they are. Similar to the Tucson results, the column base stresses predicted by the analytical study are consistently lower than those that were measured. This is attributable to the modeling of the beam-to-column connection element, as discussed earlier.

The stresses are presented graphically in Fig. 41. As in Fig. 39, this demonstrates how well the two studies correlate. Figure 42 gives the total live plus dead load stresses (computed values), providing a comparison with the level of the yield stress. It is apparent that the 100-foot monotube structure represents a more realistic design than the 60-foot one, since the margin of safety is closer to the values that are considered desirable in practice. The average total stress for all wind speeds is approximately 19 ksi; this gives a factor of safety against first yield of 1.8.

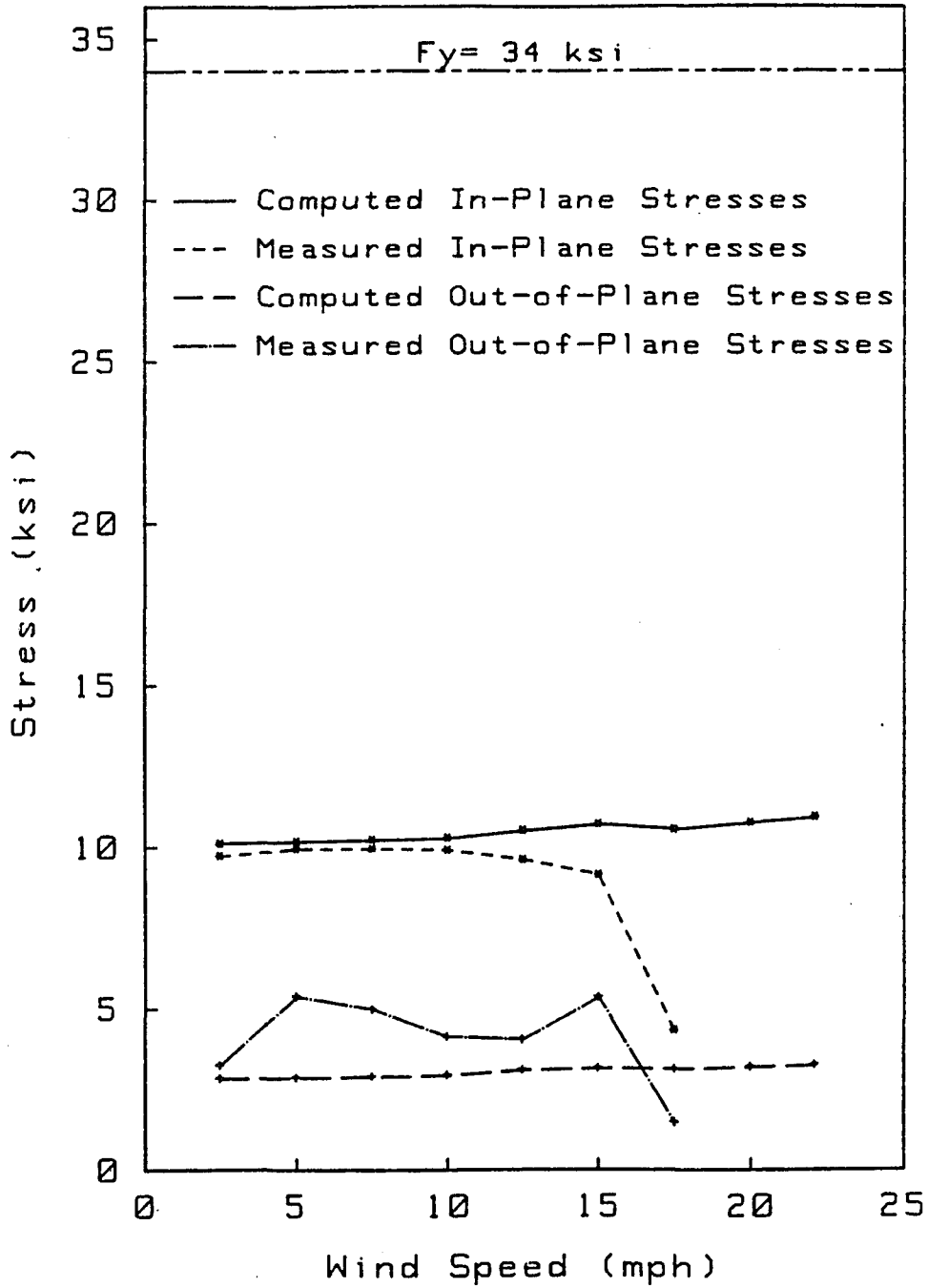


Figure 41 Correlation of Stresses for Phoenix Monotube Structure

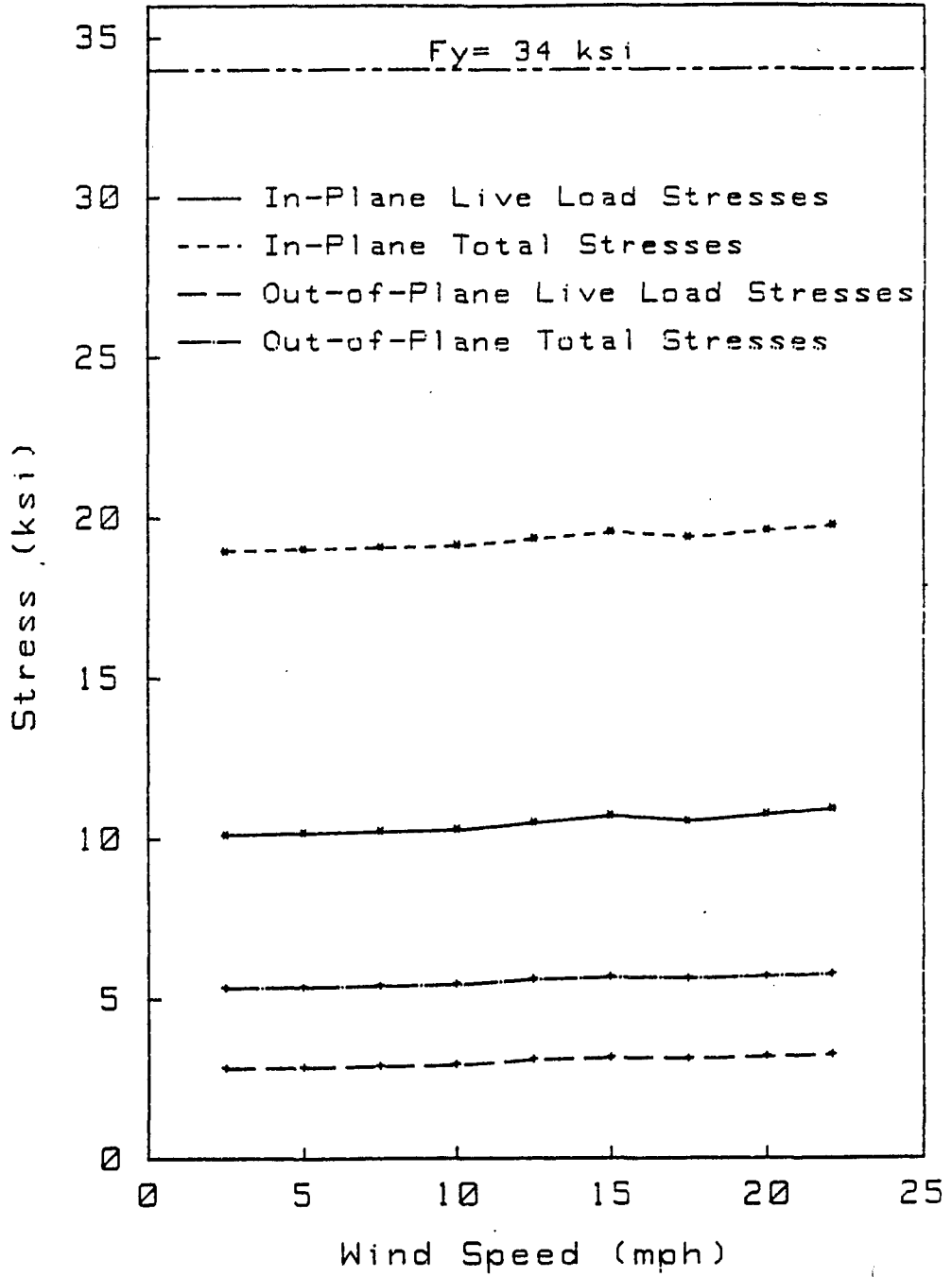


Figure 42 Total Stresses for Phoenix Monotube Structure

Chapter 7

SUMMARY, CONCLUSIONS AND RECOMMENDATIONS

The purposes of this study were to gather data on the performance of monotube sign support structures under service conditions, and to evaluate possible methods of structural analysis. Through the use of field testing and computer modeling, such data were collected, reduced and analyzed to determine the service load response characteristics of the monotube structures.

7.1 Summary and Conclusions

On the basis of the two full-scale structures that have been tested and analyzed, the following conclusions can be made:

1. The service load stresses can be accurately predicted by the use of finite element modeling. The computer models in this study correlate very well with the field measurements, as well as with the similar models studied by Ehsani and Bjorhovde (3).
2. Due to the correlation between past and present results, the recommendations that were made by Ehsani and Bjorhovde are well-founded and should be considered for adoption. These recommendations include suggested methods of analysis, new performance criteria, and topics in need of further study.

3. The two full-scale structures did not meet the $d^2/400$ dead load deflection requirement of the AASHTO Specifications.
4. The stress levels associated with the actual deflections are well below the magnitudes of the allowable stresses, even though the structures do not meet the $d^2/400$ deflection criterion.
5. As was found in the earlier study (3), the stress level at any point can be found by superimposing the stresses due to static loads and those due to dynamic loads.
6. The maximum in-plane stresses occur at midspan of the beam.
7. The maximum out-of-plane stresses occur at the column base.
8. Resonance did not occur in the field testing, even when vortices were shed at frequencies equal to the natural frequencies of the structures. This can be attributed to the inherent damping of the structure, as well as to the gusting nature of the wind.
9. A monotube structure of moderate or greater span ($> 60'$) cannot meet the $d^2/400$ dead load deflection requirement of AASHTO. In most cases, it would prove to be very uneconomical to design such a structure to meet this

requirement. A new deflection criterion was proposed in the original monotube study (3), thus:

$$\frac{\Delta}{\ell} = \frac{1}{150}$$

where Δ is the dead load deflection, and ℓ is the span length. This criterion is based on stiffness requirements, as the strength (i.e., stress level) is not likely to govern.

In the original study on monotube structures (3), a number of other recommendations also were made in regard to the analysis and design of these structures. Two of the recommendations are of particular interest in relation to the findings of the current project.

The first recommendation is to consider the analysis of the monotube structure for out-of-plane behavior independent of the in-plane behavior. The current project has shown that this is a rational approach. It makes the analysis much simpler, and does not introduce any appreciable error.

The second recommendation was to camber the beam of the monotube structure to help eliminate the undesirable visual effects of larger deflections. This is especially worthwhile if a maximum deflection-to-span ratio of 1/150 is adopted. The 100' span of the Phoenix structure that was tested in the current study had such a cambered beam. Although the dead load deflections were large, the camber kept the midspan above the end points. Thus, the visual effect

was that of a low-pitched arch, which is much more appealing than if the beam was deflected downward. Therefore, cambering the beam is a viable option in the design of monotube structures.

7.2 Recommendations for Further Studies

This study has significantly increased the pool of existing knowledge on the behavior of monotube structures. It has been shown that the design guidelines for truss-type structures cannot be rationally applied to monotube structures. New design guidelines have been recommended; however, certain additional studies of the monotube structure under high wind conditions are needed, as well as a better understanding of other characteristics. Therefore, the following subjects are in need of examination:

1. Wind Tunnel Testing - The performance of monotube structures at wind speeds up to at least 80 mph needs to be determined. This is best accomplished by using scale models in a wind tunnel. The effects of sign placement and size should also be studied.

2. Beam-to-Column Connection Behavior and Strength - The current study has indicated that the connection can play a major role in determining the stresses in the structure. More precise methods are needed to model the actual behavior of typical connections.

3. Evaluations of Fatigue Characteristics - Due to time constraints, this study did not investigate fatigue phenomena in the members or the connections of the structures. However, due to the

dynamic nature of the wind load, cyclic stress variations are common. Although the stress levels are low as compared to the yield stress, the stress ranges and the fastening details of the beam-to-column connections may make them susceptible to fatigue cracking. It is recommended that connection and base details should be tested statically and dynamically in the laboratory to determine strength and fatigue life characteristics.

4. Behavior of Cantilever Structures - The current study only addressed the behavior of span-type structures. Cantilever sign structures are also in widespread use. It is expected that the deflections will be greater than for the span-type structures, as will be the stresses at the column base. Further, the dynamic response of cantilever structures is likely to be considerably more complicated, since the torsional mode of behavior may play a major role. Fatigue also would appear to be more serious.

APPENDIX A:

DATA COLLECTION SOFTWARE
FOR HP-41CX CALCULATOR

REGISTER INPUT DATA:

The following registers must contain specific data, as given in the tabulation below, in order for the programs to execute properly.

Register No.	Value
03	Wind conversion factor = 9.2593 mph/VAC
05	Current storage pointer; must be 20 at the beginning of the data collection
06	Wind direction conversion factor; equal to 41.7633 °/VDC
12	Number of values to store before writing to tape

```
01LBL "GO"  
02 FIX 9  
03 "REG.=?"  
04 PROMPT  
05 "FILE=?"  
06 PROMPT  
07 XEQ "SEEKR"  
08 XEQ "LOG"  
09 RTN  
10 END
```

Starts program. Prompts for tape file
and beginning register.

```
01LBL "SET3"  
02 "OPN"  
03 DUTA  
04 "LS3-17"  
05 DUTA  
06 "F1RAOZON5R-1:T3"  
07 DUTA  
08 1  
09 STO 01  
10LBL 01  
11 16  
12 RCL 01  
13 X=Y?  
14 GTO 02  
15 IND  
16 XEQ "PUT5"  
17 1  
18 ST+ 01  
19 GTO 01  
20LBL 02  
21 "OPN"  
22 DUTA  
23 RTN  
24 END
```

Reads strain gages and stores values
in calculator.

```
01LBL "LOG"
02 XEQ "INI3421"      Main program. Directs program flow.
03LBL 10
04 DATE
05 XEQ "PUT5"
06 TIME
07 XEQ "PUT5"
08 "DPN"
09 DUTA
10 XEQ "WNDSPD"
11 XEQ "PUT5"
12 RCL 00
13 RCL 04
14 X<=Y?
15 GTD 20
16 3
17 ST- 05
18 GTD 10
19LBL 20
20 CF 01
21 XEQ "WNDIR"
22 XEQ "PUT5"
23 XEQ "HDCLC"
24 XEQ "PUT5"
25 RCL 02
26 RCL 08
27 X<=Y?
28 GTD 30
29 5
30 ST- 05
31 GTD 10
32LBL 30
33 XEQ "SET3"
34 RCL 05
35 RCL 12
36 X<=Y?
37 XEQ "WCASS"
38 GTD 10
39 RTN
40 END
```

```
01LBL "INI3421"  
02 AUTOID  
03 CF 17  
04 "HP3421A"  
05 FINDID  
06 SELECT  
07 RTN  
08 END
```

Selects Data Acquisition Unit as
the primary device in IL loop.

```
01LBL "WNDSPD"  
02 "RAOZO"  
03 OUTA  
04 "OPN"  
05 OUTA  
06 "CLS00"  
07 OUTA  
08 "F2N4R1:T2"  
09 OUTA  
10 IND  
11 "OPN"  
12 OUTA  
13 RCL 03  
14 *  
15 STD 00  
16 RTN  
17 END
```

Reads wind speed.

```
01LBL "WNDIR"  
02 "RAOZO"  
03 OUTA  
04 "OPN"  
05 OUTA  
06 "CLS01"  
07 OUTA  
08 "F1RAON3R1:T2"  
09 OUTA  
10 IND  
11 "OPN"  
12 OUTA  
13 RCL 06  
14 *  
15 STD 01  
16 RTN  
17 END
```

Reads wind direction.


```
01LBL "HDCLC"  
02 RCL 01  
03 COS  
04 ABS  
05 RCL 00  
06 *  
07 STD 02  
08 RTN  
09 END
```

Computes wind velocity perpendicular to the sign.

```
01LBL "PUT5"  
02 STD IND 05  
03 1  
04 ST+ 05  
05 RTN  
06 END
```

Stores values in calculator's memory in sequential order.

```
01LBL "WCASS"  
02 020.119  
03 WRTRX  
04 20  
05 STD 05  
06 RCL 12  
07 19  
08 -  
09 ST+ 13  
10 RTN  
11 END
```

Writes data to cassette tape.

APPENDIX B:

DATA REDUCTION SOFTWARE
FOR HP SERIES 200 COMPUTER

```

520 '
530 SUB Offset(Nq,Os(#))
540 '
550 First: INPUT "ENTER NUMBER OF STRAIN GAGES",Nq
560 '
570 'CHECK FOR PROPER NUMBER OF STRAIN GAGES
580 '
590 OUTPUT 2:" ": 'CLEAR SCREEN
600 PRINT USING "15/20X,""NUMBER OF STRAIN GAGES: """,2D":Nq
610 INPUT "ARE CORRECTIONS NEEDED IN NUMBER OF GAGES(Y/<Return>)",Ans
620 IF Ans="Y" THEN GOTO First
630 '
640 DISP "INSERT OFF SET DATA DISK INTO RT. DRIVE AND PRESS Continue"
650 PAUSE
660 CAT
670 INPUT "NAME OF DATA OFF SET DATA FILE",Nm$
680 ASSIGN @Fath2 TO Nm$
690 FOR I=1 TO Nq
700 OUTPUT 2:"K":
710 ENTER @Fath2.I:Os(I)
720 NEXT I
730 ASSIGN @Fath2 TO *
740 SUBEND
750 '
760 '
770 '*****
780 '* CHECK:1 *
790 '*****
800 '
810 SUB Check1(Nq,Os(#))
820 '
830 CALL Printos(Nq,Os(#)) 'PRINT OFFSETS TO SCREEN
840 '
850 'CHECK FOR CORRECT OFFSET ENTRY
860 '
870 INPUT "ARE CORRECTIONS NEEDED FOR ANY OFFSET(Y/<Return>)",Ans
880 IF Ans="Y" THEN CALL Correct(Nq,Os(#))
890 '
900 SUBEND
910 '
920 '
930 '*****
940 '* PRINTOS *
950 '*****
960 '
970 SUB Printos(Nq,Os(#))
980 '
990 OUTPUT 2:"K": 'CLEAR SCREEN
1000 '
1010 'PRINT OFFSETS TO SCREEN IN MENUE FORM
1020 '
1030 PRINT USING "31X,""GAGE #""",5X,""OFFSETS""""

```

```

10  PROGRAM REDUCE
20  !THIS PROGRAM REDUCES THE DATA COLLECTED BY MIKE MARTIN FOR HIS
30  !THIS PROJECT. IT COMPUTES THE STRESSES AND STRAINS FOR THE
40  !VARIOUS WIND SPEEDS. THIS PROGRAM HAS BEEN WRITTEN TO BE USEFUL
50  !FOR BOTH SIGNS TESTED WITHOUT MODIFICATION OTHER THAN RESIZING THE
60  !DIMENSION STATEMENTS AT THE BEGINNING
70  !
80  !DIMENSION EACH ARRAY ALONG THE FOLLOWING LINES:
90  !
100 !     1. GS(NUMBER OF GAGES)
110 !     2. D(SIZE OF DATA FILE)
120 !     3. FF(SIZE OF DATA FILE/(NUMBER OF GAGES+5)*NUMBER OF GAGES)
130 !     4. SIG(SIZE OF DATA FILE/(NUMBER OF GAGES+5)*NUMBER OF GAGES)
140 !     5. DELV(SIZE OF DATA FILE/(NUMBER OF GAGES+5)*NUMBER OF GAGES)
150 !     6. WS(SIZE OF DATA FILE/NUMBER OF GAGES)
160 !     7. F(((2*NUM. GAGES)+1)*(SIZE OF DATA FILE/(NUM. GAGES+5)))
170 !
180 OPTION BASE 1
190 DIM GS(15),D(4500),Ep(4500),Sig(4500),Delv(4500),Ws(250),F(6975)
200 OUTPUT 0:"":
210 CALL Offset(Ng,Gs(#))
220 CALL Check1(Ng,Gs(#))
230 CALL Gages(Ev,Gf)
240 CALL DataIn(Nms,Fs,D(#))
250 CALL Wind(Fs,D(#),Ws(#),Ng)
260 CALL Delta(Ng,Fs,L,Gs(#),D(#),Delv(#))
270 CALL Strain(Ng,Ev,Gf,L,Fs,Delv(#),Ep(#))
280 CALL Stress(L,Ep(#),Sig(#))
290 !
300 OUTPUT 0:"K":
310 INPUT "DO YOU WANT STRESSES AND STRAINS SAVED TO A FILE(Y/N)",An#
320 IF An#="Y" THEN
330 CALL Saveit(L,Fs,Ng,Ws(#),Ep(#),Sig(#),F(#))
340 ELSE
350 END IF
360 !
370 CALL Out(Fs,Ng,Ws(#),Ep(#),Sig(#))
380 PRINTER IS 1
390 END
400 !
410 !
420 !*****
430 !#
440 !# SURROUTINES #
450 !#
460 !*****
470 !
480 !
490 !*****
500 !# OFFSET #
510 !*****

```

```

1040 FOR I=1 TO Nq
1050 PRINT USING "3X,2D,7X,D.5D":I,Os(I)
1060 NEXT I
1070 '
1080 SUBEND
1090 '
1100 '
1110 '*****
1120 'x CORRECT x
1130 '*****
1140 '
1150 SUB Correct(Ng,Os(#))
1160 '
1170 Corr: CALL Correct2(Ng,Os(#))
1180 '
1190 'CHECK FOR MORE CORRECTIONS
1200 '
1210 CALL Printos(Ng,Os(#))
1220 '
1230 INPUT "ANY MORE CORRECTIONS(Y/<Return>)",Ans#
1240 IF Ans#="Y" THEN GOTO Corr
1250 '
1260 SUBEND
1270 '
1280 '
1290 '*****
1300 'x GAGES x
1310 '*****
1320 '
1330 SUB Gages(Bv,Gf)
1340 '
1350 OUTPUT 2:"K":
1360 '
1370 Bridges: CALL Bridge(Bv,Gf)
1380 '
1390 'CHECK FOR CORRECT DATA ENTRY
1400 '
1410 OUTPUT 2:") "':
1420 '
1430 PRINT USING "15/,30X,""1. BRIDGE VOLTAGE: ""D.DD,/,30X,""2. GAGE FACTOR:
""D.4D":Bv,Gf
1440 '
1450 INPUT "ARE CORRECTIONS NEEDED(Y/<Return>)",Ans#
1460 IF Ans#="Y" THEN GOTO Bridges
1470 '
1480 SUBEND
1490 '
1500 '
1510 '*****
1520 'x DATA IN x
1530 '*****
1540 '

```

```

1550 SUB DataIn(Nm$,Fs,D(1))
1560 '
1570 OUTPUT 2:"Y"; 'CLEAR SCREEN
1580 '
1590 DISP "PLACE DISK WITH DATA FILE IN RIGHT DRIVE AND PRESS CONTINUE"
1600 PAUSE
1610 '
1620 Corr3:CALL Correct3(Nm$,Fs)
1630 '
1640 OUTPUT 2:"K"; 'CLEAR SCREEN
1650 '
1660 PRINT USING " 15/,30X,.""FILE: """,10A,/,30X,.""SIZE: """,5D":Nm$,Fs
1670 '
1680 'CHECK FOR CORRECT DATA ENTRY
1690 '
1700 INPUT "ARE CORRECTIONS NEEDED?(Y/<Return>)",Ans
1710 IF Ans="Y" THEN GOTO Corr3
1720 '
1730 'OPEN I/O PATH TO FILE
1740 '
1750 ASSIGN @Path1 TO Nm$
1760 '
1770 'READ DATA FROM FILE INTO ARRAY D
1780 '
1790 FOR I=1 TO Fs
1800 ENTER @Path1,I:D(I)
1810 NEXT I
1820 '
1830 'CLOSE I/O PATH TO FILE
1840 '
1850 ASSIGN @Path1 TO *
1860 '
1870 SUBEND
1880 '
1890 '
1900 '*****
1910 ' * WIND *
1920 '*****
1930 '
1940 SUB Wind(Fs,D(1),Ws(1),Ng)
1950 '
1960 'READ WIND SPEEDS FROM ARRAY D INTO ARRAY WS
1970 '
1980 k=5 'FIFTH RECORD IS FIRST WIND SPEED
1990 N=1
2000 L=Ng+5 'TOTAL READINGS PER SCAN
2010 FOR I=1 TO Fs STEP L
2020 Ws(N)=D(I)
2030 N=N+1
2040 k=k+L
2050 NEXT I
2060 '

```

```

2070 SUREND
2080 '
2090 '
2100 '*****
2110 'v          DELT          t
2120 '*****
2130 '
2140 SUB Delv(Ng,Fs,L,Os(*),D(*),Delv(*))
2150 '
2160 'COMPUTE VOLTAGE CHANGE
2170 '
2180 M=Ng+5          'TOTAL READINGS PER SPAN
2190 L=1            'NUMBER OF GAGE READINGS
2200 K=1
2210 '
2220 FOR J=1 TO Fs STEP M
2230 K=K+5
2240 FOR I=1 TO Ng
2250 Delv(L)=D(I)-Os(I)          'DELTA V=READING - OFFSET
2260 K=K+1
2270 L=L+1
2280 NEXT I
2290 NEXT J
2300 L=L-1          'CORRECT FOR LAST TIME THROUGH LOOP
2310 '
2320 SUREND
2330 '
2340 '
2350 '*****
2360 's          STRAIN          t
2370 '*****
2380 '
2390 SUB Strain(Ng,Bv,Gf,L,Fs,Delv(*),Ep(*))
2400 '
2410 'STRAIN=(DELTA V)/(GAGE FACTOR*BRIDGE VOLTAGE)
2420 '
2430 L=Fs/(Ng+5)*Ng
2440 FOR I=1 TO L
2450 Ep(I)=Delv(I)/(Bv*Gf)
2460 NEXT I
2470 '
2480 SUREND
2490 '
2500 '
2510 '*****
2520 's          STRESS          t
2530 '*****
2540 '
2550 SUB Stress(L,Ep(*),Sig(*))
2560 '
2570 'STRESS = STRAIN*E
2580 '

```

```

2590 FOR I=1 TO L
2600 Sig(I)=Ep(I)*29000
2610 NEXT I
2620 '
2630 SUBEND
2640 '
2650 '
2660 '*****
2670 '          SAVEIT          '
2680 '*****
2690 '
2700 SUB Saveit(L,Fs,Ng,Ws(*),Ep(*),Sig(*),F(*))
2710 '
2720 'SAVE WIND SPEED ,STRAINS, AND STRESSES
2730 '
2740 INPUT "NAME OF NEW DATA FILE?".Nm$
2750 '
2760 M1=Fs/(Ng+5)
2770 Size=2*Ng*M1+M1          'SIZE OF NEW FILE
2780 '
2790 CREATE RDAT Nm$,Size,B   'CREAT FILE WITH SIZE RECORDS AT 8 BITS/RECORD
2800 '
2810 'OPEN I/O PATH TO NEW FILE
2820 '
2830 ASSIGN @Path2 TO Nm$
2840 '
2850 OUTPUT 2:"*":
2860 PRINT USING "10/,10X,""STORING DATA IN FILE """,10A":Nm$
2870 '
2880 'STORE DATA IN FILE
2890 '
2900 M=Fs/(Ng+5)
2910 K=1
2920 N=1
2930 FOR J=1 TO M
2940 F(N)=Ws(J)
2950 N=N+1
2960 FOR I=1 TO Ng
2970 F(N)=Ep(I)
2980 F(N+1)=Sig(I)
2990 N=N+2
3000 K=K+1
3010 NEXT I
3020 NEXT J
3030 '
3040 'CLOSE I/O PATH TO FILE
3050 '
3060 OUTPUT @Path2:F(*)
3070 ASSIGN @Path2 TO *
3080 '
3090 SUBEND
3100 '

```



```

0110 *
0120 * *****
0130 *          OUT          *
0140 * *****
0150 *
0160 SUB Out(Fs,Ng,Ws(*),Ep(*),Sig(*))
0170 *
0180 INPUT "DO YOU WANT RESULTS PRINTED ON PRINTER?(Y/N Return)",Ans
0190 IF Ans="Y" THEN PRINTER IS 701
0200 *
0210 Nr=Fs/(Ng+5)          !TOTAL NUMBER OF SCANS
0220 *
0230 FOR J=1 TO Nr-1 STEP 2
0240 *
0250 C=(J-1)/6
0260 D=INT(C)
0270 IF D=C THEN PRINT CHR$(12)          !ONLY PRINT 6 DATA SETS PER PAGE
0280 *
0290 L=J*Ng-(Ng-1)
0300 K=L+Ng-1
0310 PRINT USING "%12X,%12X,WIND SPEED: %12.2D,2D,23X,%12X,WIND SPEED: %12.2D,2D";Ws(J),Ws(J+1)
0320 PRINT USING "%12(2X,%12X,GAGE NO.%,2X,%12(2X,%12X,STRAIN(1n/1n)",2X,%12(2X,%12X,STRESS(KSI)",2X,%)"
0330 N=1
0340 FOR I=L TO K
0350 PRINT USING "%5X,2D,8X,D,5D,7X,5D,2D,9X,2D,8X,D,5D,7X,5D,2D";N,Ep(I),Sig(I),N,Ep(I+Ng),Sig(I+Ng)
0360 N=N+1
0370 NEXT I
0380 NEXT J
0390 *
0400 SUREND
0410 *
0420 *
0430 * *****
0440 *          CORRECT2          *
0450 * *****
0460 *
0470 SUB Correct2(Ng,Os(*))
0480 *
0490 CALL Printos(Ng,Os(*))
0500 *
0510 INPUT "NUMBER OF GAGE TO CORRECT",N
0520 INPUT "NEW OFFSET",Os(N)
0530 *
0540 SUREND
0550 *
0560 *
0570 * *****
0580 *          BRIDGE          *
0590 * *****

```

```
3600 '
3610 SUB Bridge(Ev,Gf)
3620 '
3630 INPUT "WHAT IS THE BRIDGE VOLTAGE?",Ev
3640 INPUT "WHAT IS THE STRAIN GAGE FACTOR?",Gf
3650 '
3660 SUBEND
3670 '
3680 '
3690 '*****
3700 's CORRECTD '
3710 '*****
3720 '
3730 SUB CorrectD(Nm$,Fs)
3740 '
3750 OUTPUT 2:"K"; 'CLEAR SCREEN
3760 '
3770 CAT 'DISK DIRECTORY
3780 '
3790 INPUT "NAME OF DATA FILE TO USED",Nm$
3800 INPUT "SIZE OF DATA FILE USED(NUMBER OF RECORDS)?",Fs
3810 '
3820 SUBEND
```

APPENDIX C:
SET UP AND OPERATION
OF FIELD TESTING EQUIPMENT

Set Up and Operation
of Field Testing Equipment

These procedures should be followed when using the HP 3421 Data Acquisition Unit to collect strain gage data.

List of needed equipment:

- A. HP3421A - Data Acquisition Unit
- B. HP-41CX - Calculator
- C. HP-IL - Module
- D. HP82161A - Cassette Drive
- E. DC Power Supply
- F. Wheatstone Bridge

Steps 1-5 must be completed in the laboratory.

1. Make sure that all battery packs in all devices are fully charged.
2. It is necessary to initialize and create a file on a tape before data can be stored on it. It is recommended to make the file big enough to fill the entire tape. Detailed instructions can be found in the HP-IL module's owner's manual.
3. For strain gage measurements, it is necessary to use a Wheatstone Bridge. The Wheatstone Bridge requires an external DC power supply. There are many different ways to configure the Wheatstone Bridge. The user should refer to the strain gage manual for these variations. Figure A1 shows a two-wire circuit.
4. Once a Wheatstone Bridge configuration has been selected, connect the appropriate wires from the bridge to the terminal block. Make sure to connect the wires to the correct channel slots. Each slot has a high terminal and a low terminal. These are clearly marked on the terminal block. Take care not to connect any wires in the unnumbered slots between slots 1 and 2, or the unit will not function properly. It does not matter which wire goes in the "Hi" slot or the "Low" slot as long as they remain the same for the entire study.

5. If it will be necessary to disconnect and reconnect the gage cables to the bridge, it is recommended to use some sort of quick disconnect device, such as the spade connectors shown in Figure A2.

Steps 6-20 are to be completed in the field.

6. Make sure all devices are turned OFF.
7. Connect the terminal blocks to the option slots on the back of the HP3421A. The block for channels 0-9 goes in slot 0, the block for channels 10-19 goes in slot 1.
8. Connect the strain gage cables to the Wheatstone bridge, following the manner of the bridge configuration selected. Use the quick disconnect devices, if available.
9. Plug the HP-IL module into an expansion port on the calculator. If the calculator has memory modules installed, the IL module must be in a higher-numbered port than a memory module.
10. Plug the lead from the IL module with the male end into the HP-IL receptacle marked "IN" on the back of the HP3421A. Only one of the leads will fit, so there is no possibility of a mixup.
11. Using the short IL cable supplied with the cassette drive, plug the female end into the receptacle marked "OUT" on the rear panel of the HP3421A. Plug the other end of the cable into the receptacle marked "IN" on the rear of the cassette drive.
12. Plug the other lead from the IL module into the receptacle marked "OUT" on the cassette drive. The HP3421A calculator and cassette drive should form a continuous, uninterrupted loop. If they do not, repeat Steps 6-12.
13. Connect the power supply to the Wheatstone Bridges.
14. Turn on all devices and check for proper operation.
15. Adjust the voltage across the Wheatstone Bridge to the desired value.

16. Place prepared data cassette in drive. It will only fit in one way.
17. Set tape to proper file and data register. Refer to IL module owner's manual for details.
18. Set any parameters required by calculator software and begin data collection.
19. Check equipment frequently to insure proper operation.
20. When disconnecting devices, make sure all devices are turned "OFF" before beginning to disconnect.

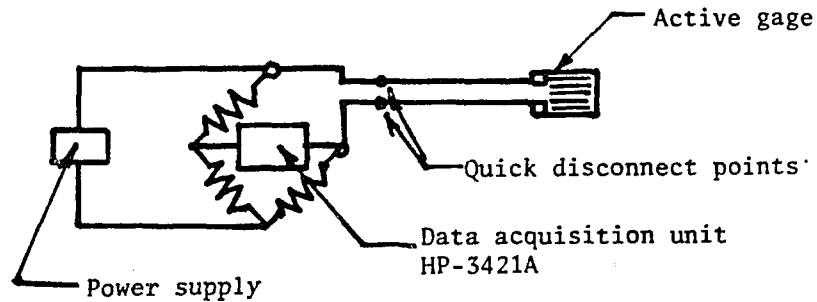


Figure A1 - Two-Wire Wheatstone Bridge

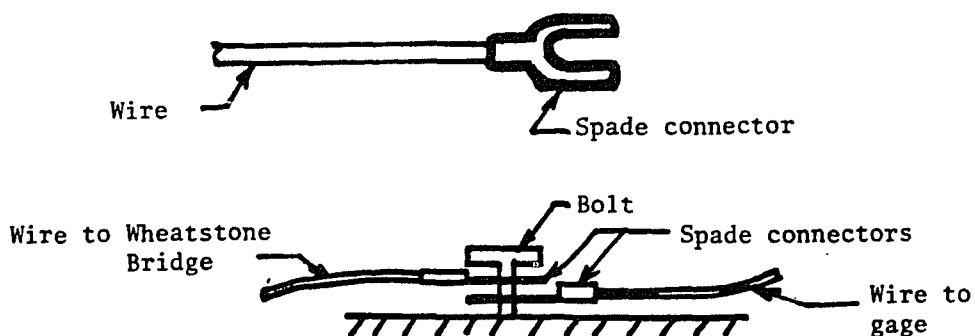


Figure A2 - Spade Connector and How to Use

APPENDIX D:
DATA TRANSFER
FROM CASSETTE DRIVE TO HP SERIES 200 COMPUTER

Data Transfer
From Cassette Drive to Series 200 Computer

These procedures should be followed to transfer data from a tape in the cassette drive to the Series 200 computer for storage on a floppy disk.

List of needed equipment:

- A. HP Series 200 Computer
- B. HP-41CX Calculator
- C. HP-IL Module
- D. HP82161A Cassette Drive
- E. HP82169A HP-IL/HP-IB Interface
- F. Floppy Disk for Storage

1. Floppy disk must be initialized before it may be used. Refer to computer manual for details.

2. To facilitate data transfer, two programs have been written. TRANS runs on the HP-41CX and TRANSFER runs on the Series 200 computer. Listings of these programs are given in Appendices E and F.

TRANS first prompts the user to enter the beginning and ending registers of the desired data, as well as the data file where the data are located. It then reads a portion of the data into the calculator's memory. One register at a time, it recalls the data into the alpha register of the calculator, selects the IL/IB interface as the primary device and outputs the alpha register to the interface.

TRANSFER also prompts the user for the beginning and ending tape registers plus the name of file where the data are to be stored. It creates this file, reads the data from the interface, and stores it.

3. TRANS and TRANSFER continue until all the data have been transferred and stored.

4. To use these programs, follow Steps 5-29. The user may wish to write his own program(s).

5. Make sure all devices are turned OFF.

6. Plug the HP-IL module into an expansion port on the calculator. Make sure that no memory modules are plugged into a higher numbered port than the IL module.

7. Plug the lead of the IL module with the male end into the receptacle marked "IN" on the IL/IB interface.

8. Using the short IL cable supplied with the cassette drive, plug the female end into the receptacle marked "OUT" on the IL/IB interface and the other end into the receptacle marked "IN" on the cassette drive.

9. Plug the remaining lead from the IL module into the receptacle marked "OUT" on the IL/IB interface and the other end into the receptacle marked "IN" on the cassette drive.

10. The calculator, cassette drive, and IL/IB interface should form a continuous loop. If they do not, repeat steps 5-9.

11. Plug an HP-IB cable from the computer into the IL/IB interface. It will only fit on one way.

12. Plug the power cord into the IL/IB interface. Turn on all devices.

13. Boot operating system on computer.

14. Make sure IL/IB interface is set to "Mailbox" mode. See IL/IB Owner's Manual for details.

15. Place proper cassette in drive.

16. Execute "TRANS" on the calculator.

17. TO "START REG?" prompt, enter the starting register of tape and press R/S.

18. TO "END. REG?" prompt, enter the ending register of the tape and press R/S.

19. To "File?" prompt, enter tape data file name and press R/S.

20. When "WRT DATA" appears in calculator display, load program "Transfer" into Series 200 Computer. DO NOT touch the calculator.
21. Re-dimension the arrays used in "TRANSFER", using the guidelines found at the beginning of the program.
22. Place the floppy disk to contain the data in the logged-in drive.
23. RUN program "TRANSFER".
24. The program will prompt the user to enter the data file name and the beginning and ending tape registers. Press the ENTER Key after each item.
25. After a short pause, the Series 200 will display "Ready to read data, press CONTINUE". When this happens, press the R/S Key on the calculator and watch the red "BUSY" light on the tape drive.
26. VERY IMPORTANT: When the "BUSY" light on the tape drive goes off (after approximately 6 seconds) IMMEDIATELY press the "CONTINUE" key on the Series 200.
27. Check the first number on the Series 200 screen to see if it is correct.
28. Wait until finished. Calculator will display "End of Data".
29. Turn all devices off before disconnecting.

APPENDIX E:
DATA TRANSFER SOFTWARE
FOR HP-41CX CALCULATOR

HP-41X program to transfer data from cassette tape
to an HP Series computer via the HP-IL/HP-IB interface.

```
01LBL "TRANS"           32 ST+ 02
02 XEQ "AUTOIO"        33 RCL 02
03 FIX 9                34 RCL 01
04 "START REG?"        35 X<=Y?
05 PROMPT              36 GTD 03
06 STD 00              37 GTD 01
07 "END. REG?"         38LBL 02
08 PROMPT              39 1
09 STD 01              40 SELECT
10 RCL 00              41 LISTEN
11 "FILE?"             42LBL 04
12 PROMPT              43 CLA
13 SEEKR               44 ARCL IND 03
14 RCL 00              45 DUTA
15 1                   46 1
16 -                   47 ST+ 03
17 STD 02              48 ST+ 04
18 STD 04              49 RCL 04
19 MANIO               50 RCL 01
20 "WRT DATA"         51 X=Y?
21 AVIEW               52 GTD 03
22 STOP                53 RCL 03
23LBL 01               54 220
24 2                   55 X=Y?
25 SELECT              56 RTN
26 10.219              57 GTD 04
27 READRX              58LBL 03
28 10                  59 "END OF DATA"
29 STD 03              60 AVIEW
30 XEQ 02              61 AUTOIO
31 210                 62 .END.
```

APPENDIX F:

DATA TRANSFER SOFTWARE
FOR HP SERIES 200 COMPUTER

```
530  DISF "Ready to read data. Press CONTINUE to procede."
540  FAUSE
550  '
560  DISF "READING DATA AND WRITING DATA TO DISK FILE"
570  '
580  !READ IN DATA FROM INTERFACE
590  '
600  N=1
610  FOR I=1 TO Size STEP 21 !STEP SIZE IS SAME AS DIMENSION OF ARRAY D(*)
620  FOR J=1 TO 21 !LOOP SIZE IS SAME AS DIMENSION OF ARRAY D(*)
630  ENTER @Ib11;D(J)
640  '
650  !USE ONLY ABLOLUTE VALUES
660  D(J)=ABS(D(J))
670  '
680  !PRINT VALUES TO SCREEN
690  PRINT USING "5X,4D,4D.10D";N,D(J)
700  !STORE DATA IN FILE
710  '
720  K=J+J-1
730  OUTPUT @Fath1,k;D(J)
740  '
750  !CONTINUE LOOP
760  '
770  N=N+1
780  NEXT J
790  NEXT I
800  SUBEND
```

8. REFERENCES

1. American Association of State Highway and Transportation Officials (AASHTO), "Standard Specifications for Structural Supports for Highway Signs, Luminaires and Traffic Signals," AASHTO, Washington, D.C., 1975 (revised 1978 and 1979).
2. Ehsani, Mohammad R. and Reidar Bjorhovde, "Deflection Criteria for Sign Support Structures," paper submitted to the Journal of Structural Division, ASCE, February 1985.
3. Ehsani, Mohammad R., S. K. Chakrabarti, and Reidar Bjorhovde, "Static and Dynamic Behavior of Monotube Span-Type Sign Structures," Report No. FHWA/AZ/194, Vols. I and II, Arizona Department of Transportation, Phoenix, Arizona, June 1985.
4. Rouse, Hunter, "Elementary Mechanics of Fluids", Dover Publications, New York, NY, 1978.
5. Hoerner, Sighard F., "Fluid Dynamic Drag", Published by Author, 1965.
6. Fung, Y. C., "An Introduction to Aeroelasticity", John Wiley and Sons, Inc., New York, NY, 1955.
7. Lamb, H. "Hydrodynamics", 6th Edition, Cambridge, London, 1932.
8. Weaver, W., "Wind-Induced Vibrations in Antenna Members," "Journal of the Engineering Mechanics Division", ASCE, Vol. 87, No. EM1, 1961, pp. 141-165.
9. American Institute of Steel Construction (AISC), "Specification for the Design, Fabrication and Erection of Structural Steel for Buildings", AISC, Chicago, Illinois, November 1978.
10. American Concrete Institute (ACI), "Building Code Requirements for Reinforced Concrete (ACI 318-83)," ACI, Detroit, Michigan, 1971.
11. Kamel, H. A. and R. R. Nagulpally, "GIFTS Primer: A First Introduction to the GIFTS-5 System," AME Department, University of Arizona, Tucson, Arizona, Rev. December 1985.
12. Micro Measurements, "Student Manual for Strain Gage Technology," Bulletin 309, Measurements Group Inc., Raleigh, North Carolina, 1983.

13. Dally, J. W. and W. F. Riley, "Experimental Stress Analysis", 2nd Edition, McGraw-Hill, New York, 1978.
14. Hoel, P. G. and R. J. Jessen, "Basic Statistics for Business and Economics", John Wiley & Sons, Inc., New York, NY, 1983.
15. Corcoran, G. F. and E. B. Kurtz, "Electrical Engineering Fundamentals", John Wiley and Sons, Inc., New York, NY, 1976.
16. Popov, E. P., "Mechanics of Materials", 2nd Edition, Prentice-Hall, Englewood Cliffs, New Jersey, 1976.
17. Hewlett-Packard, "Model 3421A Data Acquisition/Control Unit: Operating, Programming and Configuration Manual," Hewlett-Packard Company, Loveland, Colorado, 1982.